Soft Sensors in Digital Healthcare Monitoring

A thesis submitted to the

Imperial College of Science, Technology and Medicine

for the degree of

Doctor of Philosophy

By

Michael Kasimatis

Department of Bioengineering

Imperial College of Science, Technology and Medicine

London, SW7 2AZ

December 2020

Declaration of Originality

All work in this thesis, which is not explicitly highlighted to be from a third party, is my own work done over the course of the last four and a half years. Some of my work has already been published and is summarized here. All work by third parties included in this thesis is appropriately referenced.

Copyright Declaration

‘The copyright of this thesis rests with the author. Unless otherwise indicated, its contents are licensed under a Creative Commons Attribution-Non Commercial 4.0 International Licence (CC BY-NC).

Under this licence, you may copy and redistribute the material in any medium or format. You may also create and distribute modified versions of the work. This is on the condition that you credit the author and do not use it, or any derivative works, for a commercial purpose.

When reusing or sharing this work, ensure you make the licence terms clear to others by naming the licence and linking to the licence text. Where a work has been adapted, you should indicate that the work has been changed and describe those changes.

Please seek permission from the copyright holder for uses of this work that are not included in this licence or permitted under UK Copyright Law.’

List of Publications

Published

1. Max Grell, Can Dincer, Thao Le, Alberto Lauri, Estefania Nunez-Bajo, Michael Kasimatis, Giandrin Barandun, Stefan A. Maier, Anthony E. G. Cass, Firat Güder, *Autocatalytic Metallization of Fabrics Using Si Ink, for Biosensors, Batteries and Energy Harvesting,* Advanced Functional Materials 2018, 29, 1804798

2. Giandrin Barandun, Matteo Soprani, Sina Naficy, Max Grell, Michael Kasimatis, Kwan Lun Chiu, Andrea Ponzoni, Firat Güder, *Cellulose Fibers Enable Near-Zero-Cost Electrical Sensing of Water-Soluble Gases*, ACS Sensors 2019, 4, 6, 1662-1669

3. Michael Kasimatis, Estefania Nunez-Bajo, Max Grell, Yasin Cotur, Giandrin Barandun, Ji-Seon Kim, Firat Güder, *Monolithic Solder-On Nanoporous Si-Cu Contacts for Stretchable Silicone Composite Sensors*, ACS Appl. Mater. Interfaces 2019, 11, 50, 47577-47586

4. Yasin Cotur, Michael Kasimatis, Matti Kaisti, Selin Olenik, Charis Georgiou, Firat Güder*, Stretchable Composite Acoustic Transducer for Wearable Monitoring of Vital Signs,* Advanced Functional Materials 2020, 30, 1910288

5. Estefania Nunez-Bajo, Alexander Silva Pinto Collins, Michael Kasimatis, Yasin Cotur, Tarek Asfour, Ugur Tanriverdi, Max Grell, Matti Kaisti, Guglielmo Senesi, Karen Stevenson, Firat Güder, *Disposable Silicon-based All-in-One Micro-qPCR for Rapid On-Site Detection of Pathogens*, Nature Communications 2020, 11, 6176

6. Max Grell, Giandrin Barandun, Michael Kasimatis, Alex Collins, Jieni Wang, Tarek Asfour, Firat Güder, *Determining and Predicting Soil Chemistry with a Point-of-Use Sensor Toolkit and Machine Learning Model*, bioRxiv 2020, Submission for peer review

In Preparation

7. Giandrin Barandun, Max Grell, Michael Kasimatis, Yubang Shen, Chun Lin Yap, Jeremy Levy, Firat Güder, *Cellulose Fibers in a Sensor Array Enable Low-Cost Point-of-Care Diagnostics of Breath Ammonia Levels* (2021)

8. Fahad Alshabouna, Hong Seok Lee, Giandrin Barandun, Estefania Nunez-Bajo, Yasin Cotur, Michael Kasimatis, Firat Güder, *All-Organic Textile-Based Wearable Sensors by Computerized Embroidery (from Fibres to Wearable Sensors)* (2021)

9. Michael Kasimatis, Giandrin Barandun, Michael Mace, Max Grell, Paul Rinne, Nicola Goldsmith, Firat Güder, *Soft Stretchable Sensor for Enhanced Handgrip Performance in Point-of-Care Rehabilitation and Digital Therapeutics* (2021)

10. Michael Kasimatis, Firat Güder, *A Review of Monolithic Stretchable Strain Sensors in Digital Therapeutics* (2021)

11. Yasin Cotur, Selin Olenik, Ugur Tanriverdi, Tarek Asfour, Guglielmo Senesi, Michael Kasimatis, Laura Gonzalez-Macia, and Firat Güder, *Flexible Composite Pressure Transducer for Wearable Monitoring of Breathing Patterns* (2021)

Patents

1. Giandrin Barandun, Max Grell, Michael Kasimatis, Electrical Sensing of Gases in Packaged Products and Monitoring Freshness of Perishable Food Products, Application No. GB 2006737.7 (Filed May 2020)

2. Michael Kasimatis, Max Grell, Yasin Cotur, Giandrin Barandun, Firat Güder, *Component for a Stretchable Electronic Device*, Application No. GB 1907270.1 (Filed May 2019)

3. Yasin Cotur, Michael Kasimatis, Firat Güder, *Flexible Stretchable Wearable Transducer*, Application No. GB 1813568.1 (Filed August 2019)

4. Max Grell, Can Dincer, Thao Le, Alberto Lauri, Estefania Nunez-Bajo, Michael Kasimatis, Giandrin Barandun, Stefan A. Maier, Anthony E. G. Cass, Firat Güder, *Metal Fabrics and Membranes,* Application No. GB 1805131.8 (Filed March 2018)

Abstract

Stretchable sensors are a class of materials with applications across research fields from healthcare to structural engineering. Despite the extensive research aiming to improve the performance of individual materials or components, stretchable sensor devices are difficult to implement because conventional electronic components, mainly used for processing, which are rigid, have to make contact with soft components reliable enough to withstand real-world usage.

This thesis introduces a method for creating electrical contacts that can be robustly attached onto soft, stretchable conductive polymer composites on one side and soldered to metal wires on the other side. Mechanically robust electrical contacts were developed to interface (soft) silicone-based strain sensors with conventional (hard) solid-state electronics using a nanoporous silicon-copper contact. Contacts are mounted on custom-made and commercial soft strain sensitive silicone sensors. The contacts are shown to be reliable under large deformations, then compared with a commonly used alternative under real-world strain conditions. The layered structure of the device creates a complex electronic component deriving from the silicon-copper Schottky junction.

This thesis tests the versatility of the technology through a series of real-world applications. The silicon-copper contacts were used to produce a series of proof-of-concept devices, including a wearable respiration monitor, leg band for exercise monitoring, and squeezable ball to monitor rehabilitation of patients with hand injuries or neurological disorders. The sensor is shown to operate and detect multiple modes of motion regardless of placement on the body.

Next, a proof-of-concept device was employed to measure hand grip strength. The optimized sensor can detect grip strength with high sensitivity. The hardness of the device was shown to increase sensitivity when healthy humans performed manual exercises and completed digital tasks. Providing patients with these devices can help

monitor their rehabilitation following hand injuries or neurological disorders. This can be done through self-led at-home therapy which has been shown to improve treatment, engagement, long-term lifestyle adherence, while avoiding repeated visits to clinics which plays an important role in frequency of therapy, effectiveness, and accessibility.

Acknowledgements

I would really like to express my heartfelt thanks to everyone who contributed in making this work possible. This PhD thesis means much more to me than the completion of four years of a research project. It signifies a unique journey during which I challenged myself, learnt to appreciate my own time and where to devote it, and ultimately really stood on my own two feet and learned how to ask questions. Throughout this process, the role of my supervisor, Dr Firat Güder, was crucial. He inspired me to do science the way I think is right and to not compromise, he helped me even, and especially when, I was not aware that I needed it and he took the back seat when he saw that I needed to prove to myself that I could do it. I cannot find the words to thank and express my respect for him as a scientist, as a thinker, and as a person.

The privilege to work closely with him was granted to me by the EPSRC studentship, and by the Department of Bioengineering at Imperial College and I would like to acknowledge them for offering their time and efforts to help me navigate this degree.

Most importantly, I would like to thank the wonderful people that I have met these last years whose support has come in both intellectual and familial forms with the warmth and everlasting kindness that comes with it. There is a special kind of atmosphere the Güder research group creates and it is both unique and familiar. I am grateful for everyone who helped inside and outside the lab, offering the best of their abilities and showing who they really are.

I would also like to say a big thank you to my friends outside work. The people who helped me even begin this long test, and the people who lent a shoulder and even held me up with both hands when necessary during the past few years without whom it would be an understatement that I could not have done this. Above and beyond anything else, I would like to thank my family. The conviction that I received from them had a calming effect and showed me that no matter how much is going on, it is

all a matter of perspective. The simple conviction that everything looks clearer if you take a look at it from one step farther away.

Contents

Part I: Introduction

Part I Introduction 19

A Brief Introduction to Soft Devices for Wearable Sensors 20

1.1 - The History of Soft Sensors 21

1.2 - Silicone Sensors for Strain and Pressure 23

1.3 - Whole-devices with Stretchable Sensors 26

1.3.1 - Integration methods of hard and soft electronics at scale 28

1.3.2 - Compliant Strain Sensors in Healthcare and beyond 30

PART II Copper-Silicon Contacts for Soft Silicone Strain Sensors 32

Preparation and Characterisation of Silicone-CB composites 33

2.1 - Preparation & Characterisation of CB-PDMS Composite 33

2.2 - Characterisation of commercially available CB-CSC 37

2.3 - The need for robust contacts on silicone composite sensors 39

Fabrication and Characterisation of Copper-Silicon Contacts 41

3.1 - PDMS Surface Chemistry after Plasma bonding 41

3.2 - Preparation of Cu-pSi contacts 43

3.2.1 - Silicon etching overview 43

3.2.2 - Metal Assisted Chemical Etching of Silicon (Cu-pSi) 46

3.2.3 - Electroplating nanoporous Silicon with Copper (Cu-pSi) 48

3.3 - Future Development 53

Mechanical characterisation of Cu-pSi solder-on contact system 54

4.1 - Lap shear strength: Cu-pSi *vs.* AgEpoxy 54

4.2 - PDMS fracture type 57
4.3 - Cu-pSi and AgEpoxy under cyclic stress 59
Electrical characterisation of the Cu-pSi system 64
5.1 - Heterointerfaces and electrical behaviour 64
5.2 - Modelling an equivalent circuit 66
5.3 - Alternating current (AC) and sensitivity 69
PART III Applications of Cu-pSi CB-Silicone Sensors 75
Soft Sensors in Rehabilitation and Digital Therapeutics 76
6.1 - Proof-of-concept devices using Cu-pSi contact technology 76
6.2 - Wearables and Digital Healthcare 79
6.2.1 - Wearable sensors in everyday life 79
6.2.2 - Better Digital Healthcare, Remote Diagnostics, and quality of life 80
6.3 - Benefits of digital and gamification in healthcare and therapeutics 81
6.3.1 - Digital Feedback 81
6.3.2 - Telerehabilitation 82
Soft Sensor for Upper Limb Rehabilitation via Gamification and Real-Time Feedback 84
7.1 - Current standard in upper limb rehabilitation 85
7.2 - Experimental details of hand exercise monitoring using a soft sensor and digital tools 86
7.2.1 - Moulding 86
7.2.2 - Human grasp types and sensing modes 89
7.2.3 - Participants and test design 90
7.3 - Commercial outlook 95
Conclusions and Outlook 97

Bibliography 99

Appendix 113

Curriculum Vitae 116

Patents 120

Media 121

Awards & Grants 122

List of Figures

Figure 1 Evolution of electronic components 21

Figure 2 Preparation of CB-PDMS 34

Figure 3 PDMS pre-polymer components 35

Figure 4 CB-PDMS Batch & CB-CSC sample 35

Figure 5 Percolation Threshold 36

Figure 6 CB-CSC thickness *vs* DC Resistance 38

Figure 7 Sensitivity *vs* Thickness of CB-CSC 38

Figure 8 Visual contact angle of plasma-treated Si 42

Figure 9 Schematic of the plasma bonding 43

Figure 10 MACE colour change 45

Figure 11 Metal Assisted Chemical Etching 45

Figure 12 Cu-pSi preparation and assembly 47

Figure 13 Physical and Chemical Analysis at the Cu Si Interface 49

Figure 14 Si surface SEM during MACE 52

Figure 15 Cu plating and plasma bonding method 53

Figure 16 Lap Shear Test comparison Cu-pSi *vs.* AgEpoxy 55

Figure 17 Strain *vs.* CB Concentration 55

Figure 18 Stress – strain repeats (Cu-pSi *vs.* AgEpoxy) 56

Figure 19 SEM before and after stretch 57

Figure 20 Tensile strength of PDMS 58

Figure 21 Cu-pSi/AgEpoxy device pictures 59

Figure 22 Visual analysis of tensile test 60

Figure 23 Cyclic CB-PDMS tensile tests 61

Figure 24 Cu-pSi CB-PDMS Electromechanical test repeats 63

Figure 25 I-V, band diagrams, equivalent circuit #1 65

Figure 26 DC IV and sensitivity for CB-CSC 68

Figure 27 Four probe measurement 69

Figure 28 AC frequency sweeps 71

Figure 29 AC sensitivity 72

Figure 30 Raw signal AC 300 N 72

Figure 31 AC circuit modelling and equivalent circuit #2 73

Figure 32 Demo strain and pressure sensing healthcare devices 78

Figure 33 Resistance *vs.* Temperature 79

Figure 34 Hand-grip sensor manufacturing 87

Figure 35 Silicone injection moulding (two-shot) 88

Figure 36 Sensing modalities for cylindrical squeezable sensor 90

Figure 37 Screen recording from gameplay 92

Figure 38 CB-CSC/Cu-pSi devices encapsulated in Hard and Soft silicone 93

Figure 39 Closed fist using squeezable sensor 94

Appendix: Figure 40 Cyclic CB-PDMS test repeats 113

Appendix: Figure 41 Multiple contacts AC/DC measurements 114

Appendix: Figure 42 115

List of Tables

Table 3.1-1 Stress & strain values for plasma-treated and pristine PDMS 43

Table 7.3-1 Performance metrics for Test 1 (“Red Bird”) and Test 2 (“Tutu Bear”) for Hard and Soft silicone encapsulation devices; Score (Test 1): has a maximum of 30 stars collected; Peak % (Test 1): represents $\Delta R/R_0$ for the change of resistance at the maximum when the device is squeezed over the resistance at rest; Cross-correlation: shows how similar the Bird Trajectory and Star Path are (maximum 1); Score (Test 2): is the time taken to complete the level (lower is better); Peak % (Test 2): represents $\Delta R/R_0$ between the maximum squeeze and at rest states; # Peaks: is the mean number of squeezes the subjects needed to complete the level (n = 10) 93

Part I

Introduction

Chapter 1

A Brief Introduction to Soft Devices for Wearable Sensors

This thesis explores mechanically robust strain and pressure sensors made of soft materials. Specifically, we used conductive polymer composites (CPC) made of silicone as soft strain and pressure sensors.

In the first Chapter, we introduce the concept and need for sensors made with soft, stretchable materials and their applications in healthcare. We look at methods to manufacture these soft sensors made of silicone at scale and address the challenge of reliably connecting soft electronics with conventional "hard" electronics like wires and circuit components needed to make up an electronic device.

In Chapters two & three, we present a custom-built CPC using polydimethylsiloxane (PDMS), which is a versatile and stable silicone rubber, filled with Carbon Black (CB) conductive fillers. We also tackle the problem of connecting soft and hard electronics by creating specific sites on CB-PDMS to solder on. These sites are made of copper-plated nanoporous Silicon (Cu-pSi).

The mechanical strength under real-world strain conditions and the CB-PDMS/Cu-pSi sensor's electrical response and sensitivity are explored in Chapters four & five. Industrially-made Carbon-black filled conductive silicone composite (CB-CSC) is also connected to Cu-pSi contacts to test the scalability of the Cu-pSi contact technology.

Chapters six & seven are focused on devices that can be manufactured using this technology and how they can be applied in monitoring motion of humans and upper limb rehabilitation in clinical practice.

1.1 - The History of Soft Sensors

Solid-state electronics began as complex structures, with Bardeen, Brattain, and Shockley's "three-electrode circuit element utilizing semiconductive materials" composing of rigid "blocks" of material several centimetres long. [1,2] Developments in materials science allowed for the miniaturization of "blocks" needed to assemble electronic "circuit elements" which we now call integrated circuits (ICs – "chips", Figure 1). While electronics grew into one of the world's largest industries, their shape remained flat and rigid.

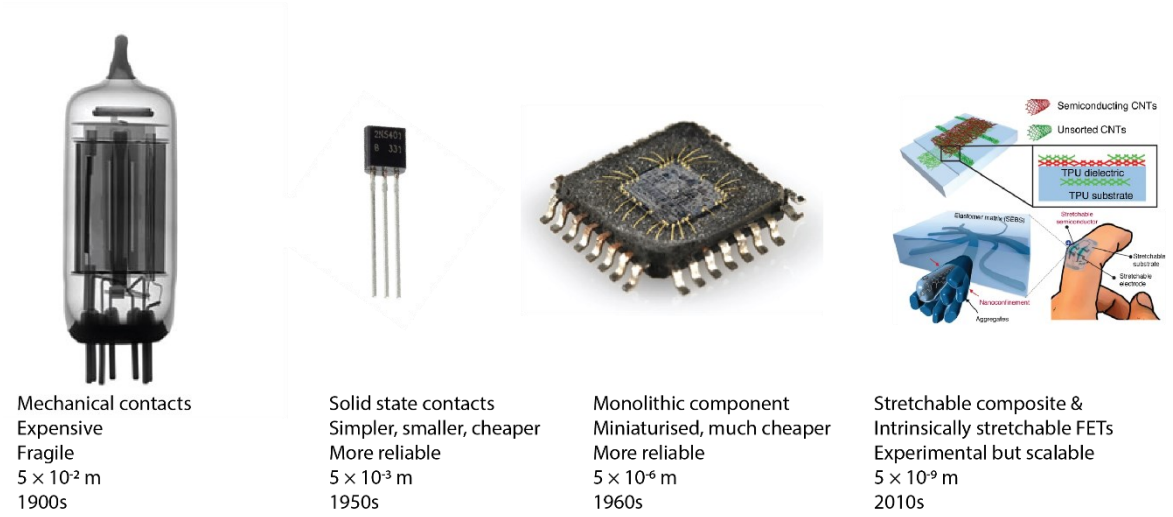


Figure 1 Evolution of electronic components (from left to right) Vacuum tube, transistor, integrated circuit, carbon nanotube composite field effect transistor (FET) [3] & intrinsically stretchable transistor [4]

Silicon-based ICs have not yet been substituted by stretchable equivalents but conformal, stretchable devices can be created when combining rigid circuit components with stretchable components and sensors. These "hybrid" electronic devices have found applications in healthcare when intimate and conformal interaction with human tissue is required. [5] Recent advances in the development of conformal hybrid devices where functional layers interface and integrate towards a monolithic device are discussed in later sections.

The first soft electrically conductive materials, surprisingly, came from an unlikely place in the beginning of the 20th century: car tires. Manufacturers added carbon black

(micro-nanoscale carbon powder) to the rubber used to make tyres. Natural isoprene, and synthetic styrene-butadiene rubbers which are typically white, now turned black and were improved in three ways: 1) they became harder and more resistant to wear, 2) they were more resistant to UV radiation which weaken rubber, 3) they were heat conductive and could dissipate heat away from the car. Although this application was not related to electronics, manufacturers became familiar with large scale fabrication techniques for conductive polymer composites, with production and demand reaching high levels such that research is now focussed on creating more sustainable CB production routes. [6]

Through the years between 1960 and 1980 conductive composites were studied as fatigue indicators and gaskets. [7] Since the '80s soft conductors started being used as transducers and tactile mechanical sensors. Unconventional forms of electronics began in the mid-'90s with the first polymer transistors appearing (which could enable innately stretchable ICs). [8–10] Since 2000, low-modulus materials engineering and processing of composite elastomers using nanoparticles gave rise to the manufacturing of compliant functional sensing elements with tuneable properties. For example, Carbon Nanotube (CNT) composites, first discovered in 1991 and since then other carbon derivatives of various sizes (from nm to mm realms) have been used to tune electrical and mechanical properties of the polymer they are composited with depending on requirements. Research in capacitors, resistors, inductors, diodes, batteries, fuses, and transistors made from stretchable materials continued. By 2011, hybrid devices for signal filtering, analogue-to-digital conversion, microcontrollers, memory and wearable computing devices have been developed in labs around the world. [11,12] These innovations have created a whole new research field of multifunctional monolithic stretchable electronic circuits and fields of applications including thin-film memory, all-purpose strain-sensors, skin electronics and great progress in the field of wearable sensors in healthcare. [13,14]

1.2 - Silicone Sensors for Strain and Pressure

Conductive polymer-based composite sensors have been around since the late '90s and can convert large mechanical deformations (i.e. strain) into an electrical signal through changes in resistance and/or capacitance. Such enabling technology is extremely suitable for developing soft wearable devices for physiological monitoring. Silicone-based stretchable CPC strain sensors are particularly easy to fabricate (in standard laboratory environments) and consist of conductive particle fillers dispersed in a silicone polymer matrix to measure applied strain. The sensors can be moulded into the shapes desired using 3D-printed moulds or printed directly at room temperature via screen or stencil printing. [15,16] Among others, carbon black-filled polydimethylsiloxane (CB-PDMS) composites are widely used as strain sensors because of the long-term chemical and mechanical stability of silicones, tuneable mechanical and electrical properties of these composites, and their low cost. [17]

There are three methods to create a stretchable conductor regardless of the specific materials used. In a first case, one obtains elasticity by adjusted patterning of intrinsically stiff conductive materials. Rigid materials like metals (Au, Ag, Al, Ti and Mo) are most commonly used to create stretchable conductors. When thinned down they can become stretchable up to 1% strain in unidirectional stretching with constant resistance, then a linear response up to strains of 10-20% when cracks due to the Poisson effect of the substrate meet the transverse buckling of the deposited metal get large enough and the conductors fail electrically. Using special 2D and 3D geometries to mount these rigid materials on elastomeric substrates allows for mechanical reliability at higher strains. Buckled conductive strips can be prepared via metal evaporation on pre-stretched substrates (10-25%) which can allow for deformation up to 100% strain in some cases, although device-level stretchability is limited to around 12% by contacts with other rigid components. [18] A second approach makes use of intrinsically stretchable conductive polymers (e.g. polyaniline, poly(3,4-ethylenedioxythiophene) – poly(p-phenylene sulphide) as a comparison can be stretched up to 5% strain. [19] The advantage metals have, however, is their conductivity over composite (soft) conductors.

[20] Neither of these two classes of materials are stretchable enough for real world applications without a stretchable substrate. A third method disperses stiff conductive fillers in an elastomeric matrix in order to form a stretchable electrically conductive composite. This allows for larger strain values (above 300%) which presents the challenge of mounting less stretchable materials and component on such substrates. [21] A key determinant for stretchability is the adhesion between the metal or composite film with the substrate. When this is the case, strain does not localise around specific spots, instead the strain is distributed over the entire area of the conductive material. [22] A final approach is to create localised strain-isolated areas by having a more compliant elastomeric substrate around rigid areas where the rigid components are mounted and thus have the majority of the strain be transferred to the stretchable interconnecting areas. [23,24]

PDMS can be used as a substrate or encapsulant to support all three methods to create stretchable electronics. Wavy structures of metal can be deposited on a pre-strained silicone substrate and maintain a relatively stable conductivity although localised stress causes damage and degradation of conductivity upon cycling. This can be controlled by forming a periodic pattern of chemical bonding sites of the conductive material on PDMS. A common way to do this, which originated from the field of microfluidics, is plasma bonding. Exposure to oxygen (O_2) plasma through a protective mask selectively activates areas on the surface of PDMS. Oxygen converts the hydrophobic surface, which comprises mainly of methyl-functionalised silane groups (–$OSi(CH_3)_2O$–) into activated –$O_nSi(OH)_{4-n}$– groups. The silanol functional groups can form strong covalent bonds with a variety of materials including inorganic and other Si-containing species resulting in –O–Si–O– covalent bridges.

Inner-chain chemical modification of PDMS can partly tune the mechanical properties, including hardness, of the PDMS substrate which in turn modifies the mechanical properties, including sensitivity, of the conductive materials deposited on the surface. A straight-forward way of tuning the mechanical properties of Pt-cured PDMS is modifying the amount of curing agent (siloxane cross-linker) $(CH_3)_3Si[OSi(CH_3)_2]_nSi$

$(CH_3)_3$ added to the base siloxane oligomers. Localised stiff "island" structures which diffuse stress from surrounding areas created this way have been used to mount components that do not stretch (e.g. ICs).

Finally, silicone chemistry has extensively been explored to enhance self-healing properties. Although silicones are quite resistant to punctures, tears can lead to catastrophic failure when devices are repeatedly strained. [17] Amino, carboxyl, hydroxy, epoxy, and isocyanate terminated siloxane chains have been explored to prevent any subsequent fracture by allowing small cracks to heal. Manipulating both the sensing conductive composite as well as the substrate polymer at this level allows a high degree of tuneability in tensile properties (modulus, ultimate strength, maximum elongation) as well as in electrical and thermal properties (sensitivity, dielectric properties, thermal conductivity). In this way, conductive fillers that are difficult to disperse can be used with controllable alignment to increase the aforementioned sensing properties. Advanced circuit components are also enabled by this control over conductive, semiconductive and dielectric properties of stretchable composites, such as organic field effect transistors (OFETS). [25]

The interaction between conductive filler particles within the polymer matrix and between surfaces is important in determining the behaviour of the dispersed system. This means that the sensing parameters of the devices as well as the bulk mechanical properties of the composite polymer are determined by the type and dimensionality of the conductive fillers. [26] Control over mechanical properties such as stretchability, hardness, sensitivity and responsiveness is essential in personalised healthcare systems and commercial wearables. For instance, choosing CNTs over silver nanowires (AgNWs) can significantly enhance the stretchability of a CPC sensing element, but because the conductivity of CNT-composites is usually lower they are more widely used in voltage-controlled devices where high conductivity is not required such as sensing elements for strain and pressure sensors as well as capacitive touch screens. Metal-NWs, on the other hand, are more suited for current driven devices such as solar cells and light emitting diodes but they produce an overall more rigid device because of the

higher stiffness of their composites. Composite polymers with metal-oxide fillers are usually very sensitive as piezoresistive sensors, which means that a small change in strain can produce large resistance changes, and this is a desirable sensor feature. However, metal-oxide composites have very limited stretchability so they are not suitable for wearable applications where materials need to conform to the shape of and move freely with the body. Research on these composite materials and functional structures has produced insight into tuning sensor properties like stretchability and sensitivity. [27,28] For commercial applications, however, it is necessary to further integrate the materials acting as stretchable sensing elements into whole circuits and later to consumer device level.

1.3 - Whole-devices with Stretchable Sensors

When integrating stretchable components with conventional electronic components, whole-device considerations become important. They have to be addressed specifically taking into account the nature of the polymer matrix and conductive filler used to prepare the "active" CPC used as a sensor, as well as the material used to house the electronic components. These considerations extend to the inclusion of conventional, rigid components, the mechanical transition from soft components to rigid components, the integration of sub-circuit elements (such as power supply and logic ICs), the maturity and scalability of manufacturing techniques used, and the safety of the materials used.

Strategies to mount conventional electronics on stretchable substrates include locally reducing the elasticity around the component to prevent mechanical mismatch, or by mounting conventional components on rigid "isles" connected via stretchable traces. A mechanically simpler strategy is to combine stretchable components with stretchable interconnects. This is less frequently used because the development of stretchable counterparts of traditionally rigid components is still complex. [29,30]

There still is no industry standard method to mount rigid components onto stretchable surfaces. This is in part due to the complex or hybrid structures needed to create

stretchable electronic devices. Technologies to robustly interface soft and hard materials are essential for commercialization. Unreliable adhesion of the stretchable sensing element at the interface with (rigid but necessary) electronic components, such as wiring, integrated circuits, or other conventional devices is a key barrier than needs to be overcome.

Currently, the most common connection method relies on brittle conductive adhesives (AgEpoxy), although some commercial products use large solid mechanical connections, such as clamps and clasps, that are not suitable for miniaturized devices. Successful outcomes from these efforts have the potential to fundamentally change our conception of electronics, from hard, rigid, planar chips to soft, stretchable, curvilinear sheets. For this to happen, mechanical design is as important as electrical design in the formulation of new systems. The state of stretchable electronics at the moment is examined below. We will look into manufacturing techniques used and the steps towards having more of the sensing materials described above in the market. We present a simple, low-cost, scalable method of creating solderable contacts onto PDMS CPCs in Chapters two & three.

The largest market segment for conductive elastomers, since their invention, is electrostatic protection in the automotive and electronic device packaging industries has a valuation close to three times larger than the stretchable circuits market globally. [31] In the next sections, the relationship between silicon packaging development and stretchable electronic development is examined and how this is crucial to have stretchable sensors available outside of academic laboratories. In the next five Chapters, this thesis will address the interface between hard and soft electronic materials. In the final two Chapters, the need for soft stretchable devices in healthcare is explored, the need for stretchable sensors that interface with the human body established, and a solution that makes rehabilitation more effective via gamification is presented.

Some of the latest flexible sensor products that conform with the human body in the field of diagnostics and healthcare include MC10's BioStamp nPoint – a motion and surface electromyography (sEMG) sensor, Samsung's stretchable OLED display, and

Drynode by IDUN Technologies – a dry electrode for heart and brain monitoring. [32,33] These products use soft materials that are active either as light emitters, or sensors, but to date the strains achievable by commercially available devices are still low <10%. This is partly due to the lack of mechanically robust connections between soft and rigid electronic components. In the next section we look at materials and manufacturing strategies around high strain stretchable electronics.

1.3.1 - Integration methods of hard and soft electronics at scale

A process that is already mature in industrial scale manufacturing is screen printing of conductive filler-elastomer composites to create stretchable sensors. That said, most conductive or "active" filler-elastomer sensor components have not reached maturity and their material properties are still being studied. Even though most stretchable sensors at the moment have not left academic laboratories yet, there is a growing ecosystem of small and large companies focussed around their development. One path towards commercialisation involves the creation of stretchable sensing elements, followed by devices with limited stretchable configurations and discrete functionality, and eventually achieving highly functional, distributed systems. To date, non-stretchable components like clamps are used to connect stencil printed or other filler-elastomer sensors to build a device. Start-ups using sensors for strain and pressure measurements, where a CPC layer is embedded between two layers of a support substrate, have focused on upscaling the manufacturing processes and real-world reliability of their sensing elements while keeping the read-out electronics on a separate, rigid base communicating via pins or magnetic connectors (e.g. Tacterion[34], Stretchsense - technology developed by Parker-Hannifin Corporation[35], Flexosense[36] have mechanical connectors, and Heddokol[37] use magnetic connectors).

ICs and surface mounted electronic components (SMCs) used in all electronic devices today are soldered-on. A number of attempts have been made to create solderable CPCs which were not tested for durability. [38–44] The need for standardised testing was put forward as a foundation for future guidelines on reporting of the performance of

stretchable electronics including stretchability and sensitivity limits. [26,45,46] The reliability of adhesion at the point of contact with hard electronics and ICs and whole device (CPC and connected components) should certainly be included in these standards. There currently is no standard for connecting stretchable and non-stretchable electronics, and this is in part because silicon, a flat and rigid material, has been at the epicentre of electronics since the early days of this field.

It is important to mention that advances in stretchable devices have been aligned with the developments in silicon packaging technology, which albeit incremental, are significant. By incorporating these design and manufacturing strategies parasitic effects that reduce the performance and mechanical robustness of stretchable devices introduce promising new paths to commercialisation with much shorter time scales than typically required for technologies translated from academic research. As a first example, the commercial success of hinged displays in laptops and ultrathin cell phones with sliding parts has inspired the development of multi-layered flat flexible cables and circuit structures that can accommodate some degree of flexibility. A second example is the technology to produce micrometre thick silicon chips that allow for advanced thermal management and stacked device level integration of miniaturised form factors. Finally, the latest efforts are centred around materials research to evolve chips into form factors that accommodate strain and that blur the distinction between stretchable and rigid components.

The task of connecting stretchable sensors to rigid electronic components in discrete, distributed, or hybrid systems may still be challenging from an engineering viewpoint because although the materials and mechanics strategies described above are promising there are engineering challenges that still need to be overcome. For instance, if we focus on the task of connecting a silicon device on a PDMS-composite sensor we are presented with extreme mechanical mismatches. The modulus of silicon is about 10^6 times as high as a typical substrate elastomer (Si: 130 GPa, PDMS: 2 MPa); the thermal conductivity is 1000 times as high (Si: 1.3 W cm^{-1} $°C^{-1}$, PDMS: 0.15 W m^{-1} $°C^{-1}$) , and the thermal expansion coefficient is 100 times as small (Si: $2.6 \cdot 10^{-6}$ $°C^{-1}$, PDMS: 9.6×10^{-4} $°C^{-1}$). [47–

[49] As an example, research on nonlinear behaviour in hard and soft laminates is providing new insights into the mechanics of their deformation, particularly their nonlinear behaviour in buckling modes, with explicit relevance to stretchable electronics. Expensive materials like CNTs and nanoparticle composites can yield materials better matching the desired mechanical properties but they cannot easily be manufactured using mass processes. In terms of scalability and real-life applicability, lower cost, industry friendly materials like CB may be enough. From an engineering standpoint, we investigate extensively the mechanical stability of solderable contacts on PDMS-based stretchable sensor devices in Chapter four.

1.3.2 - Compliant Strain Sensors in Healthcare and beyond

Some of the most compelling applications for stretchable sensors are in biomedical devices that address important problems in human health diagnostics, treatment, and rehabilitation. Stretchable sensors made of elastic materials with curvilinear layouts can provide both mechanical modulus and shape matching to biological tissues. Such devices, when implemented reliably and matched with the right application for their properties, will rapidly expand into fully distributed, multifunctional devices for clinical use.

In Chapters six & seven, we analyse the potential that wearable technologies have for healthcare, especially when combined with rapidly developing digital technologies both hardware (portable computers) and software (user interface and digital feedback). Beyond biology, stretchable sensors can be used in conjunction with conformal antennas and other components for communications, perhaps even in smartphones of the future. [50,51]

This thesis addresses the knowledge gap in connecting hard electronics, necessary for useable devices, and soft silicone based sensors with applications in improving the useability, comfort, and gamification of healthcare applications, including rehabilitation and therapeutics, of mechanical and strain sensors. These and related opportunities for engineering in areas of application with important societal implications, taken together

with the broad range of interesting scientific topics, provide strong motivation for continued and expanded efforts in this emerging field.

PART II

Copper-Silicon Contacts for Soft Silicone Strain Sensors

Chapter 2

Preparation and Characterisation of Silicone-CB composites

In this chapter we characterise two Conductive Silicone Composites based on PDMS and CB – the first custom-made (CB-PDMS) and the second industry-made (CB-CSC). Initially, we explore structural and design parameters that affect the behaviour of the composite as a strain sensor by developing a custom manufacturing protocol in-house. In later chapters, we use an industrially manufactured composite and further investigate electromechanical device properties to demonstrate scalability of our technology. Silicone is a primary candidate for wearable sensors because it is chemically stable, compatible for cutaneous and sub-cutaneous applications, mechanically robust, and has scalable, low-cost manufacturing pipelines. [52,53] Among numerous carbon fillers and manufacturing strategies we kept focus on the commercial viability of the material. In initial experiments, we found that Multi-walled carbon nanotubes (MWCNTs) required longer and more power intensive mixing and sonication cycles manufacturing processes (although mechanically they prevented stiffening of the base silicone). Ground carbon fibre (GCF) produced composites of acceptable conductivity levels at low loadings but disrupted the mechanical integrity of the silicone due to their dimensions (length = 100 μm, EasyComposites) which reduced overall stretchability of the sensing element. We used custom-made CB-PDMS using stencil printing, then tested commercially available Carbon-Black filled Conductive Silicone Composite (CB-CSC) to demonstrate the feasibility of scaling up our novel contact technology.

2.1 - Preparation & Characterisation of CB-PDMS Composite

In this section, we present the preparation of custom-made CB-PDMS and a simple and rapid micropatterning stencil printing protocol. A suspension of powdered CB is

mixed with 50-nm average particle size (Vulcan XC 72 made by Cabot Corporation) with PDMS (Sylgard 184 by Corning Inc.) in a five step process modified from works previously reported in literature [54–56]: i) We suspended CB in hexane in a 1:10 (w/w) ratio and sonicated at 220 W for 10 min. ii) We dissolved base elastomer in hexane in a 1:2 (w/w) ratio in a different container. iii) We mixed the CB suspension with the base-solution (from step ii) to produce 5, 8, 10, 12, 15, and 20% (w/w) CB-PDMS precursor. iv) We then dried the dispersions in air overnight to remove the solvent – i.e. hexane. v) And added the cross-linker to form the CB-PDMS composite pre-polymer.

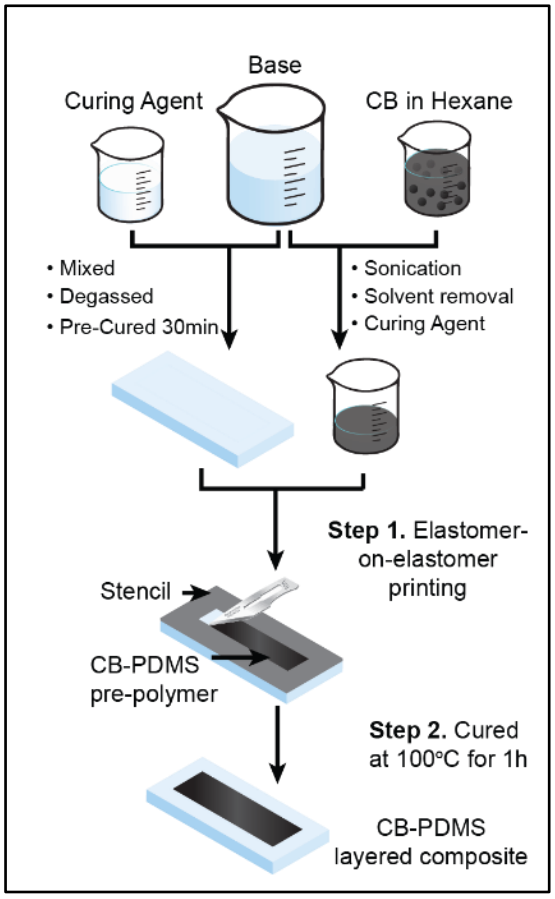


Figure 2 Preparation of CB-PDMS Schematic representation of the stretchable CB-PDMS layered composite protocol.

With this dispersion we prepared composites with concentrations between 5 and 20% w/w CB in PDMS-base by mechanical stirring, followed by ultra-sonication using a Pro Scientific VCX sonicator, and solvent evaporation (Figure 2). We mixed the CB-

PDMS-base with the curing agent and deposited a 0.1 mm conductive layer on a carrier PDMS layer through elastomer-on-elastomer printing using a stencil mask.

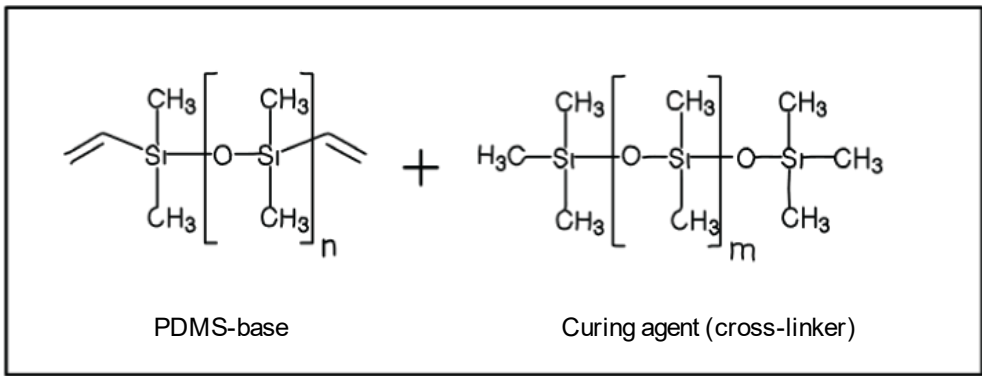


Figure 3 PDMS pre-polymer components Oligomer parts of Pt-cured PDMS with base (left) and curing agent (right).

The PDMS substrate was prepared by mixing degassed base elastomer and cross-linker in a 10:1 ratio (w/w) (Figure 3). We casted on a mould treated with Ambersil PTFE mould-release and pre-cured at 100 °C for 30 min. As a result, a PDMS carrier substrate with a thickness of 3/6/9 mm was obtained and cut into strips of 10×30 mm^2 using a scalpel.

The liquid (uncured) CB-PDMS composite and PDMS substrates were then co-cured in a conventional oven at 100 ℃ for 1 h (Figure 4).[57]

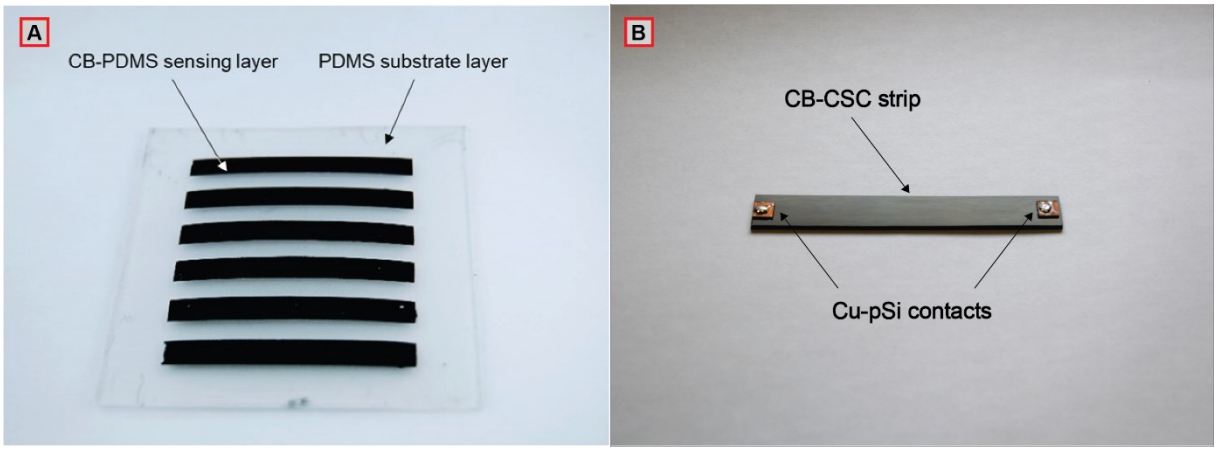


Figure 4 CB-PDMS Batch & CB-CSC sample (A) Picture of a batch of stencil-printed CB-PDMS sensing elements (5 mm x 60 mm) on PDMS substrate 3 mm thickness, (B) Picture of 1 mm thick

commercially available Carbon-Black filled Conductive Silicone Composite strip sample (12 mm x 110 mm) with solder-on Cu-pSi contacts attached

The electrical resistance of CPCs is determined by the number of connections between conductive fillers within the polymer matrix, which in turn is determined by their volume fraction in relation to the percolation threshold. The percolation threshold is reached when the various junctions created between filler particles for current to pass along the material abruptly cause the resistance to drop. This happens when the volume fraction of conductive fillers (Φ) reaches the critical volume concentration for the percolation threshold (Φ_c, Figure 5). The network of junctions between filler particles can either be physical contacts with no contact resistance or near contacts whose resistance decreases with inter-filler distance. [58] We measured the electrical resistance of unstrained CB-PDMS layer using a commercially available UT171 (Uni-Trend Technology Co., Ltd) multimeter (current measurement with 5 V applied voltage) and flat alligator clips, with a CB concentration range between 5 – 20% (w/w) of PDMS (Figure 5). The electrical resistance of CB-PDMS decreased rapidly with increasing concentration of CB particles from 9.5±1.5 MΩ for 5% to 4.1±0.3 kΩ for 20% CB due to formation of conductive percolative networks within the polymer matrix, reaching values around 200 kΩ for 12% CB.[59]

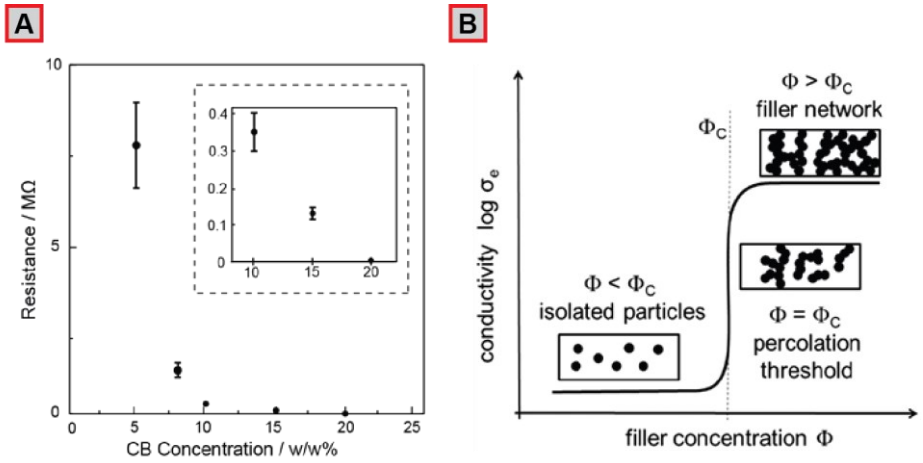


Figure 5 Percolation Threshold (A) Resistance vs. CB concentration for the CB-PDMS conductive polymer composite (n=7), (B) Percolation curve schematic for conductive fillers in an insulating matrix showing the volume fractions Φ, Φc where percolation networks form [60]

2.2 - Characterisation of commercially available CB-CSC

In this section, we present and discuss the electrical properties and selection criteria for the commercially available Carbon-Black Conductive Silicone Composite (CB-CSC) sensing element used in later chapters based on thickness and sensitivity to pressure. A commercially available sensing element is used to demonstrate the scalability of the technology developed in this thesis.

CB-CSC sheets with thicknesses of 0.5, 1.0, 1.5, and 3.0 mm (± 5%) sourced from J-Flex (Retford, Nottinghamshire, UK), were compared in terms of conductivity measured solely on the surface and conductivity measured throughout the bulk using single side and double side two-probe measurements. In Figure 6A, we see I-V scans of CB-CSC sheets of equal area and four different thicknesses. Dotted lines represent measurements taken solely from the surface of the material, and solid lines represent measurements taken by having the clamp make contact with both the top and bottom surfaces of the material. We investigated the relationship between thickness and resistivity because our contacts are surface mounted and found that the difference between single surface and double surface (bulk) conductivity increases at a decreasing rate (Figure 6B). This indicates that the bulk of the material contributes to its conductivity but at a decreasing rate beyond 1.5 mm. More testing is required to confirm this effect which may be negligible as Figure 6C shows that both bulk and surface resistances closely agree with the theoretical value for a conductive material. Figure 6C compares the theoretical variation of the Resistance of the materials according to $R{=}\varrho L/A$, where ϱ is the resistivity of the material, in this case 45.3 Ω·cm (datasheet available on J-Flex.com – "Electrically Conductive Silicone Sheet"), L is the length of the test sample, and A the cross-sectional area.

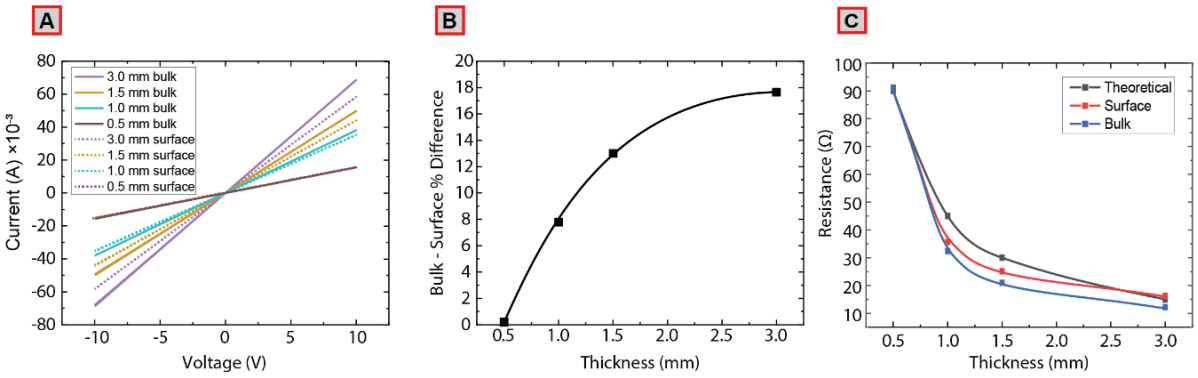


Figure 6 CB-CSC thickness *vs* DC Resistance (A) IV diagrams for all J-Flex CB-CSCs for measurements taken with both sides of the material clamped (bulk) and only one side clamped (surface) (B) Percentage difference between the bulk and surface resistance values for CB-CSCs of the same area but increasing thickness (C) Comparison between the theoretical resistance values for the CB-CSC in question *vs* the measured bulk and surface values (n=3).

To select the appropriate thickness we compared the CB-CSCs in terms of their electromechanical sensitivity. When the conductive composite is pressed, a decrease in cross-sectional area and conversely an increase in length take place according to the material's Poisson ratio ($v = \Delta\varepsilon_{longitudinal} / \Delta\varepsilon_{compressive}$). Figure 7 shows that when 12×110 mm^2 strips were tested using a custom built 50 mm compression plate in 50 and 300 N compression experiments, 1.0 mm thick samples showed the highest response.

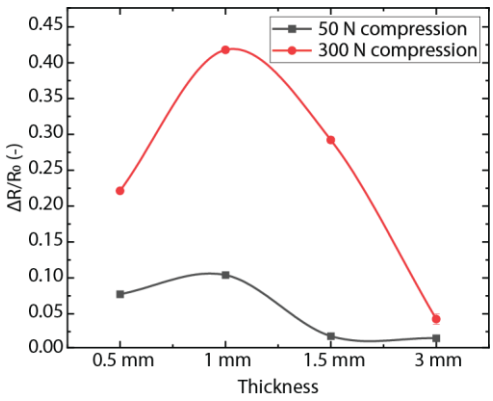


Figure 7 Sensitivity *vs* Thickness of CB-CSC (n = 6 for each thickness)

The resistance of the bare CB-CSC strips was measured using a constant voltage of 5 V using a Keithley 2450 Interactive SourceMeter® connected directly. This device will

be used as a power supply and measurement device for all subsequent DC experiments. All tensile experiments were performed on a MultiTest 2.5-i 1000 N Mecmesin compression tester and Mecmesin force and Torque Test Software (Mecmesin Ltd., Slinfold, West Sussex, England).

2.3 - The need for robust contacts on silicone composite sensors

Works reported to date have optimized the sensing properties (sensitivity, modulus, maximum operational strain, thermal properties, etc.) and the manufacturing of stretchable CB-PDMS sensing elements, however, reliable adhesion of the stretchable sensing element with electronic components, such as wiring, integrated circuits, or other conventional devices, still remains a problem. [61–63] Currently, the electrical connection between CB-PDMS sensors and external electronics primarily relies on brittle conductive adhesives, although some commercial products use large solid mechanical connections, such as clamps and clasps, that are not suitable for miniaturized devices. [64] Silver-based conductive epoxy (AgEpoxy) is, by far, the most widely used adhesive to create electrical contacts between CB-CSC sensing elements and electrical read-out devices. [65–72] Even though AgEpoxy is an excellent electrical conductor ($<10^{-4}$ Ω·cm), it is susceptible to cracking and debonding from the silicone-based stretchable strain sensors and usually the first interface to fail under rates of strain higher than 10 mm/min (120 mm/min is physiologically relevant). [73] This is due to the brittle nature of the adhesive and poor wetting of silicones by AgEpoxy. Silicones bond weakly with most adhesives due to their lower surface energy (the surface energy of epoxy is 40-50 mJ/m^2, while silicones have a range between 19-25 mJ/m^2). Hence, a reliable method is needed for bonding electronic components with silicones. [74]

To overcome the limitations of AgEpoxy, several groups explored vacuum deposition of metallic structures on silicone elastomers and subsequent soldering of wiring and components to achieve bonding. [75–77] Vacuum deposition of metals on silicones, however, requires complex processes that generally involve patterning through photolithography, deposition of additional adhesion enhancement layers and liquid-phase transfer of films. Despite the complex fabrication methodologies, such metallic

contacts are still susceptible to delamination and failure, especially in applications (such as physiological monitoring) where they may experience high levels of applied stress (>1 MPa) and high rates of strain (>2 mm/s). [78,79]

In the next Chapter, we present a method for creating solderable, mechanically robust, electrical contacts to interface (soft) CB-PDMS strain sensors with conventional solid-state (hard) electronics using a nanoporous Si-Cu composite. The Si-based solder-on electrical contact consists of a copper-plated nanoporous Si top surface formed through metal-assisted chemical etching (MACE) and electroplating, and a smooth Si bottom surface which can be covalently bonded on CB-CSCs through one-step plasma bonding. In Chapters four & five, we investigate the mechanical and electrical properties of the contacts proposed under relevant ranges of mechanical stress for applications in physiological monitoring and rehabilitation.

Chapter 3

Fabrication and Characterisation of Copper-Silicon Contacts

PDMS does not adhere well to non-silicon-based substrates, due to low surface energy, even after special treatment and so there are still few, sophisticated, and complex ways to connect wires, microcontrollers and other connections made on the surface of silicone composites. Wu *et al.* have reported bonded silicone to various materials including metals like copper using silane derivatives but this method is costly and requires a lot of optimisation, even in a controlled lab environment. [80] We use plasma bonding to bond our nanoporous Si chip to the surface of our PDMS-based sensing element. In this chapter we compare the tensile performance of plasma bonded Si on PDMS against widely used conductive silver epoxy adhesive (AgEpoxy) and PDMS.

3.1 - PDMS Surface Chemistry after Plasma bonding

PDMS can be cast in any shape and size and the surface of this elastomer can be prepared to be very smooth with nanometre features. [81,82] As-prepared surfaces have contact angles near 100° and this has been addressed in the field of microfluidics by surface chemistry modification techniques such as chemical vapour deposition (CVD), sol-gel and other coatings. A simple, single step way to produce hydrophilic PDMS is UV or O_2 plasma irradiation. [83] Figure 8 shows the decrease in contact angle after plasma treatment as evidence of increased hydrophilicity on a Si wafer which is chemically similar to PDMS (see Figure 9).

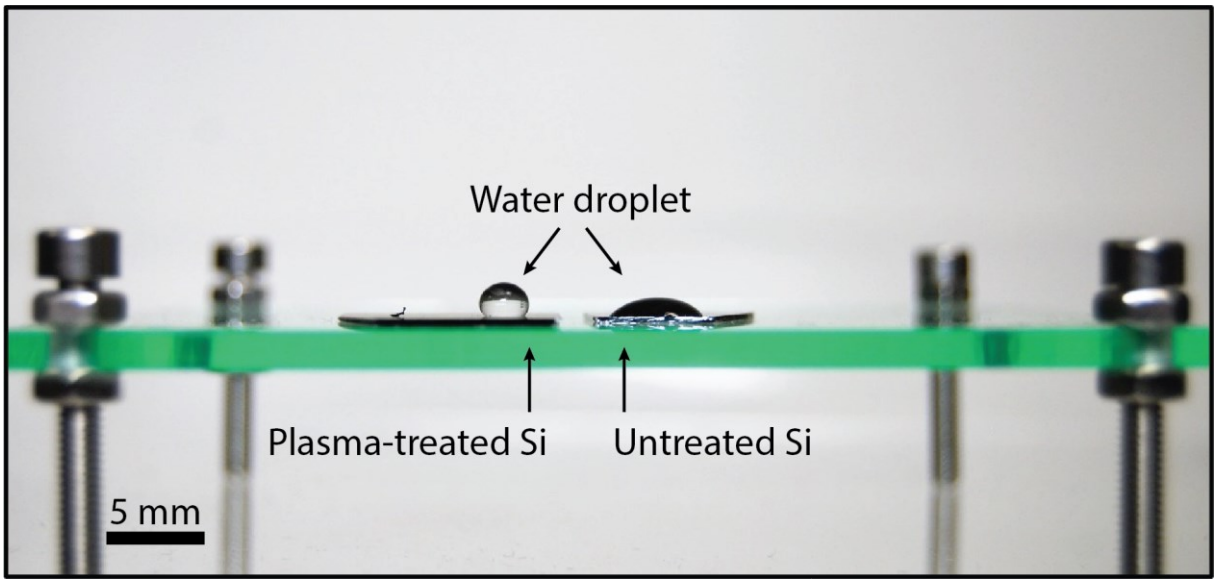


Figure 8 Visual contact angle of plasma-treated Si Visual difference in water contact angles between as-received polished Si wafer (left) and plasma treated Si wafer (right).

Oxygen plasma treatment functionalises the PDMS surface by oxidation to generate a silica surface which is further reacted after conformal contact with the Si wafer surface (Figure 9). We treated the polished side (as-received) of the Cu-pSi contact and CB-PDMS with O_2 plasma for 35 s which forms SiO_x species on their respective surfaces and when in contact, the materials irreversibly bond together through a condensation reaction. [84] After plasma treatment we standardised the duration and force applied on the annealing interfaces by pressing the Cu-pSi and conductive silicone together overnight using plastic clamps (Tooltime UK Ltd, East Kilbride, Lanarkshire, UK).

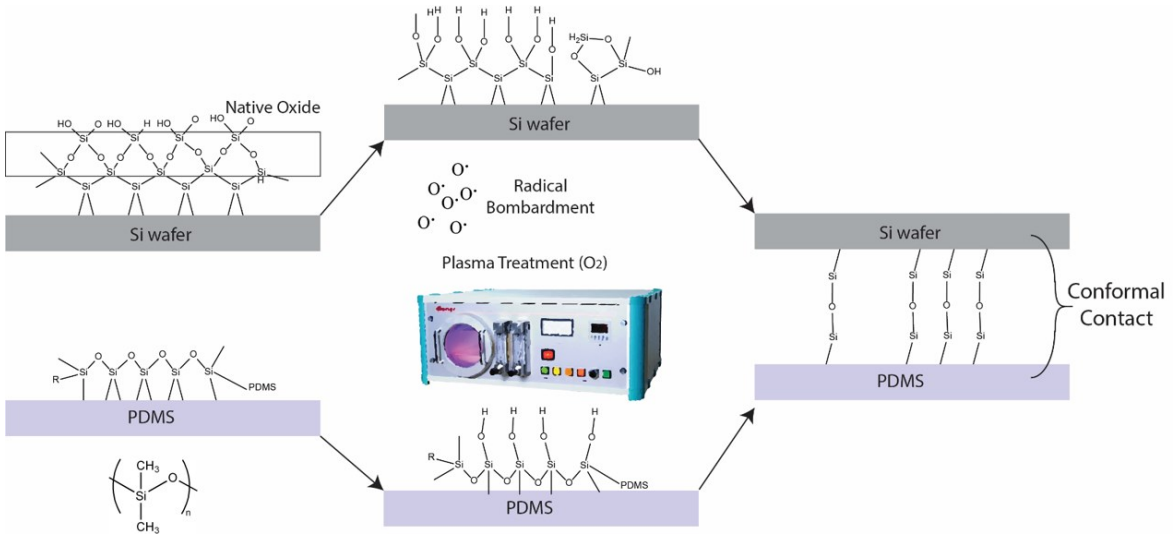


Figure 9 Schematic of the plasma bonding Schematic presents the condensation reaction between a Si surface (Si wafer) and a silicone surface (PDMS) after coming into conformal contact.

Chemisorption and covalent bonding are involved in the Si-PDMS bond as opposed to AgEpoxy-PDMS physisorption adhesion. [85] Further mechanical studies of the Si-PDMS detachment system would also shed light on the role of covalent bonding *vs.* cross-linking in silicone-on-silicone "monolithic" systems, and simple physisorption of epoxy adhesives. In this Chapter, we explore the macroscopic mechanical adhesion strength between the Cu-pSi surface and the CB-PDMS multi-layered structure.

Because plasma treatment modifies the mechanical properties of PDMS (increased brittleness – Table 3.1-1), a physical mask was used to limit areas of exposure to plasma, only at the sites of bonding. All samples tested were plasma treated at the contact bonding sites for equivalence as it is a common industrial method to improve bonding. [86]

Table 3.1-1 Stress & strain values for plasma-treated and pristine PDMS (n=5, standard deviation is reported).

Material	Max Stress (MPa)	Max Strain (mm/mm)	Young's Modulus hyperelastic region (MPa)	Young's Modulus (MPa)
Plasma-treated PDMS	1.0 ± 0.1	0.8 ± 0.1	0.6 ± 0.3	1.3 ± 0.6
Pristine PDMS	1.4 ± 0.2	1.0 ± 0.2	0.8 ± 0.2	1.5 ± 0.6

3.2 - Preparation of Cu-pSi contacts

3.2.1 - Silicon etching overview

Metal Assisted Chemical Etching (MACE) of Silicon, based on ongoing research works as follows: Ag catalyst particles are deposited on the Si surface through a substitution reaction between $AgNO_3$ and HF (Equation 1 found below). The particle size of Ag

particle layer can be controlled with the concentration of $AgNO_3$. Under the conditions used in our method, the size and distribution of Ag particles were visible from top view SEM images. Although the shape and size distribution can be optimized by thermal annealing, we used the as-deposited Ag layer. [87] After Ag deposition, in an etching solution of H_2O_2 and HF, 1) H_2O_2 is catalytically reduced at the surface of the noble metal (Equation 2); 2) Holes (h^+) are injected from Ag into Si at the Si/Ag interface; 3) This oxidises Si which etches by HF to form soluble silicon hexafluoride (Equation 3); 4) Both the direct dissolution of Si accompanied by H_2 evolution as well as the formation of SiO_2 on the metal-Si interface before Si dissolves (Equations 4a, 4b) have been proposed. We observe an array of colours (Figure 10) on the surface of the Si/SiO_2 wafer before any observable H_2 gas was visible in our own experiments; 5) The concentration of holes has its maximum at the Si/Ag interface. Therefore, the Si that is in contact with the metal is etched much faster at the interface; 6) The progression of the etching reaction and hole diffusion from Si under the Ag, to off-metal areas or to the wall of the pore are matters of extensive investigation.

$$4Ag^+ + 6HF \rightarrow {SiF_6}^{2-} + Ag + 6H^+ \quad (1)$$

Reduction reaction (Ag catalyst/solution interface)

$$H_2O_2 + 2H^+ \xrightarrow{Ag} 2H_2O + 2H^+ \rightarrow H_2 \uparrow + 2h^+ \quad (2)$$

Oxidation reactions (Catalyst/Silicon interface)

$$Si + 6HF + 2h^+ \rightarrow H_2SiF_6 + 2H^+ + H_2 \uparrow \quad (3)$$

$$Si + 2H_2O \rightarrow SiO_2 + 4H^+ + 4e^- \quad (4a)$$

$$SiO_2 + 6HF \rightarrow H_2SiF_6 + 2H_2O \quad (4b)$$

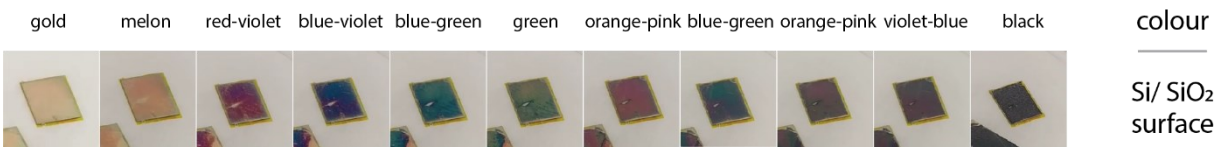


Figure 10 MACE colour change Colour change on the surface of Ag electroless plated Si upon addition of HF + H_2O_2 etchant, t=2 s after addition (far left), pictures taken every 5 s for approx. 1 min (far right). See Section 3.2.1 for details on the MACE process

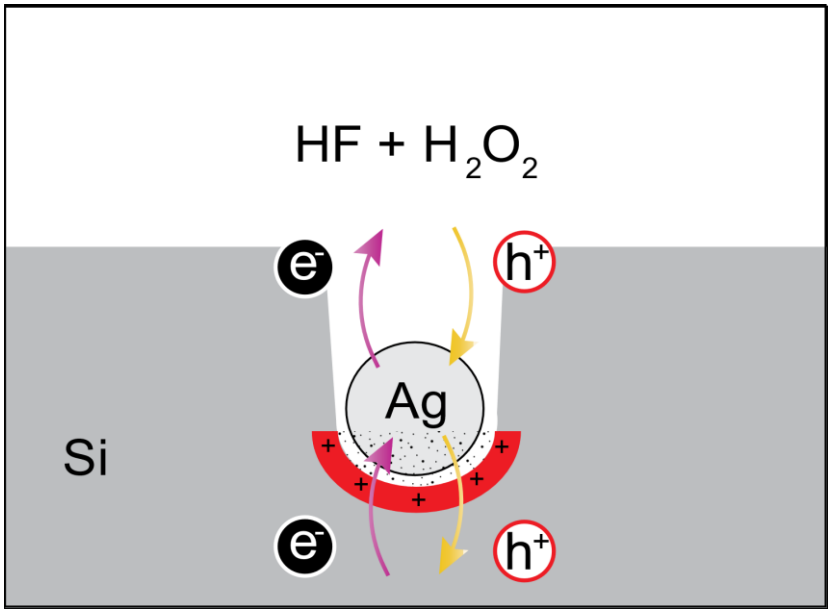


Figure 11 Metal Assisted Chemical Etching at the Si/Ag/Aqueous interface

Both anisotropic and conical shaped pores can be created and Si parameters such as doping type and level, crystal plane orientation, HF to oxidising species (H_2O_2) concentration, catalyst species, and etching duration all affect the size, orientation, and shape of the pores. [88] Briefly, etching direction initially depends on the orientation of the Si substrate, but at high (>20%) [HF]/[HF]+[H_2O_2] ratios etching becomes anisotropic (perpendicular to the surface). [89] The direction of etching is controlled by the number of holes injected by the oxidant and the rate of removal of SiO_2 by HF oxidation. When [H_2O_2] is low most atoms would get etched from the surface {100}, but when [H_2O_2] and [HF] increase Si atoms would get removed quickly given many holes would get produced allowing increased etching in the bulk {110} and {111} planes. In general, the etching rates of n-type Si is faster than p-type Si, however, we optimise etching time based on how well our Cu layer adheres onto the porous surface. [90] We have adapted the practices found in literature and present our methodology below (Sections 3.2.2 and 3.2.3). [91–97]

3.2.2 - Metal Assisted Chemical Etching of Silicon (Cu-pSi)

Etched Si contacts were manufactured in-house using 100 mm Si wafers (*heavily doped n-type*: Siegert Wafer, 525 ± 25 µm thickness, <0.005 Ω·cm, *heavily doped p-type*: Pi-Kem, 525 ± 50 µm thickness, 0.001 - 0.005 Ω·cm, *lightly doped n-type*: Pi-Kem, 525 ± 50 µm thickness, 1-10 Ω·cm, *lightly doped p-type*: Pi-Kem, 525 ± 50 µm thickness, 1-10 Ω·cm). In this section, we will present the protocol developed to prepare solder-on Si contacts regardless of Si wafer dopant and doping level. In the next chapter, Chapter four, the mechanical robustness of Cu-pSi contacts will be demonstrated by comparing devices using p-type Cu-pSi with devices using AgEpoxy adhesive contacts. Then, in Chapter five, the best Si type based on electrical characterisation for our application will be chosen.

To begin the preparation, the top surface of a pristine silicon wafer was cleaned, electroless plated with Ag particles and placed in an etching solution (containing H_2O_2 and HF) to create a nanoporous Si surface through MACE. [98,99] The surface resulting from etching consisted of 50-300 nm wide pores with a depth of ≈ 2.4 µm (*highly doped*

p-type Si shown in Figure 12A). [98,100,101] The multi-layered device, including the CB-PDMS sensing element and Cu-pSi solder-on contact are shown in Figure 12B.

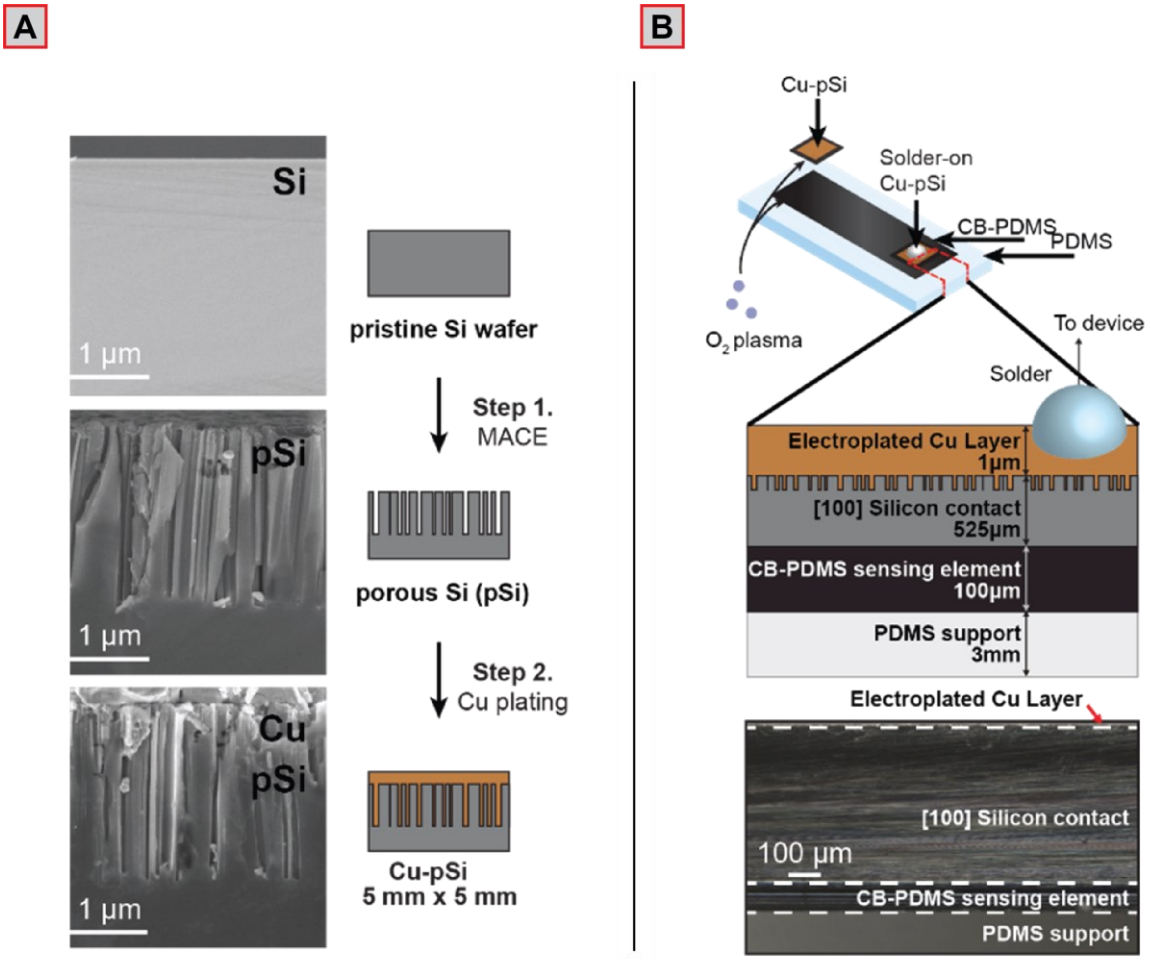


Figure 12 Cu-pSi preparation and assembly (A) Cross-sectional SEM images taken during MACE and Cu electroplating on p-type Si (100) wafer. (A) Schematic illustration of (top) and cross-sectional optical micrograph (bottom) of Cu-pSi contacts after plasma bonding on the CB-PDMS sensing element.

All Si wafers were initially cleaned with acetone, rinsed with distilled water, and then immersed in a 3:1 piranha solution (95% H_2SO_4/30% H_2O_2 v/ v) at 80 °C to remove organic residues. After drying in air the polished side of each wafer was protected from chemical attack with adhesive polyimide tape. *Lightly doped p-type and n-type* wafers were immersed in a bath of 2.9 mM $AgNO_3$ for 2 min for electroless plating to take place. The etching solution was made up of 2.7 M HF with 0.2 M H_2O_2 for 7 min to form nanoporous silicon (pSi) on the surface of the protected wafers. The electroless plating solution for *heavily doped n-type* Si contained 7.25 µM Ag^+ for 30 s deposition,

and the *heavily doped p-type* Si additionally required a modified etching solution with 2.2 M HF and 0.25 M H_2O_2 for 10 min.

3.2.3 - Electroplating nanoporous Silicon with Copper (Cu-pSi)

Following etching, the wafers were treated with 10% HNO_3 to remove all Ag from the surface. Right before electroplating with Cu, each wafer was cleaned one last time with 5% HF to remove the native oxide from the surface of Si and produce an electrically conductive surface. The wafers were plated with Cu in a bath containing an aqueous solution of 0.8 M $CuSO_4$ (and 1ml ethanol) using a Pt-wire as anode. Plating of *highly-doped p-type* wafers was performed with a current density of 0.2 mA cm^{-1} for 15 min to produce a film of Cu approximately 1 µm. All other wafers were electroplated in 0.08 M $CuSO_4$ (and 1 ml of ethanol), at a current density of 40 µA cm^{-1} for 1 h or until a uniform shiny Cu surface formed.

The nanoporous surface was then electroplated in a 0.8 M $CuSO_4$ aqueous bath *vs.* a Pt wire, to create a ≈ 1 µm Cu film on the nanoporous Si (Cu-pSi) surface that can be soldered to external wiring and components. Elemental analysis by energy dispersive X-ray spectroscopy (EDX) and close-up electron micrographs show a clear separation between the Si and Cu surfaces for unetched Si. For pSi, however, the Cu layer extends inside the porous surface with decreasing amounts with increasing depth, likely due to limitations in mass transfer during electrodeposition (Figure 13). This limitation

could be overcome through further optimization of the process parameters or using other electroplating regimens such as pulsed electrodeposition. [102]

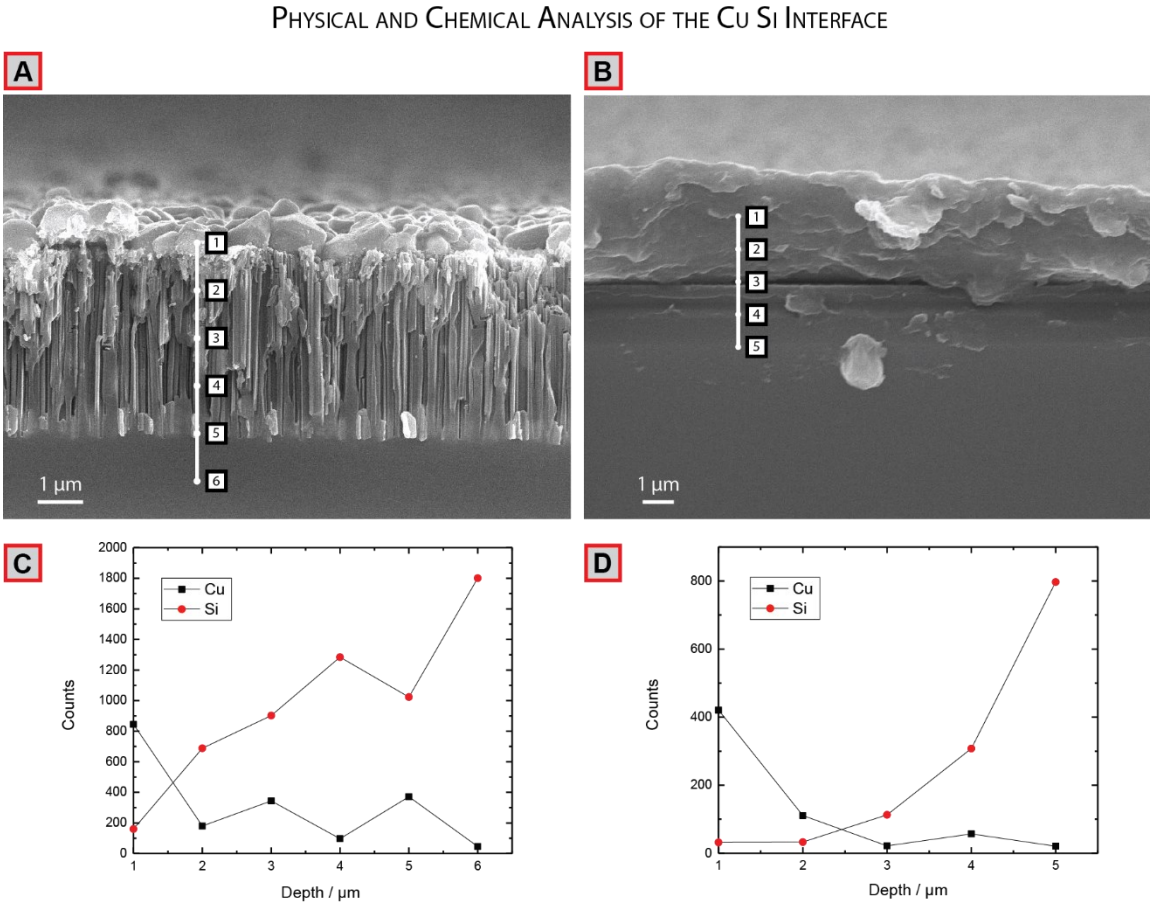
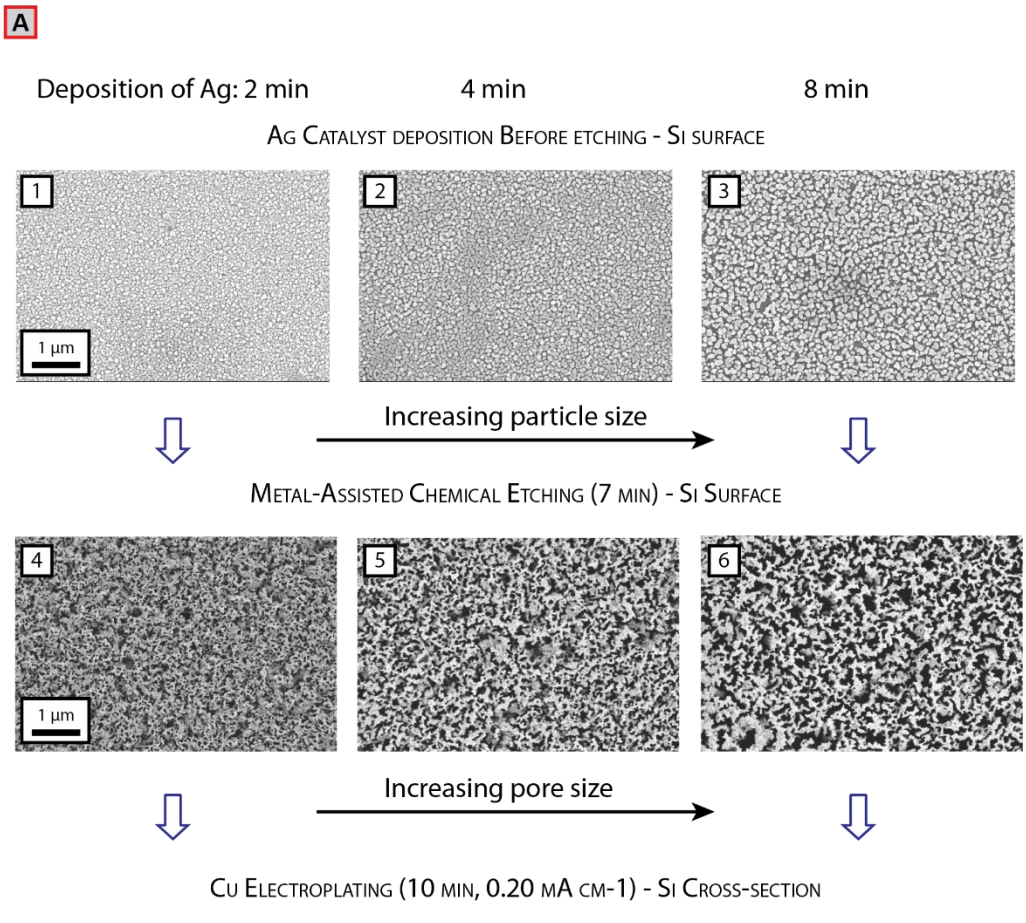
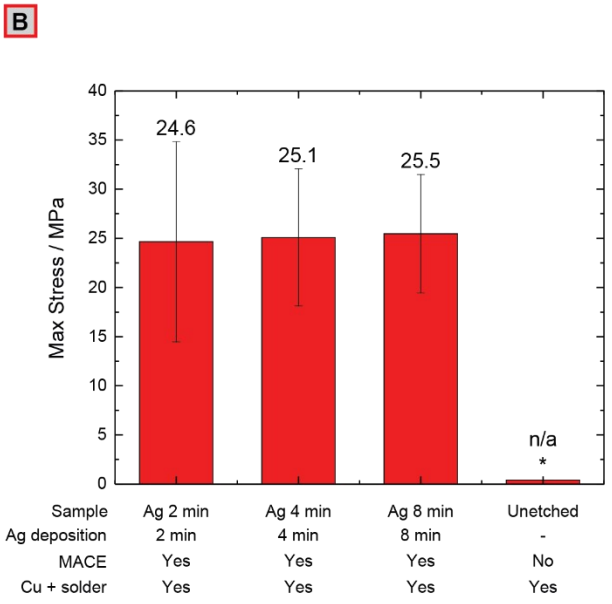


Figure 13 Physical and Chemical Analysis at the Cu Si Interface (A) Electron micrograph of Cu-pSi interface (Ag deposition time of 2 min). The numbers indicate the location of each spectra acquired by EDX analysis (note that each measurement is 1 µm apart); (B) Electron micrograph of unetched Cu-Si interface. The numbers indicate the location of each spectra acquired by EDX analysis (note that each measurement is 1 µm apart); (C) EDX spectra for Cu and Si taken from the cross-section of electroplated pSi shown in (A); (D) EDX spectra for Cu and Si from the cross-section of electroplated unetched Si shown in (B); Intensity values for Cu and Si were calculated using the peaks at 0.79 keV for Cu and at 1.74 keV for Si.

The nanostructured pSi surface plays the important role of improving the adhesion of the Cu layer without any additional adhesion enhancement layers on the Si surface, by increasing the surface area and morphological complexity to create interlocking structures. We performed tensile testing by soldering a 4 mm thick multicore Cu wire on the electroplated Cu layer on the surfaces of unetched Si and nanoporous Si with

varying pore sizes. We did not observe a difference on adhesion strength of the Cu layer on pSi when we increased the pore size since in each experiment the Si substrate failed before the Cu film could detach from the surface. The unetched Si surface electroplated with Cu, however, delaminated during handling, hence we were not able to perform tensile testing for these samples (see Figure 14 below for more information).


A
Deposition of Ag: 2 min
4 min
8 min
Ag Catalyst deposition Before etching - Si surface
1
2
3
1 µm
Increasing particle size
Metal-Assisted Chemical Etching (7 min) - Si Surface
4
5
6
1 µm
Increasing pore size
Cu Electroplating (10 min, 0.20 mA cm-1) - Si Cross-section
7
8
9
1 µm


B
Max Stress / MPa
40
35
30
25
20
15
10
5
0
24.6
25.1
25.5
n/a
*
Sample
Ag deposition
MACE
Cu + solder
Ag 2 min
2 min
Yes
Yes
Ag 4 min
4 min
Yes
Yes
Ag 8 min
8 min
Yes
Yes
Unetched
-
No
Yes

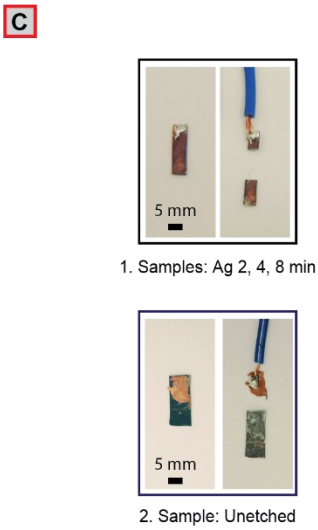

C
5 mm
1. Samples: Ag 2, 4, 8 min
5 mm
2. Sample: Unetched

Figure 14 Si surface SEM during MACE (A1-A3) Electron micrographs of the surface of Si wafers after depositing Ag catalyst (deposition times: 2 min, 4 min, 8 min for A1, A2, A3 equivalently) with increasing particle size; (A4-A6) Electron micrographs of the surface of pSi with increasing Ag catalyst size after etching which produced a Si surface with larger pores; (A7-A9) Electron micrographs of pSi with varying pore sizes after Cu electroplating showing the interface of Cu and pSi. The Cu layer was not deposited with an even thickness throughout the cross-section of the pSi, likely due to the limitation in mass transfer during electroplating; (B) Max. stress values for Cu-pSi samples pulled to failure after a 4 mm thick multicore copper wire is soldered on the electroplated surface of pSi samples of varying pore sizes and flat, unetched Si. (C1-C2) Representative photographs of the samples tested in B showing the wafer before soldering the 4 mm multicore Cu wire (C1-left) and the wafer breaking before the soldered connection (C1-right) and showing the unetched Si wafer just after Cu electroplating (C2-left) and showing the Cu film detaching from the surface of unetched Si during soldering (C2-right). * Max Stress = n/a, unable to perform test; Cu film delaminated during soldering and handling.

Electroplated wafers were diced using a fibre laser (Speedy 100 fiber 20 W, Trotec) to produce 5×5 mm^2 Cu-pSi contacts (Figure 15) and the unmodified side of each piece (smooth, non-plated, non-porous side of the starting Si wafer) was plasma bonded to the CB-PDMS (Figure 15 - Step 5) as described in Chapter two. A summary of the Cu-pSi contact attachment is presented in Figure 15. MACE creates a nanostructured rough surface on one side of a whole 10×10 cm^2 Si wafer. The wafer is inserted in a custom-made holder

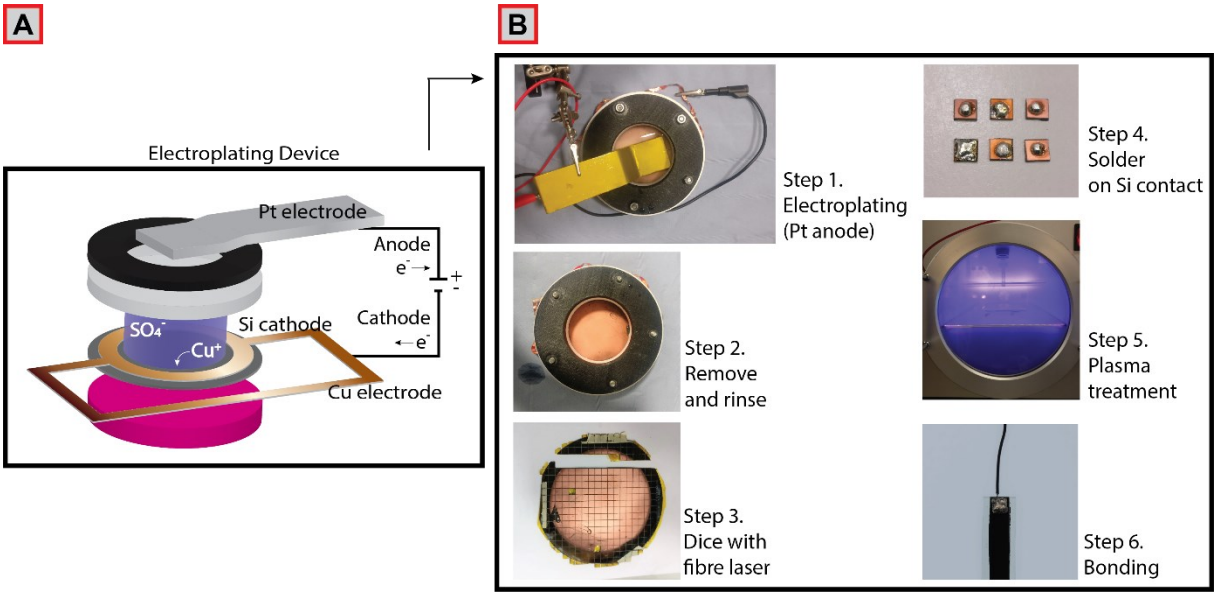


Figure 15 Cu plating and plasma bonding method (A) Graphic of custom built electroplating Si wafer holder also visible in Step 1 and 2 – the pink and white layers form a reservoir for $CuSO_4$ electrolyte to come into contact with the etched and activated Si wafer, the black layer applies pressure to the layers below to prevent leakages; (B) Step-by-step Cu-pSi contact preparation after etching showing whole wafer to individual 5×5 cm^2 contacts to bonding onto a CB-PDMS sensing element.

3.3 - Future Development

The Cu-pSi contact technology has the following three disadvantages which can be addressed in future iterations: i) For the moment, Cu-pSi can only be covalently bonded to silicone-based CPCs, therefore more research is needed for using this solution for other elastomeric materials. ii) Formation of nanoporous Si using metal-assisted chemical etching requires HF, a highly toxic chemical. This process, however, can be performed with HF solutions with a lower concentration, in-line with household cleaning products. [103] Surface roughening for Si may also be performed using less-hazardous compounds such as KOH or potentially even mechanically, eliminating the need for HF. iii) Si substrates we used in this study were not stretchable nor flexible, but using stress-diffusion geometries and thin layers, Si can be rendered highly flexible and to some extent also stretchable. [104,105] In the next Chapter, the mechanical robustness of CB-PDMS sensors with Cu-pSi and AgEpoxy contacts is investigated. In Chapter five, CB-PDMS and CB-CSC devices with Cu-pSi contacts are characterised electrically using DC and AC, and proposed equivalent circuits are presented based on the electrical behaviour of the devices.

Chapter 4

Mechanical characterisation of Cu-pSi solder-on contact system

Once we assembled the CB-PDMS sensor with Cu-pSi contacts and soldered wires on the two Cu pads, we characterised the contact technology developed and compared it with widely used alternative contact integration method using conductive epoxy, AgEpoxy. In this Chapter, we look at the contact adhesion strength during a single stretch to failure of Cu-pSi and AgEpoxy bonded CB-PDMS sensing elements. The device was held stationary at one end and pulled to failure at the other end.

4.1 - Lap shear strength: Cu-pSi *vs.* AgEpoxy

To measure the electromechanical contact reliability under stress we performed shear strength testing to compare the mechanical characteristics of Cu-pSi and AgEpoxy electrical contacts on the interface of both with the CB-PDMS layered composite (please note that we used AgEpoxy to attach a copper wire to the CB-PDMS layered composite to pull the substrate and make electrical measurements). The samples were stretched from each end until the device-under-test (DUT) failed mechanically (Figure

16). First (Figure 16A), we investigated the effect of CB content (0-20%) on the maximum stress to failure (strain relationship is shown in Figure 17, below).

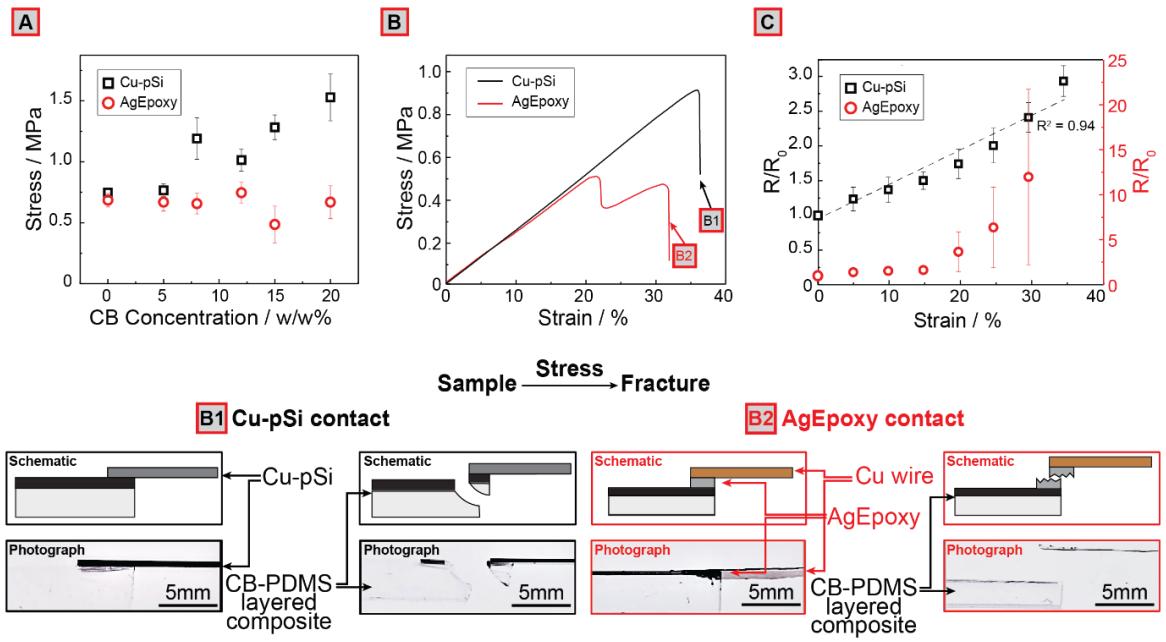


Figure 16 Lap Shear Test comparison Cu-pSi *vs.* AgEpoxy (A) Dependence of maximum stress to failure of Cu-pSi and AgEpoxy contacts in relation to CB filler concentrations (n=5) in the CB-PDMS layer; (B) Representative curves for stress *vs.* strain for CB-PDMS layered composite devices with AgEpoxy and Cu-pSi contacts during a single stretch to failure (n=7 shown in Figure 18). (B1, B2) Modes of failure for 12% CB-PDMS layered composite devices (12% CB content) with AgEpoxy and Cu-pSi contacts used in the experiments shown in (B); (C) Electromechanical characterization of 12% CB-PDMS layered composite devices using different with Cu-pSi and AgEpoxy contacts (n=9).

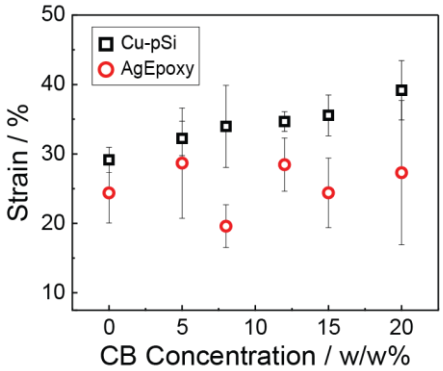


Figure 17 Strain *vs.* CB Concentration Dependence of maximum strain at failure of Cu-pSi and AgEpoxy contacts in relation to CB filler concentrations (n=5) in the CB-PDMS layer.

CB-PDMS layered composite devices fabricated using the Cu-pSi electrical contacts exhibited an increase in maximum stress (n=5) to failure with increasing CB content in the composite while the maximum stress to failure for samples with AgEpoxy contacts (n=5) did not change with increasing CB in the composite conductive layer. Strain stiffening in layered composites can be used in the future to form contact strain relief islands. [106] This result indicates that each system has a different point of failure (e.g., failure of the contact-substrate interface, failure of the CB-PDMS layered substrate itself, etc.). To investigate the mode of failure of the CB-PDMS layered composite devices with Cu-pSi and AgEpoxy contacts in more detail, we characterized the mechanical behaviour of the devices under shear stress up to 40% strain (Figure 16B and Figure 18). We used CB-PDMS layered composites with 12% CB content for these experiments because it falls in the desired range of electrical resistance ≈200 kΩ (a current in the μA range is desired for further experiments using a 5 V Arduino).

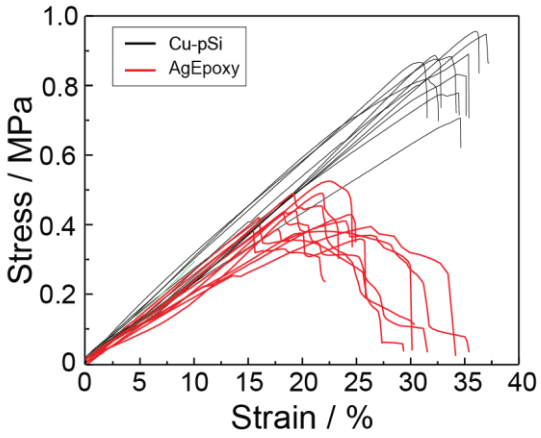


Figure 18 Stress – strain repeats (Cu-pSi *vs.* AgEpoxy) Detailed strain – stress characteristics for samples of CB-PDMS (3 mm thickness, 12% CB content) with AgEpoxy and Cu-pSi contacts. The gradual mode of failure for AgEpoxy and abrupt mode of failure (i.e. catastrophic) for Cu-pSi samples are shown.

We found that the samples with Cu-pSi contacts produced a highly repeatable, linear strain-stress behaviour up to approximately 1.0 MPa (or nearly 35% strain) after which the DUT failed catastrophically with further increases in stress. On the contrary, the CB-PDMS layered composite devices with AgEpoxy contacts exhibited repeatable and

linear stress-strain behaviour only up to 0.4 MPa (or 15% strain). Further increases in strain caused devices with AgEpoxy contacts to slowly fail (i.e. no catastrophic failure in this case) as indicated by decreasing stress beyond 15% strain. Visual inspection of the samples before and after shear testing (Figure 16 B1, B2) revealed that, in the case of AgEpoxy contacts, the electrical contact – CB-PDMS composite interface failed slowly due to the brittleness of AgEpoxy and non-covalent, weak bonding between the adhesive and silicone substrate. In devices with Cu-pSi contacts, the catastrophic mechanical failure was caused by fracturing of the CB-PDMS layered composite and not the Cu-pSi contact, suggesting that the bonding strength of Cu-pSi contacts was higher than the yield strength of the CB-PDMS layered composite. Electron micrographs of the CB-PDMS layer before and after stretching to 20% showed no cracks on the surface of the composite (Figure 19).

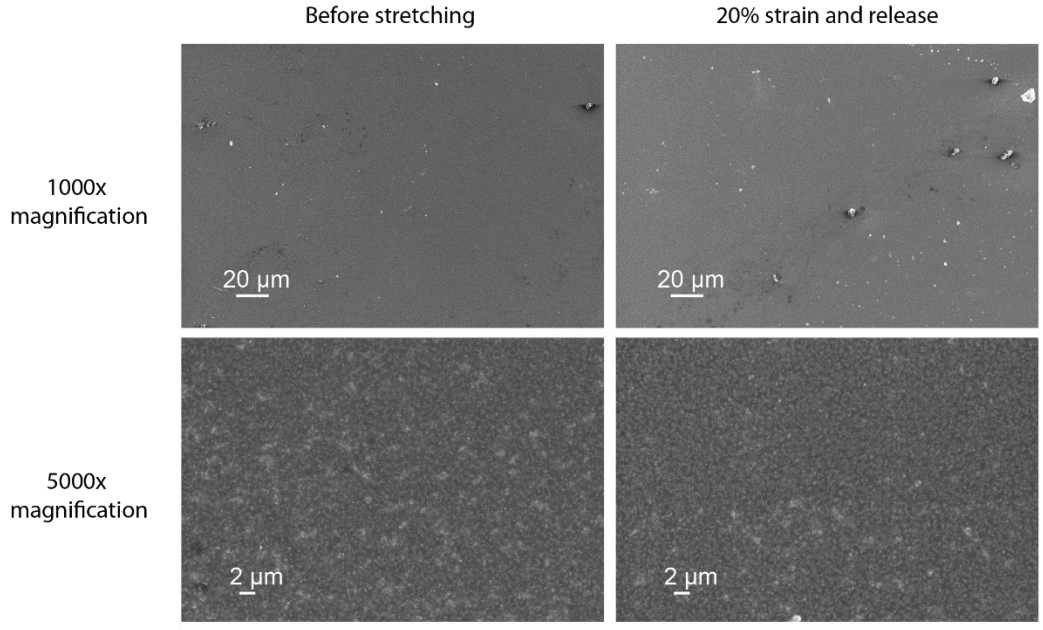


Figure 19 SEM before and after stretch SEM micrographs for 12% CB-PDMS surface before and after stretching to 20% strain at 1000x and 5000x magnification.

4.2 - PDMS fracture type

We further studied the mechanism of failure of the CB-PDMS layered composite (CB-PDMS on PDMS carrier substrate) under tensile stress; regardless of the thickness of the PDMS carrier substrate, plasma-treated PDMS always fails around 0.5-0.7 MPa

(Figure 20). It follows that when subjected to plasma, PDMS becomes more susceptible to forming microscale cracks on its (somewhat hardened) surface. These cracks may subsequently propagate under applied tensile stress (normal to the direction of the crack) and cause failure (i.e. Mode I type crack propagation). [107] This claim is further supported by the fact that increasing CB content in the CB-PDMS layer also increased the maximum stress to failure (Figure 16A) since composite materials are more resistant to Mode I type crack propagation. [108] Given that the substrates are flexible, for numerical analysis of the system, a superposition of Mode I and II loading should be considered.

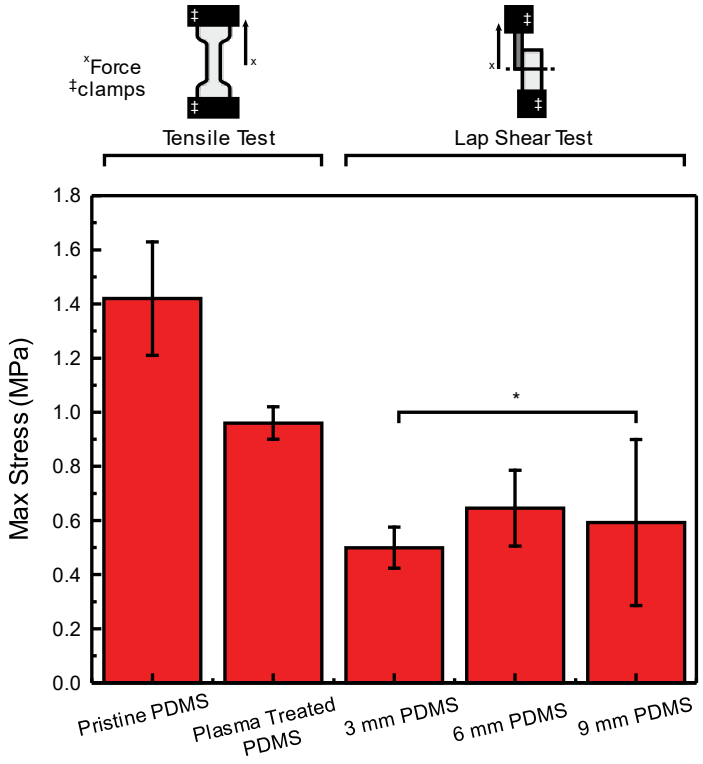


Figure 20 Tensile strength of PDMS Maximum stress experiments using 3 mm pristine PDMS and plasma-treated PDMS (unmasked) dog-bone samples, and samples with Cu-pSi contacts prepared on PDMS substrates with 3, 6 and 9 mm thickness. No difference was observed in the values of maximum stress to failure for each thickness indicating that the fracture mechanism is a surface phenomenon only (* no significant difference).

Figure 16C illustrates the electrical resistivity-strain behaviour of 12% CB-PDMS layered composite devices connected to read-out electronics via copper wiring soldered on Cu-pSi or adhered with AgEpoxy (see Figure 21). We measured the

electromechanical characteristics during a single stretch to failure at a strain rate of 2 mm/s (physiologically relevant rate for breathing). [79] The resistance response of the CB-PDMS stretchable conductive layer (Response = R/R_0 where R is the measured resistance and R_0 is the initial or baseline resistance) with Cu-pSi contacts produced a repeatable and slightly nonlinear response up to a maximum strain of 35% (please note that beyond 35% strain the devices fail catastrophically). Sensors with AgEpoxy, however, produced a highly nonlinear response across the range of strains between 0-30% due to gradual mechanical failure of the AgEpoxy electrical contact beyond 15%.

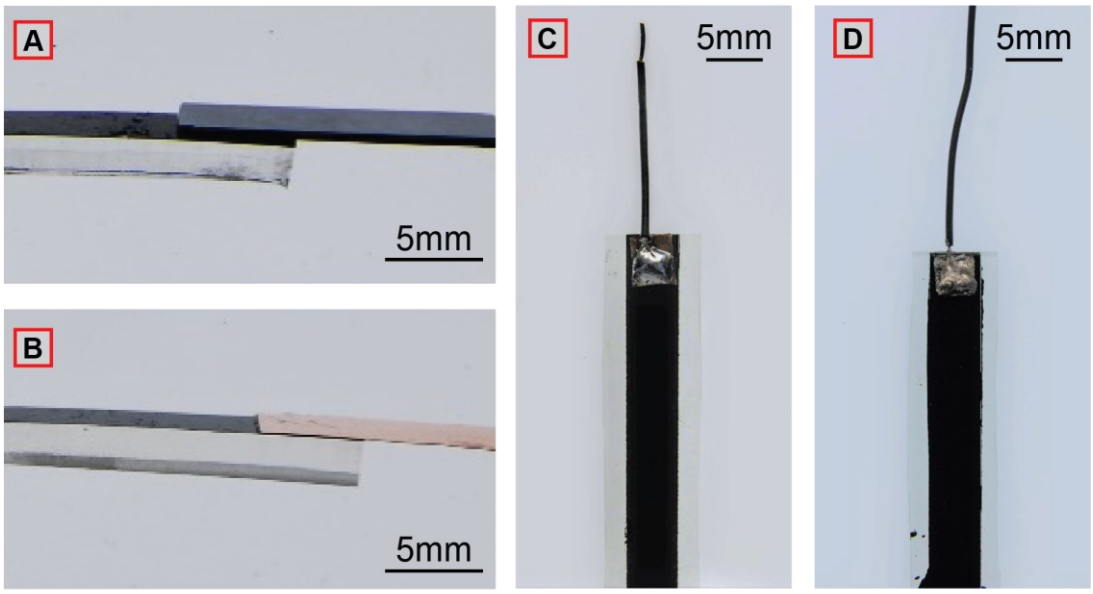


Figure 21 Cu-pSi/AgEpoxy device pictures (A, B) Picture of the samples used in lap shear tests (A - sample with Cu-pSi contact on CB-PDMS; B - sample with Cu wire bonded on with AgEpoxy on CB-PDMS). (C, D) Pictures of the assembled sensors with plasma-bonded Cu-pSi contact (C) and stencil-printed AgEpoxy contact (D).

4.3 - Cu-pSi and AgEpoxy under cyclic stress

Since physiological monitoring (such as breathing) or rehabilitation exercises often involve repeated application of mechanical stress, we also characterized the electromechanical behaviour of the CB-PDMS layered composite strain sensors with Cu-pSi and AgEpoxy contacts under cyclic stress. We subjected each sample to 20 cycles of repeated deformation at a strain rate of 2 mm/s at each level of strain starting

from 5% to account for stress relaxation in a method modified from Seyedin *et al.* [109] After every 20 cycles, the level of strain was increased by 5%. The procedure was repeated until the sample (gradually or catastrophically) failed. Figure 23A shows a representative cyclic stress measurement (see Appendix: Figure 40 for repeats for n=5) of the sensors with Cu-pSi and AgEpoxy contacts. Under cyclic stress, the devices with AgEpoxy contacts started failing gradually at strains higher than 10% with complete failure beyond 15%, barely withstanding stress (σ) = 0.2 MPa (we captured gradual cracking and failure of the brittle AgEpoxy contacts and robust stretching of Cu-pSi devices – Figure 22). The gradual formation of hairline cracks on AgEpoxy causes the wired connection to become weaker, thus straining the device required lower levels of stress until complete disconnection of the AgEpoxy fragments still connected to the DUT (Figure 23A, top).

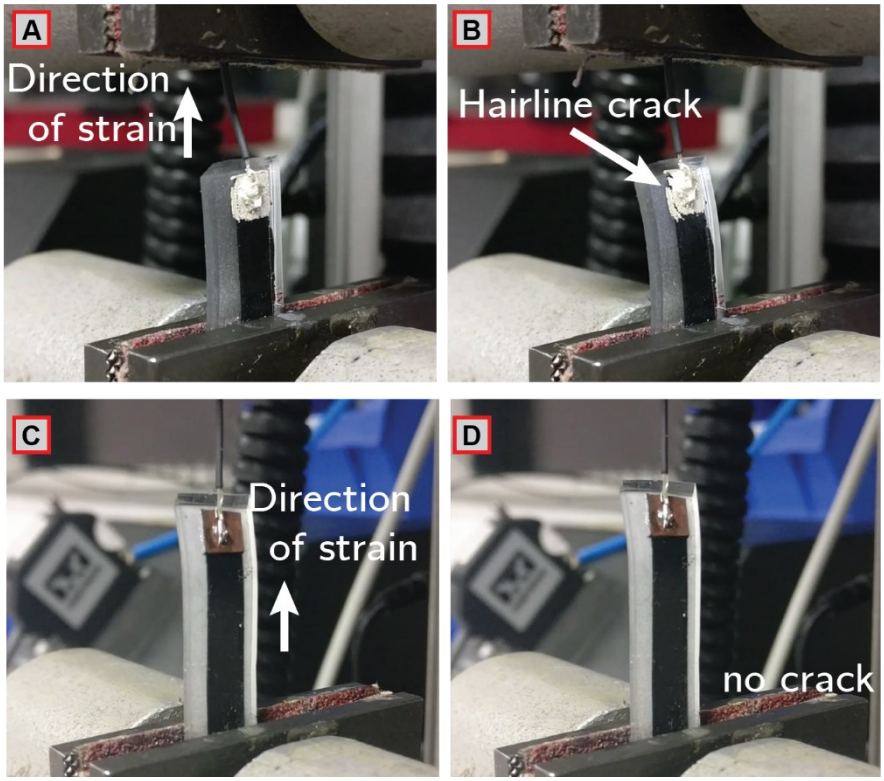


Figure 22 Visual analysis of tensile test Lap shear test for AgEpoxy (A, B top) and Cu-pSi (C, D bottom) devices showing initial cracking (cracking of adhesive) for AgEpoxy, but no such effect in Cu-pSi devices

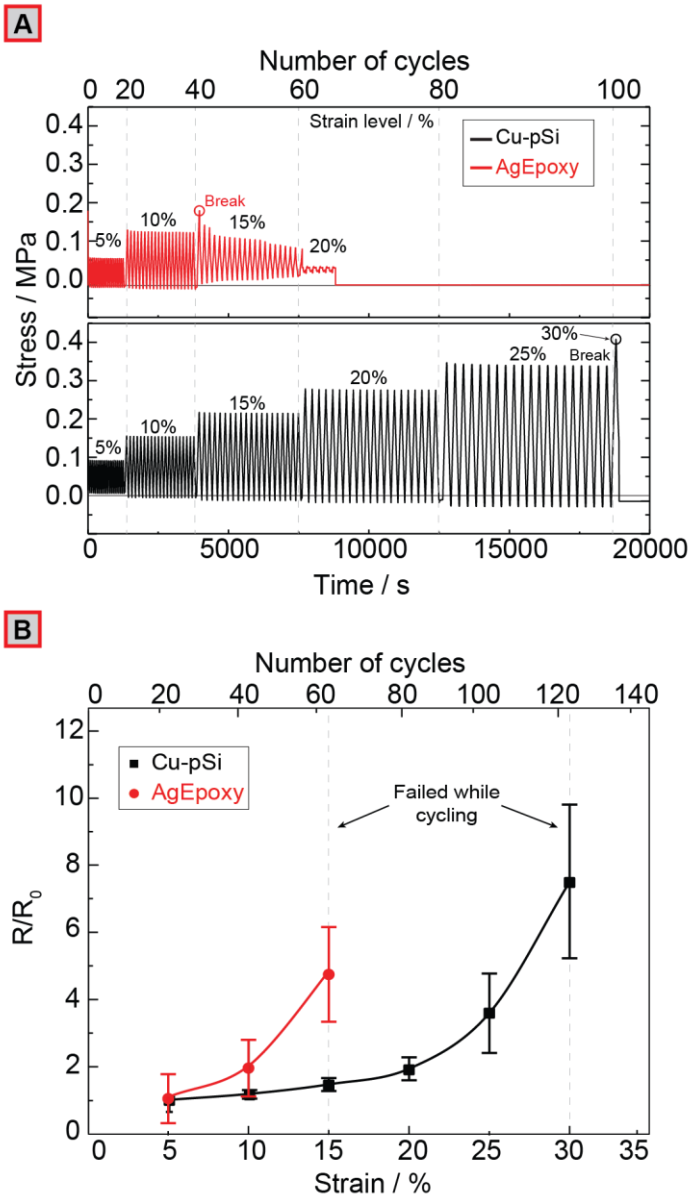


Figure 23 Cyclic CB-PDMS tensile tests (A) CB-PDMS layered composite with AgEpoxy and Cu-pSi contacts subjected to cyclic strain; AgEpoxy (top) showing gradual failure beyond 15% strain, and Cu-pSi (bottom) showing abrupt failure beyond 30% strain. (B) Electrical resistance after 20 cycles of strain and release at different strain levels (n=5).

Devices with Cu-pSi contacts, however, would only fail at 30% strain (σ = 0.5 MPa) and remain fully functional under repeated strain until catastrophic failure of the substrate (after about 100 cycles at strains lower than 30%). The electrical measurements under cyclic stress (Figure 23B) also followed a similar trend. At 15% strain, the resistance increased and was eventually lost for the CB-PDMS layered composite devices with AgEpoxy contacts before reaching 20 cycles whereas the sensors

produced with Cu-pSi contacts could reach 30% strain before failing abruptly. The sensors with Cu-pSi contacts, however, produced a non-linear electrical response with hysteresis especially when subjected to high levels of cyclic stress (>20%) owing to the Mullins effect (i.e. softening due to previous loading) in which the physical connections between the filler (CB) particles are modified to a greater extent when multiple cycles of high levels of strain are applied to the composite material.[110,111] Since this mechanical effect is prevalent in all in-filled rubbers regardless of the type of contact, we expect that the devices with AgEpoxy contacts would also exhibit a similar behaviour of hysteresis at higher strains if they could withstand such levels before failure (for more information on hysteresis see below - Figure 24). Hence, in all electromechanical tests performed, Cu-pSi appeared to be more robust compared to AgEpoxy electrical contacts for CB-PDMS samples.

In summary, we compared the new Cu-pSi contacts prepared with standard AgEpoxy contacts in static shear strength tests and cyclic deformation. The maximum strain and stress levels achieved by the new contacts was on average higher than the standard contacts. What is more, the mode of failure is different. For Cu-pSi contacts the bond with the silicone surface does not fail, rather the substrate forms a crack and subsequently tears. This can be improved by uniformly distributing the area under strain.

In terms of evidence for fatigue of the system, visually the substrate looks identical after stretching and releasing at 20% strain. The Cu-pSi devices fail at 30% strain and the devices made with AgEpoxy at 15%. Higher strain levels can be achieved by stress dissipation structures such as stiffer "island" structures where the contacts are placed,

however, we also see the AgEpoxy contacts failing gradually which is undesirable as explained above, and this is not observed in Cu-pSi devices.

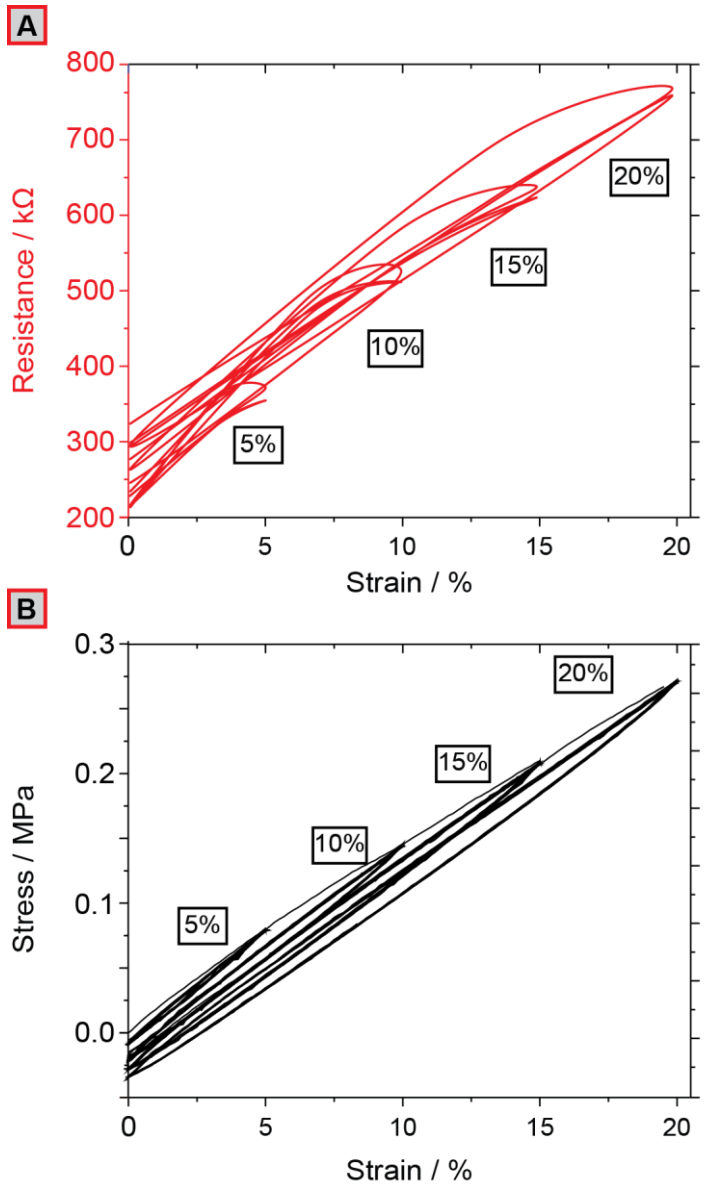


Figure 24 Cu-pSi CB-PDMS Electromechanical test repeats (A) Representative curves for electrical hysteresis due to previous loading demonstrated on a 12% CB-PDMS layered composite. (B) Mechanical hysteresis during cyclic stretching tests.

Chapter 5

Electrical characterisation of the Cu-pSi system

In this Chapter, we focus on studying the electrical characterisation of our contacts and strain sensor CPCs (both CB-PDMS and CB-CSC) as electrical components of a circuit. We test devices under DC and AC conditions in order to make an informed decision on the electronic components and operating conditions required to operate these sensors as well as create portable devices. We also test the sensitivity of each type of device and devise an equivalent circuit model which introduces a guide for future development based on our empirical observations. As an example, the asymmetric conductance observed in one of our preliminary experiments that used DC voltage led to the hypothesis that the device's characteristics resemble those of a diode and as a result, operating in AC would higher sensitivity and noise reduction.

5.1 - Heterointerfaces and electrical behaviour

In order to understand the electrical behaviour of the devices formed and to construct an equivalent circuit model, we performed two-probe I-V measurements using CB-PDMS layered composite strain sensors with two Cu-pSi contacts.

Because of the metal-semiconductor-metal nature of each electrical junction (i.e. Cu-Si-C), the two-probe I-V measurements (n=7) were highly non-linear (i.e. non-ohmic), as shown in Figure 25A. In the range -2 V to 2 V, the devices exhibited a diode-like behaviour due to the formation of Schottky barriers (because of the metal-semiconductor interface) with an exponential increase in electrical current for voltages beyond 0.5-1.0 V.[112] An applied voltage with a magnitude higher than 1.0 V is therefore required for strain-sensing with the Cu-Si-C junction. The Cu-Si-C contact

structure leads to Schottky junctions at both Si heterointerfaces (Cu-Si and Si-C), for both p-type and n-type Si (equilibrium diagram shown in Figure 25B).

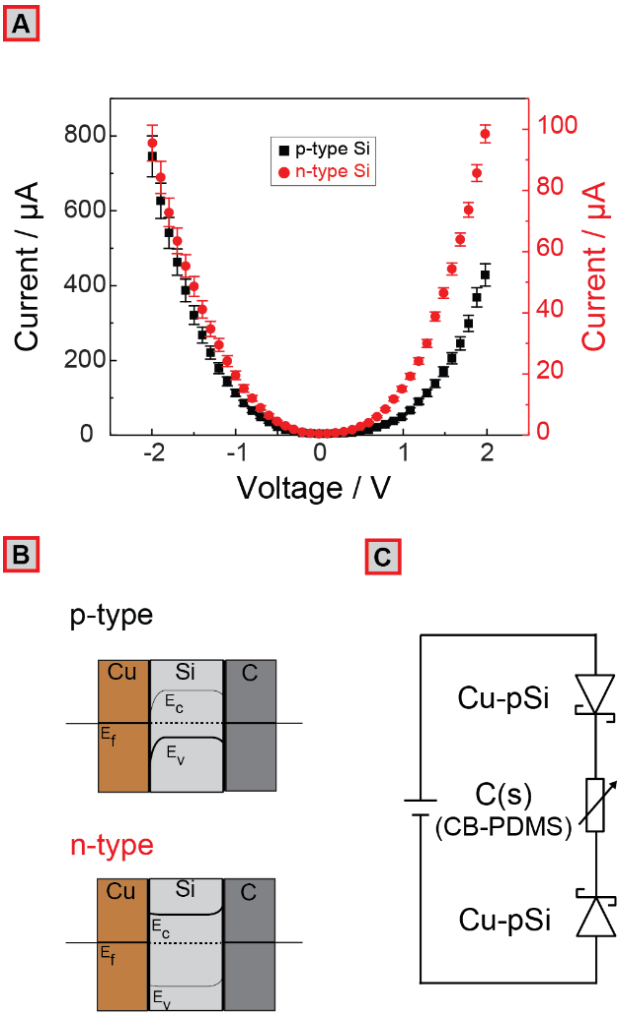


Figure 25 I-V, band diagrams, equivalent circuit #1 (A) I-V measurements for a 12% CB-PDMS layered composite strain sensor with Cu-pSi contacts created using *lightly doped p-type and n-type* Si (100) (n=7); (B) Equilibrium band diagrams for the Cu-Si-C interface. (C) Equivalent electrical circuit for the CB-PDMS layered strain sensor with two Cu-pSi contacts.

Fermi level pinning causes bending in the Si conduction and valence bands, which restricts the conductance at low potentials (Figure 25B). The devices constructed using p-type Si, however, were substantially more conductive than the devices created using n-type Si beyond the voltage of operation (i.e. >1 V). This is because the injection barrier height for the metal-Si interface for p-type Si is lower than that of n-type Si, leading to overall larger currents at the same potentials for devices with similar doping levels.[113] The I-V graph for the junctions constructed using p-type Si indicates a more

asymmetric barrier properties due to the differences in work functions (Φ_M) of Cu and C. For example, in the case of p-type Si, because Cu has a work function $\Phi_{M\text{-}Cu}$ of 4.6 eV and C, 4.8 eV the barrier height for the Si-Cu junction is larger.[114] The height of the Schottky barrier can be reduced by using Si with higher doping levels, leading to higher charge carrier density, thereby reducing the width of the depletion layer. Using thin Si layers (<100 μm) as contacts would also effectively reduce the total width of the depletion layer, as the depletion layers for each junction would begin to overlap.

5.2 - Modelling an equivalent circuit

An equivalent circuit diagram is presented in Figure 25C representing the circuit where the CB-PDMS piezoresistive layer is connected via the solder-on Cu-pSi contacts to a power source. Since, regardless of the polarity of the potential applied, one of the junctions is always reverse-biased, the entire device can be modelled as a variable resistor with two Schottky diodes connected in reverse polarity. This model is an over-simplification of the system, however, it represents the electrical behaviour of the devices measured with sufficient accuracy. In this section, commercially available CB-CSC will be used to further study the electrical behaviour of our contact – silicone strain sensor system.

The metal-semiconductor junction which forms by attaching a Cu electroplated Si contact on the sensing element gives rise to Schottky-barrier type behaviour whose rectifying characteristic need to be investigated. As expected, the resistance of the sensing device greatly depends on applied voltage with values ranging from 170 kΩ at 1 V to 1 kΩ at 10 V, whereas the resistance of the bare conductive silicone strip is independent of applied voltage at approx. 900 Ω (Figure 26A).

We compared the sensitivity of devices with no contacts and assembled devices connected via the Si contacts as described above at pressures of 50 and 300 N (Figure 26B). A comparison of relative magnitude differences at rest and under compression for the specified range of applied voltages shows that voltage level does not affect the sensitivity or response for sensing strips connected without contacts. On the contrary,

the devices with Si contacts could not reliably detect a pressure of 50 N due to high levels of noise for 1-10 V. Similarly, noise and signal drift produced unreliable responses at 300 N pressure for all voltages up to 10 V where a small significant change from the baseline is observed. Given that 300 N is the maximum grip force for humans and a higher sensitivity is required for the current device to be applicable in hand rehabilitation situations.

In Figure 26C the turn on voltage for different doping levels and dopants of the Si contact is visible on an I-V graph. *Lightly doped n-type and p-type* contacts have a visible turn on voltage levels at approximately 5 and 1.5 V. Devices prepared using *heavily doped* Si contacts do not have visible turn on voltages as they are degenerately doped and behave similarly to a conductor. Devices using *heavily doped p-type* Si exhibit the highest conductivity.

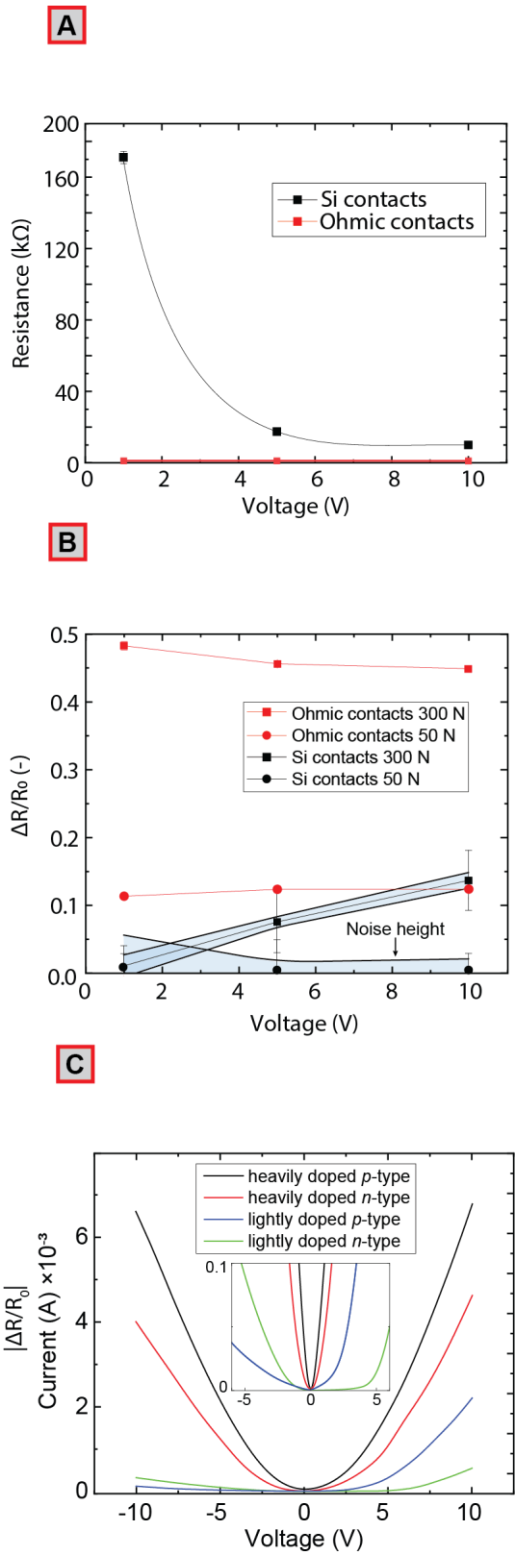
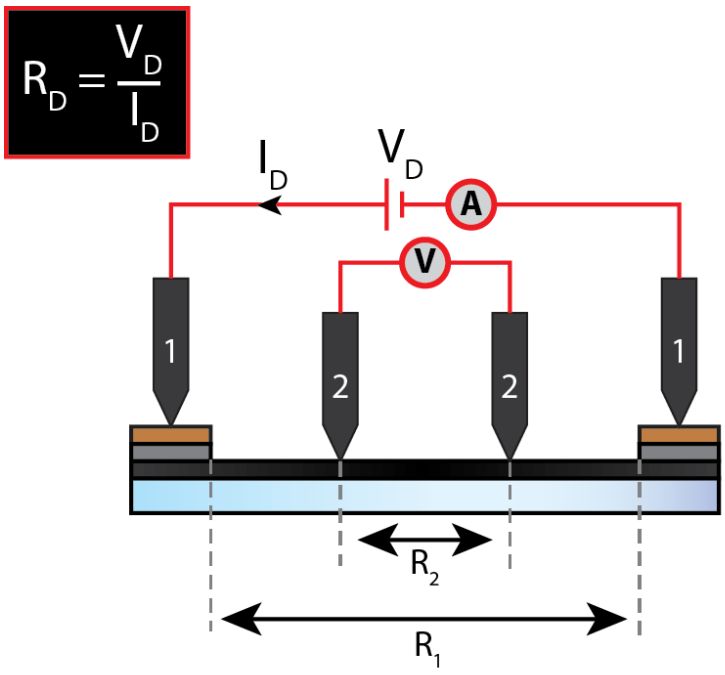


Figure 26 DC IV and sensitivity for CB-CSC For devices made using clamps on CB-CSC (Ohmic contacts) and Cu-pSi contacts on CB-CSC (Si contacts of various doping levels) (A) DC Resistance at rest: The black line shows the decrease in resistance with increasing voltage which is in accordance to the equivalent circuit presented in Figure 25 compared against the stable resistance of the ohmic resistor which is the CB-CSC (red line) (B) DC sensitivity ohmic *vs.* Si contacts: Presentation of lower sensitivity

(resistance change from baseline) for devices with Si contacts (black) when under 50 N and 300 N of compressive force compared to devices with ohmic contacts (C) I-V diagrams for all Si wafer types used to create CB-CSC devices for Voltages from -10 to 10 V.

We also performed four-probe electromechanical tests to determine the contribution of contact resistance to the overall change in resistance under strain. Our results indicate that the Cu-pSi contacts, when attached to the CB-PDMS layer, increase the resistance of the entire device by ~100 kΩ at an applied bias (V_D) of 2 V; this resistance does not change under strain (see Figure 27).



Strain/ %	R_D/ kΩ	R_2/ kΩ	R_1/ kΩ	Contact contribution R_D-R_1/ kΩ
0	669.7±1.2	104.8±3.2	564.8±17.5	104.8±4.6
10	665.6±0.2	99.3±1.1	566.2±17.6	99.3±4.3
25	675.6±0.3	109.1±1.3	566.5±17.6	109.1±4.8

Figure 27 Four probe measurement Schematic of the four-probe measurement setup to determine the change of contact resistance at different strain levels; Table: Derivation of contact resistance contribution for strain levels of 0%, 10%, and 25% (n=3).

5.3 - Alternating current (AC) and sensitivity

We continued our investigation using the commercially available CB-CSC sensing element sourced from J-Flex with a volume resistivity of 45.3 Ω·cm and 65 Shore A

hardness to which we attached Cu-pSi contacts as described previously. Devices made with *heavily doped p-type* Si were still showing rectifying behaviour. We tested the response of all Si types (presented in Section 3.2.2, §1) using AC with a Model 891 Bench LCR Meter (B&K Precision Corporation, Yorba Linda, CA).

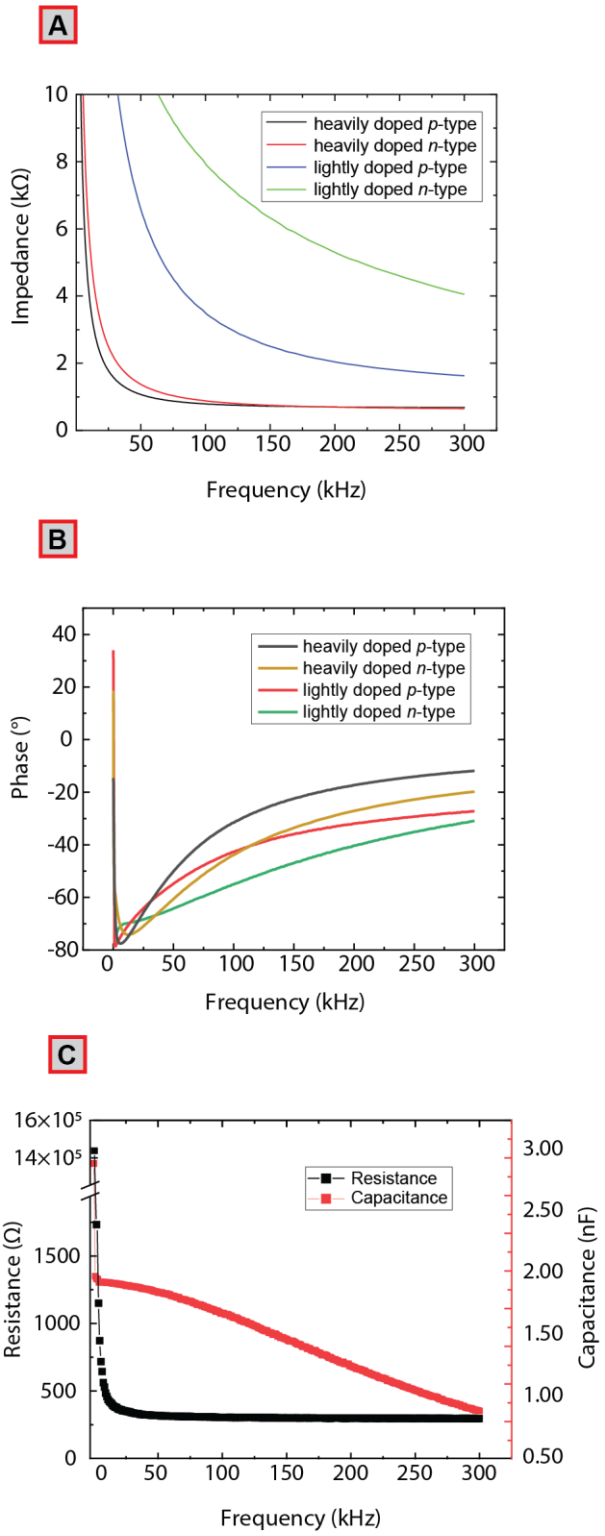


Figure 28 AC frequency sweeps (A) Linear AC frequency sweep *vs* Impedance for devices made with Cu-pSi contacts attached to all Si types (B) AC frequency *vs* Phase graph for the same devices (n=5) (C) Resistance and Capacitance *vs* Frequency for *highly doped p-type*

Figure 28 presents the complex impedance and phase of the Si contact device systems during a frequency sweep of all frequencies from 10 Hz to 300 kHz using an LCR meter (B&K Precision Corporation, Yorba Linda, CA). It is visible that the *heavily doped p-type* systems show the lowest Impedance. Interestingly, the real part of impedance (resistance component in $Z = R + 1/j2\pi fC$) at 300 kHz is the same as the resistance of the bare strip with no contacts. We also measure a significant nF capacitive component to the devices that decreases at higher frequencies (Figure 28C).

We iterated on the measurement system for the CB-CSC/Cu-pSi devices. Among others we built a simple sine oscillator, a peak detector circuit, and investigated a True RMS to DC chip (AD8436, Analog Devices). We decided to make all measurements using an LCR meter. Briefly, our initial setup consisted of a simple voltage divider and transimpedance amplifier in series using an input voltage of 10 V. This circuit produced signals lacking in quality and reliability as described in the previous section (see Figure 26B). We decided to operate the device using AC and built two iterations of a peak detector circuit which produced some component instability, and finally used an integrated RMS-to-DC circuit.

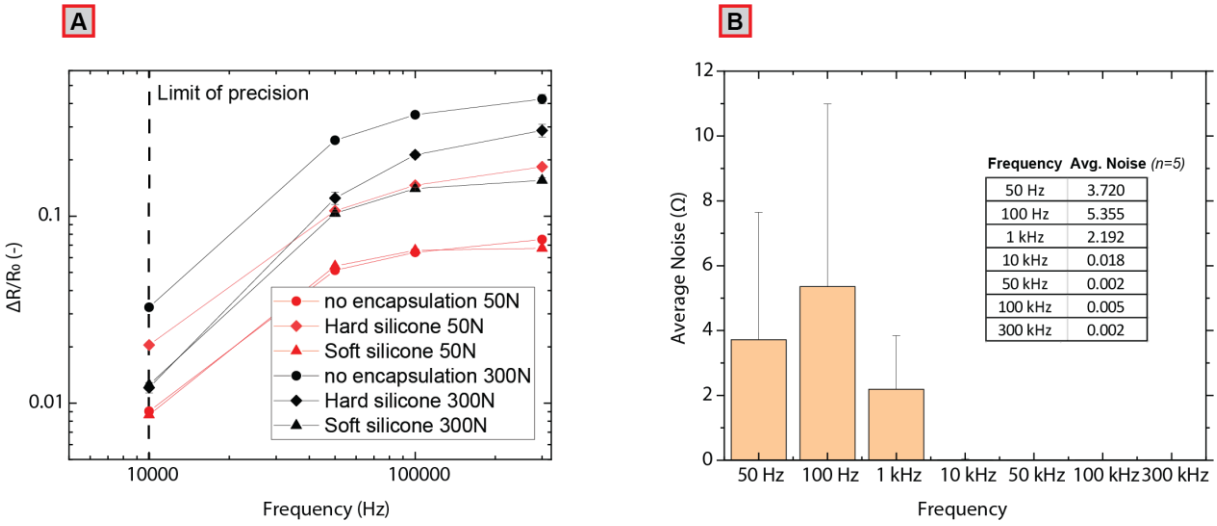


Figure 29 AC sensitivity (A) Relative change in resistance from baseline ($\Delta R/R_0$) for devices without encapsulation, in soft encapsulation, and in hard encapsulation, under 50 and 300 N of pressure, at different AC frequencies starting from the limit of precision where the Signal-to-noise ratio was smaller than the relative change in Resistance (B) Average Noise height for signals obtained using AC frequencies between 50 Hz and 300 kHz reporting average differences between smooth and raw signals

Average Noise height is calculated by taking the difference between the signal produced after a third-degree polynomial filter and the raw signal. There is a 2 order-of-magnitude reduction of noise between 1 and 10 kHz, which we set as the precision limit for pressure measurements, and a further order reduction at 300 kHz. An additional point to be made about cut-off level of signal reliability is signal stability visible in Figure 30.

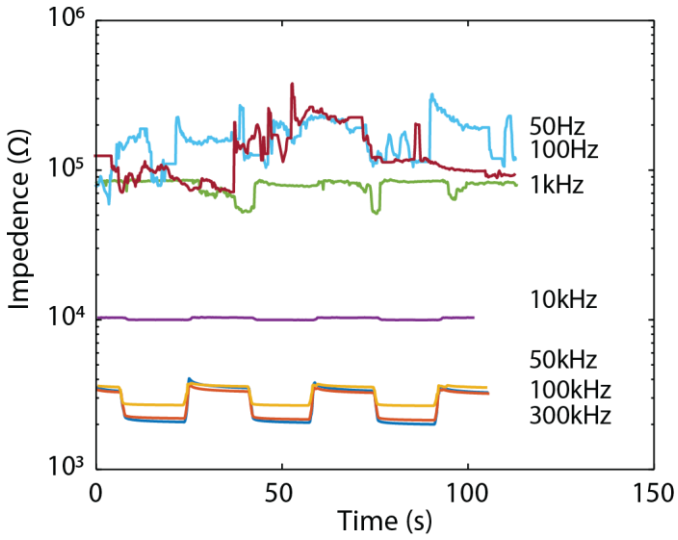


Figure 30 Raw signal AC 300 N Raw signal for all frequencies tested (50-300 kHz) with different baseline Resistance for each frequency as shown in Figure 28A. The compressive force applied is 300 N on a sensor without encapsulation.

Signals below 10 kHz are unreliable, whereas for signals above 10 kHz sensitivity increases at a decreasing rate as frequency increases to 300 kHz. Electromechanical sensitivity tests were repeated for a range of AC frequencies from 50 Hz to 300 kHz. Signal-to-noise ratio was too low below 10 kHz (Figure 29B shows average noise for all frequencies). The highest sensitivity is at 300 kHz, this could be because contact resistance and capacitance change effects are reduced and the piezoresistive changes of the sensing element are most prominent (Figure 29A). The contact resistance is

negligible at 300 kHz to the point that the sensitivity of CB-CSC (considered as a variable resistor) with Cu-pSi contacts at 300 kHz is the same as the sensitivity of CB-CSC with metal (ohmic) contacts using DC (Figure 26B). As a result a more suitable equivalent circuit is presented in Figure 31 which accounts for the increasing sensitivity at higher frequencies presented in Figure 29. In Figure 31A, we model (using modelling software LT Spice) the amount of voltage through our circuit in Figure 31 B as the AC frequency increases. The model shows an increasing amount of signal through our equivalent circuit at higher frequencies with a sharp change at 10 kHz. This agrees with the trend seen in Figure 28A and the variability and noise change that occurs at 10 kHz presented in Figure 28C. That said, this device is a complex structure with multiple interfacial contacts and a complex band structure. Further investigation could reveal extra components that better model the behaviour of our devices.

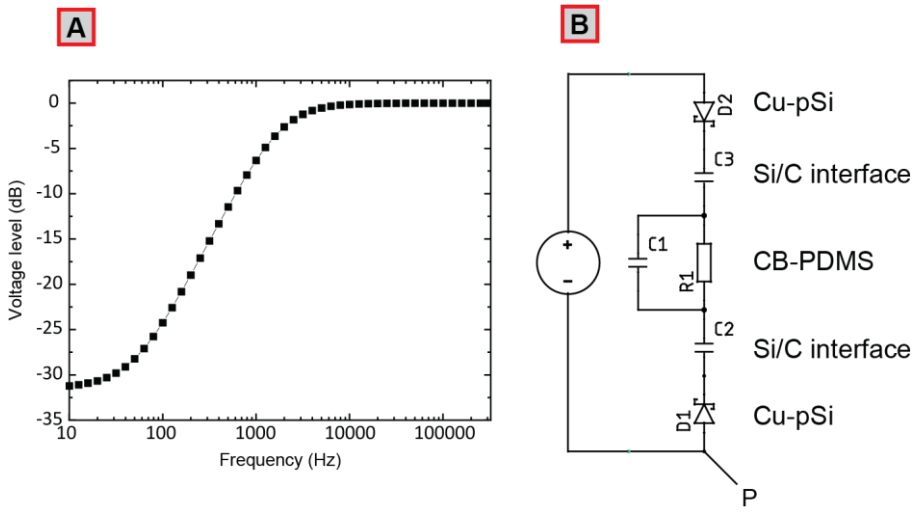


Figure 31 AC circuit modelling and equivalent circuit #2 (A) Voltage level after AC analysis measured after connecting the circuit in B to a potential divider (1 MΩ resistor) at point "P" (B) Equivalent circuit representing the Cu-Si interface of the Cu-pSi contact, C3 represents the Si-C (silicon-carbon) interface where the Cu-pSi contact adheres on the CB-CSC, the C1 and R1 (both variable) in parallel represent the piezoresistive CB-CSC sensing element, and C2, D1 are the equivalent Cu-Si-C interfaces on the other side.

In the next two Chapters, several proof of concept devices for physiological monitoring are presented and then the possibility of rehabilitation and gamification is further investigated using a connected squeezable sensor.

PART III

Applications of Cu-pSi CB-Silicone Sensors

Chapter 6

Soft Sensors in Rehabilitation and Digital Therapeutics

In this Chapter, we present the soft exercise and wearable devices (breathing harness, pressure sensing stress-ball, and more) we prepared and tested on volunteers. After that, we present the state of digitally connected wearable devices in the market today, and the benefits of such technologies once combined with soft sensors.

For about ten years now, a number of wearable products started to appear in the market. These were roughly divided in two categories: fitness trackers, which measured basic physiological functions such as the users' heart rate, and smartwatches, a cross between a fitness tracker and a smartphone. The commercial success of these product groups functioned as a driver for the rapid development of health related software-first solutions. Applications use algorithms that analyse the user's health or well-being-related behaviour. Limited hardware capabilities have pushed the capabilities of software and stretchable, body-conformable hardware is required for next-generation wearable healthcare devices.

6.1 - Proof-of-concept devices using Cu-pSi contact technology

We have fabricated a series of proof-of-concept devices to demonstrate the mechanical robustness of the technology we developed in real-world applications (Figure 32). In the first example, we printed a CB-PDMS (12% CB) conductive layer with Cu-pSi contacts on an unmodified (non-conductive) silicone-based chest strap (Smooth-On Inc., Ecoflex® 00-30 used as carrier substrate) to measure breathing rate to demonstrate the applicability of our technology in wearable physiological monitoring. [115] Figure 32A shows the change in electrical resistance during inhalation and exhalation due the expansion and contraction of the chest. During inhalation, as the

chest expands, the strain sensor stretches, which leads to an increasing in the resistance of the CB-PDMS sensing element. As soon as the exhalation starts, the volume of the chest decreases leading to a decrease in the electrical resistance. Every peak in the signal corresponds to a cycle of respiratory activity. We were able to monitor breathing at rest (normal breathing), during fast and paused breathing, as well as heavy panting using the device we developed. Other devices, with a similar form-factor to the chest strap, can also be produced for various applications in exercise monitoring and rehabilitation such as a leg band (Figure 32B). Compared to alternatives currently available, the devices presented allow for conformability and comfort above what a rigid device can offer. A simple case in point would be a chest health tracker with electronics housed in a rigid casing in the middle of the chest. This would be uncomfortable for a person lying on their chest. For more information on conventional health monitors refer to Section 1.3.1.

In another example we fabricated a silicone-based, ball-shaped device (i.e. Squeeze-ball) with embedded CB-PDMS (12% CB) and Cu-pSi contacts for monitoring rehabilitation of patients with hand injuries or neurological disorders such as stroke (Figure 32C). Squeezing the ball compresses the sensing element embedded inside which in turn changes the resistance relative to the force applied. Although we did not fully quantify, the sensors were sensitive to both light and tight grip forces and could function reliably for repeated application of force through squeezing of the ball. We have also measured different baseline resistances for the sensing element in a range of physiologically relevant temperatures (Figure 33). A detailed comparison of this soft, pressure-sensitive hand-held solution with conventional rehabilitation devices is given in Chapter 7. The main two advantages of a soft device over a rigid device for measuring grip-strength are as follows: 1) the hardness of the whole device can be tuned to fit the needs of weaker patients or age groups and change depending on their progress, 2) a

soft device can measure modes such as bending and stretching, in addition to pressure, which current rigid devices are not able to.

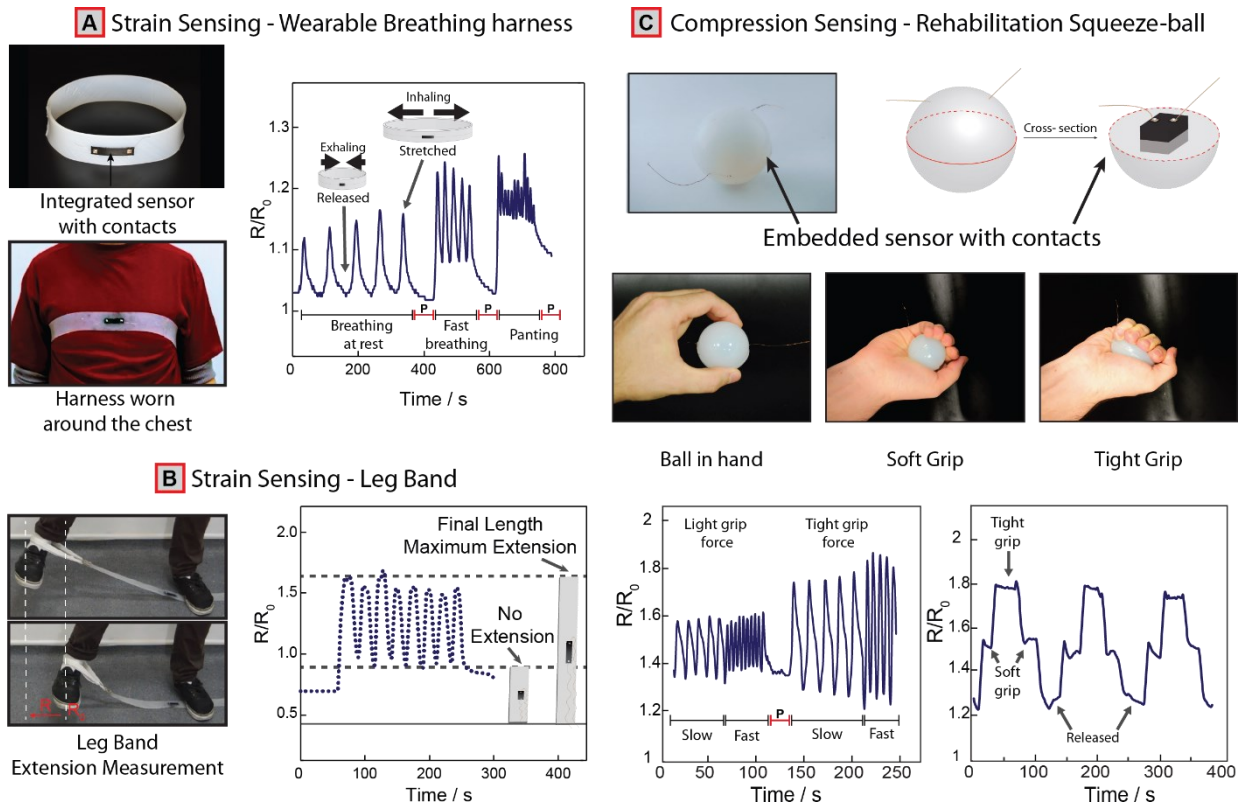


Figure 32 Demo strain and pressure sensing healthcare devices (A) Picture of completed stretchable harness and human subject wearing the device (i.e. CB-PDMS sensor with Cu-pSi contacts); Physiological data collected from chest during inhalation (stretched) and exhalation (released) recorded with the harness in real-time; (B) Picture of a leg band containing the CB-PDMS sensor with Cu-pSi contacts during a leg extension exercise. The electrical signals indicate the level of extension; (C) Picture and graphical illustration of the cross-section of the rehabilitation ball and a subject holding the ball for size comparison; Resistance data (equivalent to force) collected using the rehabilitation ball during exercise at light and tight gripping force at different exercise rates; Testing the sensitivity of the device by applying different grip forces (Soft grip → lower force, Tight grip → higher force). P = Paused.

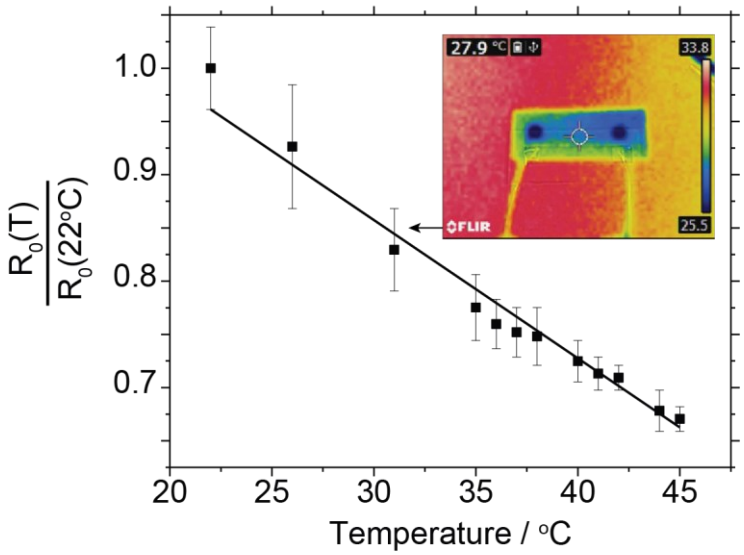


Figure 33 Resistance *vs.* Temperature Resistance of 12% CB-PDMS layered composite with Cu-pSi contacts as a function of temperature (normalized to resistance at 22°C).

6.2 - Wearables and Digital Healthcare

Intuitively, we need soft electronics to match the advances of engineering, electronics, and sensors with the versatility of biological systems and their compound movement. We need them to create robots for personalised therapy, prosthetics, handheld and wearable electronics compliant enough to be compatible with our bodies, skin, even internal tissues. The fields of Artificial Intelligence and Virtual Reality are moving into applicable maturity and gaining commercial interest very quickly. These predictive software capabilities and comfortable, imperceptible sensors find ways to seamlessly integrate in our daily lives.

6.2.1 - Wearable sensors in everyday life

Compliant electronics (wearable, flexible, stretchable) enabled by the composite systems described throughout Chapter one have enabled the creation for low-cost, portable, accessible, unobtrusive, personalized sensors with potential to alter more aspects of our lives than smartphones: from daily task completion like brushing our teeth and driving, to the way rehabilitation is practiced in the clinic. Soft sensors can be positioned where it was never before possible using rigid devices. Examples include

"sensorising" everyday objects in order to more intuitively control digital devices by clenching our teeth, practice surgeries with great fidelity, or navigating a virtual environment as easily as writing on a piece of paper.[116–118] As Nagels *et al.* put it "Devices with soft electronics have inherently greater mechanical degrees of freedom, and therefore provide new opportunities of interaction". [26] "Stretch to enter full-screen" and "twist to start camera" have the potential to be as strongly naturalized concepts as "swipe to unlock". The *squeeze dimension* found its way into mass market in Google's Pixel 2 smartphone (released October 2017). [119] More importantly, however, everyday objects like smartphones and pens to measure grip strength, and car seats to monitor posture are transformed into diagnostic devices.[120,121] Stretchable sensors made from elastomers like silicone can be easily and rapidly customised and personalised for a patient.

6.2.2 - Better Digital Healthcare, Remote Diagnostics, and quality of life

Wearable digital sensors offer quantification of motor behaviour, activity recognition and motor tracking across patient population with the potential to identify recovery mechanisms, remote monitoring, telerehabilitation, injury prevention and motor skills development in children as well as neurorehabilitation patients like stroke survivors. [122] Monitoring body motion can even offer clues to a patient's health status and aging process. [123] Studies tracking the movements of patients have been used to enhance occupational wellbeing and develop guidelines to prevent sports injuries. [124,125] Continuous monitoring of body movement can provide feedback on injury rehabilitation and give early detection of disorders that affect motor control like Parkinson's disease and cerebral palsy, and assessment of fine motor skills is one of the screening tests for conditions such as epilepsy. Gamification of treatment leads to greater engagement mainly due to the visual, direct feedback patients get throughout the duration of their activities. Faster recovery and faster task completion times are observed in numerous studies. [126]

Visual feedback and soft rehabilitation materials help patients who have been weakened by neurological disease or injury more easily communicate their movement. A study

showed that users could discriminate four times more discrete levels of motion with full visual feedback than without. [127] Automated decisions to improve treatment during a session using real-time sensor data and decision algorithms have also been implemented. [126] Big data enable personalisation of treatment and cloud computing can be used to identify and instruct healthcare professionals to take appropriate course of treatment. [123] Digital input from sensors resulting in visual feedback can also be provided in an interactive task to direct the patient to the appropriate therapeutic course. Another important feature of digital monitoring is the quantification of the patient's response. The approach currently employed by clinicians involves observing the patients performing certain movements, and then raking the patient's level according to qualitative descriptions in a benchmark classification scales. This method is often subjective and the scores can be inconsistent because they do not capture slight, progressive changes in patients' progress in response to therapy. There is a critical need to tackle the issue of imprecise assessment of motor disorders.

Consistent, objective metrics are using conforming, consistent, use-appropriate sensors to accurately track whether a treatment effectively treats symptoms are critical in the rehabilitation process. Point-of-care sensor systems allow frequent monitoring, which is highly desirable to offer a better understanding of the patient's short and long-term response to therapies, to tailor treatment and improve outcome and quality of life for patients. Finally, the potential for democratisation of rehabilitation, access to wider audience, at home is worth mentioning. Tailored state-of-the-art treatment can become available to weaker patients, tailored to their needs, young children, no more one size fits all, with self-improving digital solutions.

6.3 - Benefits of digital and gamification in healthcare and therapeutics

6.3.1 - Digital Feedback

Rehabilitation protocols involving physical, digital, and virtual reality feedback have been proven to improve the rehabilitation and engagement of patients and thus

speeding up their recovery. [128] Patients often fail to comply with the prescribed course of treatment or exercise given by their doctors, or do not have a way of measuring how effectively they have been performing an prescribed exercise, or if they have been doing it for the appropriate duration. Patient compliance is an important factor in improving health outcomes. Our soft sensor is aiming to improve feedback and information available to patients, and increase the available age groups that can use these digital rehabilitation devices. Devices available in the market or described in research are too large for children to use, or they are too rigid for senile and weaker patients to perform gripping exercises on. Our device addresses these issues in two ways: 1) They can be custom moulded to fit the desired shape and size of the user, 2) their hardness can be tuned over a range from 0.01 to 20 MPa, while gradients in modulus can target the exercise at specific areas of the hand (e.g. higher modulus for specific fingers). [129]

Digital technologies can massively improve recovery time and patient comfort. That said, in order to ensure patients adhere to their prescribed rehabilitation course, the digital devices and tools need to be easy to use and easy to understand. Our devices are easy to understand and use intuitively as they can be used instead of the soft training tools already used in clinics (Theraputty, foam blocks). Systems that are difficult to use put patients in risk of misusing them and this has a reportedly negative effect in the rehabilitation workflow and causes distrust for such systems. [130]

6.3.2 - Telerehabilitation

Compared with conventional rehabilitation, telerehabilitation reportedly offers easier access, mentoring for disabled patients (e.g. due to stroke), and greater involvement for patients who can record their mood, pain, and activity themselves. [131,132] As in the case of cognitive assessment, easy use soft sensors can offer unique insights on this front by providing in-depth analytics capabilities of not only the patients' quality of life, but also through the automated assessment of mental health condition.

Remote access to healthcare tools and courses of treatment enables the culmination of features such as autonomy, convenience, feedback on the course of treatment, increased

engagement, namely the gamification of treatment. The straightforward advantage of gamification is the higher level of adherence. Besides lessening the negative sentiments around diminished bodily function, neurological disease, or injury, as well as proven increased adherence numbers, gamification allows for personalisation of the course of treatment based on the patients' performance. In the next and final Chapter, the role of gamification in upper limb rehabilitation is explored and the technology developed to create mechanically robust soft pressure sensors is employed to improve the hardware used in hand therapy. Soft sensors are ideal for grip exercises because of the mismatch that exists between conventional monitoring tools (rigid electronics), and conventional exercise tools (soft materials). Movement disability can impact any part of the body, and we initially focus on hand rehabilitation, as recovering hand and arm function is the number one priority for disabled subjects in order to improve their quality of life. [133]

Chapter 7

Soft Sensor for Upper Limb Rehabilitation via Gamification and Real-Time Feedback

Digital and connected devices are essential for monitoring of progress and recovery in a patient's ability in today's upper limb rehabilitation course of therapy. Current assessments rely on therapist observation and static, inconsistent, analogue tools. The most prominent of these tools is the hand-dynamometer, a technology that has been around for more than 60 years, and which is hydraulic, insensitive, inflexible, yet found in the majority of clinics globally.

Following damage to the upper limb, assessment, rehabilitation and monitoring are essential if individuals are to regain independence. However, there is a large mismatch in the number of therapists and sessions available to the number of, as a result, underprovided patients, with inpatients in Europe receiving only approximately 10 mins of supervised hand and arm training per day. [134] There is a need for simple, objective, repetitive and remote tracking measures to that can be used by patients from hospital to home.

Beyond physical therapy, hand-grip strength, as a measure of whole-body strength in general is emerging as a top marker for wellness and chronic disease prediction e.g. cardiovascular disease, general ageing and frailty. Research suggests that grip strength testing should be done with every patient, alongside tests such as blood pressure. The current hand-dynamometer is not scalable for this purpose. [135]

The state of the art in sensorised devices for rehabilitation are robot-assisted devices which cost in excess of €10k, and specialist rehabilitation centres are needed. [136] Portable, lower cost app-based exercise platforms could also be used to improve hand

grip and rehabilitation; however these solutions are designed for able-person use and proper outcomes are not guaranteed for less-abled patients due to hardware limitations, including too few degrees of freedom in movement capture, limited range of motion, and lack of movement differentiation. [137] Most importantly, however, there is a general lack of soft stretchable sensors in the market. We address a market that uses soft devices as the standard of care, but also broadens the applicability of sensorised devices to weaker, more severely disabled patients as well as children. [138]

7.1 - Current standard in upper limb rehabilitation

Measuring grip strength is an important diagnost It also plays a key role in rehabilitation and occupational therapy to help with a range of neurological and musculoskeletal diseases such as arthritis, Cerebral Palsy, Parkinson's Disease, stroke, as well as with amputations and burns. [139] Grip strength exercises are frequently prescribed to patients as a form of rehabilitation to initiate and accelerate recovery, however, such forms of therapy do not provide immediate feedback to patients or healthcare professionals concerning the effectiveness of the rehabilitation strategy. The current standards of care for rehabilitation are soft objects like foams and putties but these do not provide any quantitative ways of measuring grip strength. Tools that doctors have to actually measure grip strength and monitor progress over time are bulky devices that are made of hard materials, restraining the range of motion of patients. These devices can only be used in a clinical setting and as such cannot be part of the patient's regular rehabilitation routine, especially for patients that are immobilised, frail, too young or depend on carers.

Soft elastomeric polymers, such as ethylene-vinyl acetate (foam blocks) or silicones (Theraputty) are used widely by occupational therapists when to provide therapy for patients of all ages and sexes, although decade old dynamometers are still used for grip strength assessment. Currently, digital monitoring equipment used in the clinic is expensive and inaccessible to patients with diminished prehensility due to malformation or smaller hand size (17% of people with hand disability are children).[140]

Providing patients with digital tools that allow self-led at-home therapy has been shown to improve treatment, patient engagement, long-term lifestyle adherence, while avoiding repeated visits to clinics plays an important role in frequency, effectiveness, and accessibility.

A low-cost, silicone-based soft sensor is presented here for hand therapy monitoring outside a clinical setting which harnesses the power of digital healthcare tools to promote adherence and accelerate recovery.

7.2 - Experimental details of hand exercise monitoring using a soft sensor and digital tools

This work has focused on creating devices to capture grip strength from a position where the hand is completely relaxed, to where a fist is fully formed. The technology developed is used to manufacture soft, unobtrusive strain sensors that allow for full range of motion during everyday activities and rehabilitation exercises for stroke and neurological patients to monitor their physiological condition and rehabilitation progress.

The hand rehabilitation device comprises an elastomeric silicone-carbon composite piezoresistive sensing element, solder-on Si contacts, and a silicone encapsulation classified as soft (30 Shore 00) and hard (20 Shore A).

Liquid Silicone Rubber (LSR) Ecoflex 30 Shore 00 and Dragon Skin 20 Shore A (Smooth-On Inc., Macungie, PA, USA) were used to encapsulate the sensing element and distribute the gripping force. Different device hardness is possible by layering silicones of different stiffness to accommodate the strength level of different patients.

7.2.1 - Moulding

We used 3D-printed moulds and an iterative methodology to manufacture the device at laboratory scale, based on feedback by specialist clinicians. The manufacturing methods presented were developed with industrial processes like injection moulding

batch manufacturing in mind. We use the methodology described in Chapter three to attach Cu-pSi solder-on contacts onto the CB-CSC to connect to read-out electronics.

Firstly, the assembled sensor was placed on a flat surface, and covered with the first half of the mould which was filled with silicone. This assembly was placed in the oven to allow for the silicone encapsulation to semi-cure. It has been shown that the optimal way to join silicone parts is by partially curing one before joining them. [141] The resistance of some devices increased two days after manufacturing which we believe is due to silicone penetration in the spongy CB-CSC matrix so a protective cellophane membrane was used in later iterations. To test this we made devices using pre-stretched CB-CSC sensing elements and observed a larger change in resistance. After 30 min at 40 °C the mould was fully assembled (Figure 34) and after a second silicone injection placed in the oven to fully cure overnight. The same procedure was used for both hard and soft silicone encapsulations. A schematic of the sensing element, contacts, and the proposed cylindrical mould for the grip force sensor are presented in Figure 34.

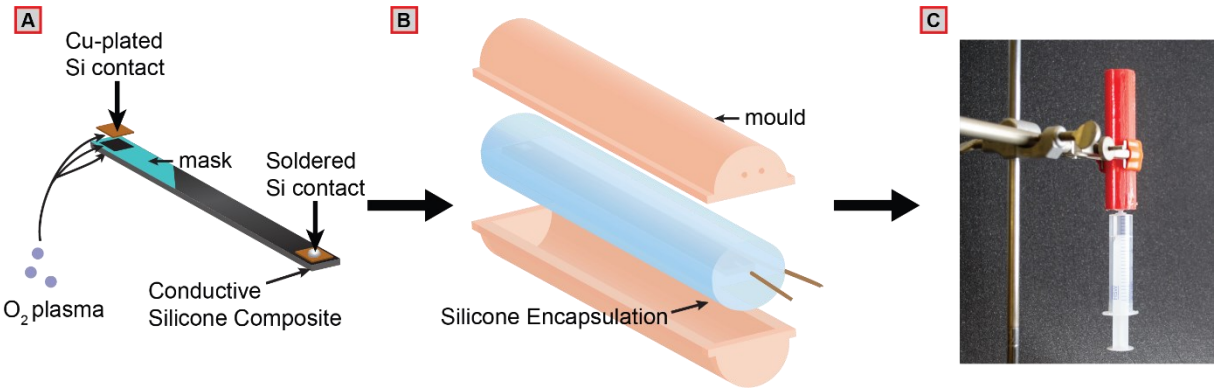


Figure 34 Hand-grip sensor manufacturing Squeezable cylinder manufacturing (A) Brief overview of CB-CSC/Cu-pSi sensing element manufacture (B) Mould fitting and sensing element encapsulation (C) Injection of silicone before the mould is transferred to cure

The lab-scale mould was designed to easily transition to injection moulding. Figure 35 shows the steps towards creating a two-shot overmoulded silicone sensor. The device consists of four key parts: 1) the sensor and contacts, 2) the first and 3) second silicone injections (Figure 35 B and C respectively), 4) the electronics housed in the hollow end of the dumbbell component (orange component, cavity visible in Figure 35E).

The two-shot mould has several design improvements. The sensing element is held securely in place at the centre of the mould by two holders (Figure 35A). This is to ensure that the sensor will be correctly aligned with a hand gripping this device and measure as closely as possible the total amount of force applied by the person gripping. The design of this first-stage component is such that when inserted in the second cylindrical mould the silicone material can flow throughout this component and reach the other side of the mould unobstructed. The transverse cross-section of the first mould resembles a smoothened quatrefoil (✦) in eclipsed conformation. The second-stage mould creates a simple dumbbell shaped component of the desired diameter which also houses the required electronics and batteries for wireless monitoring and communication with smartphones and tablets for real-time digital feedback, or the cloud for data storage.

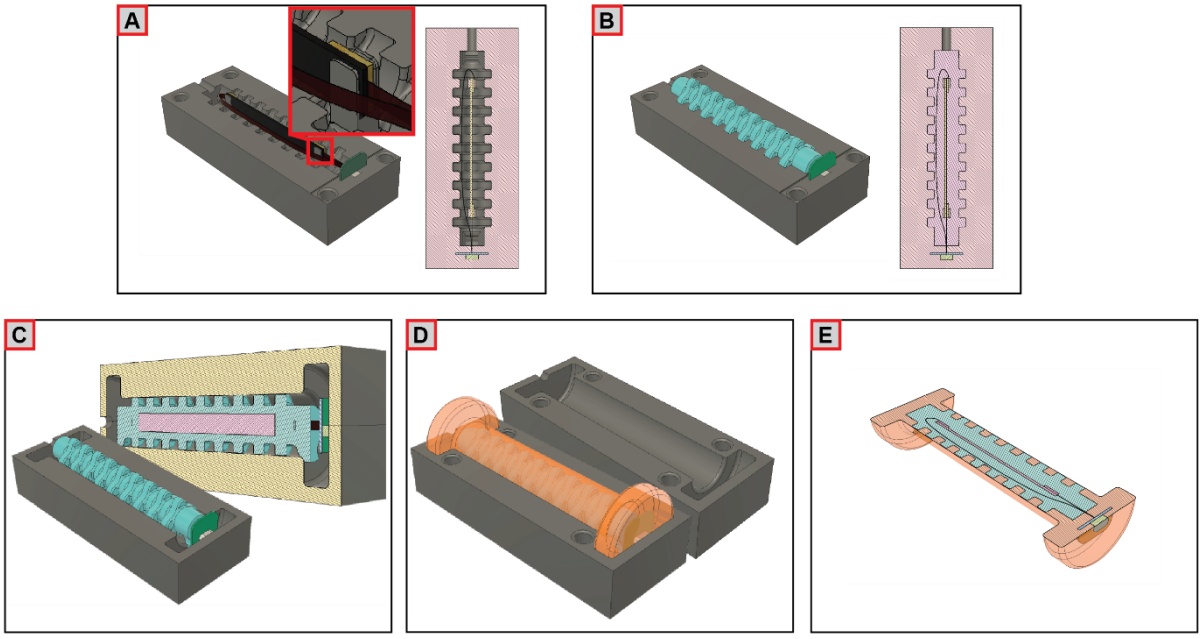


Figure 35 Silicone injection moulding (two-shot) (A) Mould for the encapsulation of the sensing element and contacts, there are two support holders at the centre of the mould to keep the sensor centred and in place (inset) (B) The mould in A after the first silicone injection; note the overspill ducts for excess silicone to escape during the injection (C) The component in B is placed in the second mould, the channels to allow for the second silicone injection to flow throughout the mould are visible in the cross-section (D) Finished moulded part with sensor encapsulated, two part mould vidible (E) Cross-section of finished part showing sensor in the same position as in A.

7.2.2 - Human grasp types and sensing modes

Silicone rubber can be prepared in a very wide range of hardness to match patient strength level and is ideal for skin contact application as it is already used for most special effects prosthetics. [142] The versatility of our manufacturing method and the combined flexibility of soft sensors and software, has the potential to build an interactive system to sense virtually all 33 identified GRASP types by integrating multiple sensors and device form factors and decoupling the signal digitally. [143,144] This can be done by conformally attaching our sensors on the surface of everyday objects. The complete list of grasp types (available online at http://grasp.xief.net) use an object that makes contact with the fingers or palm. By making these objects out of silicone or by attaching thin (1 mm) silicone sensors at the contact points, the pressure at these points can be measured.

Furthermore, we tested the capabilities of our sensors by applying different modes of strain. In Figure 36 we test twisting, bending, rolling and stretching and observe similar sensitivity for all modes with stretching being slightly higher. It is important to note that the behaviour and sensitivity in these experiments will depend on the shape of the CB-CSC sensing element we use. We have used a flat sensing element but depending on the requirements of the application cylindrical or non-uniform in terms of thickness elements can be used. A strain rosette can be constructed to indicate the direction of the principal strain direction and identify complex strain modes like the ones presented below. Strain data from various physical scenarios (e.g., stretching, rotating and squeezing) could be used to train machine learning classifiers (e.g., support vector machines, decision trees or K nearest neighbour) to identify the physical scenario. This could further provide diagnostic insights such as identifying individual finger strength when forming a closed fist. [145]

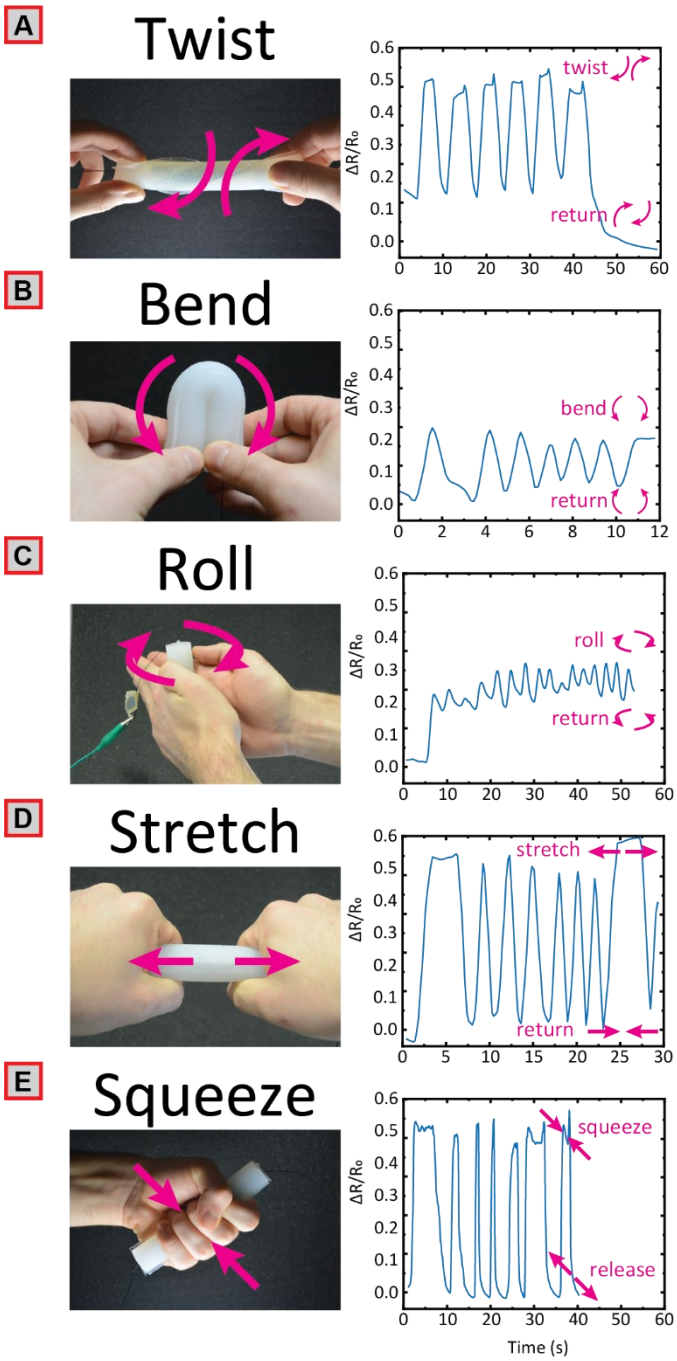


Figure 36 Sensing modalities for cylindrical squeezable sensor (A) Demo and resistance change signal for twisting (B) bending (C) rolling, which can also be done on a flat table surface and (D) stretching (E) squeezing.

7.2.3 - Participants and test design

A sample size of ten healthy participants, which is standard for hand grip sensor trials as seen in systematic reviews of the literature assessing post-stroke rehabilitation, three female and seven male, between 24 and 36 years old, volunteered for the study (nine

were right handed and one was left handed). [122,146,147] The participants took two different hand grip exercise tests in random order:

- Test 1 was a feedforward exercise which involved controlled grip strength to guide a flying cartoon character ("Red Bird") through the level and collect as many floating stars which were arranged in a sinusoidal path while following this path closely and smoothly (Figure 37A).
- Test 2, involved an activity with visual feedback on a tablet, whereby a cartoon character ("Tutu Bear") speeds up when continuously gripping to maximum strength (Figure 37B). The goal is to get the character to the finish line as quickly as possible (the selected level takes approximately 30 s to complete).

All participants understood the purpose of the study and the instructions for each test and a safety assessment was carried out beforehand. The software (both Test games) and hardware (tablet) the games were played on were provided by Gripable Ltd.

The purpose of Test 1 was to assess the ability of the test subjects to follow a smooth sinusoidal path by exerting the force necessary to keep the "Red Bird" on that path. We characterise the effectiveness of each test subject in three ways: 1) the Score counts how many stars the subject collected, which is an indication of whether the "Red Bird" followed the star path, 2) peak signal ($\Delta R/R_0$) averaged over the number of times the subject squeezes during the Test, 3) Cross-Correlation is a normalised coefficient which describes how similar the path followed by the test subject is with the smooth sinusoidal star path, the closer to 1, the more similar the signals are (Figure 37E).

For Test 2, the participants were instructed to squeeze to the maximum of their ability and fully release their grip before squeezing again. The faster they repeat this the faster the "Tutu Bear" character moves forward. The goal of the game is to cross the finish line in the shortest amount of time. The performance metrics are: 1) Time to reach the finish line; 2) $\Delta R/R_0$ peak, as above; 3) The frequency of squeezing measured in number of squeezes per level.

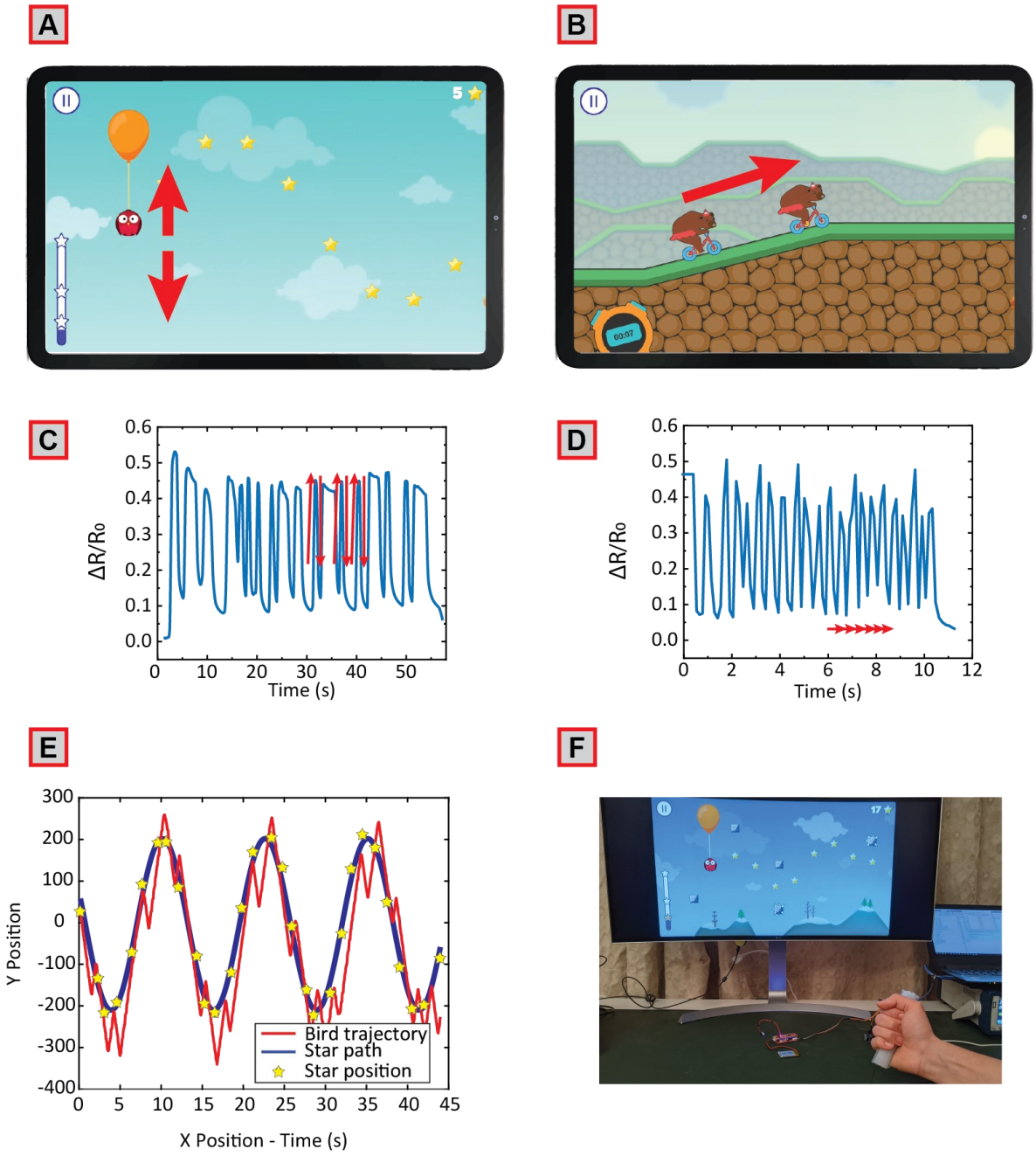


Figure 37 Screen recording from gameplay (A) activity used for Test 1 showing the "Red Bird" character and moving capabilities (squeeze to rise, release to drop) (B) gameplay from activity used in Test 2 showing how "Tutu Bear" moves (C) Collected data from a Test 1 participant, red lines show upwards direction when squeezing and downwards when releasing (D) Collected data from a Test 2 participant, red arrows show how movement occurs when pressure is released (E) Graph showing part of the data analysis used to determine cross-correlation between the bird's trajectory and the smooth star path in Test 1 (F) Live action during Test 1 showing participant's hand and squeezable device in hand

We initially expected that the Tests would require less force to get a high signal using the Soft devices. However, subjects needed to apply more pressure to the Soft devices

compared to the Hard devices to reach the same signal which is reflected in the higher sensitivity of the hard silicone device (Figure 38). Stress, strain shows that strain required to reach 300 N is lower with dragon skin, same for 50 N and 100 N. The Hard devices were also more responsive as evident in Figure 38B – stress *vs* $\Delta R/R_0$ which could also drive subjects to apply more force. The soft material dampens the sensitivity of the sensors and the observed result is that participants squeeze harder especially in a Test 2 scenario. Other soft robotic assistive actuators have been specifically designed to assist the variable moving parts of the hand. [148] Similarly, we can accommodate the requirement for non-uniform pressure coming from ulnar and radial parts of the hand or fingers depending on the patient's requirements. Soft actuators have the long term disadvantages of significant hysteresis and budging due to the combination of materials used to achieve variable stiffness. [149] Our devices use Si-based materials and semi-cured bonding (silicone layer fuse together) which creates a monolithic structure.

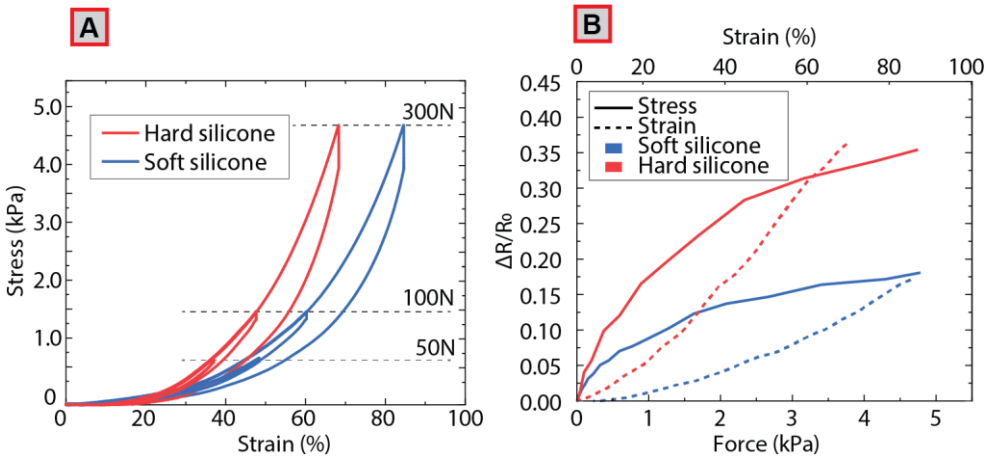


Figure 38 CB-CSC/Cu-pSi devices encapsulated in Hard and Soft silicone Electromechanical characterisation: (A) Stress – strain relationship at various pressure levels (B) Force – sensitivity and Strain – sensitivity relationships

Table 7.2-1 Performance metrics for Test 1 (Red Bird) and Test 2 (Tutu Bear) for Hard and Soft silicone encapsulation devices; Score (Test 1): has a maximum of 30 stars collected; Peak % (Test 1): represents ; R/R_0 for the change of resistance at the maximum when the device is squeezed over the resistance at rest; Cross-correlation: shows how similar the Bird Trajectory and Star Path are (maximum 1); Score (Test 2): is the time taken to complete

the level (lower is better); Peak % (Test 2): represents ; R/R_0 between the maximum squeeze and at rest states; # Peaks: is the mean number of squeezes the subjects needed to complete the level (n = 10)

Test 1	Hard (Dragon Skin)	Soft (Ecoflex)
Score /30	29.75 (SD 0.43)	29.5 (SD 0.76)
Peak %	24.5 (SD 4.1)	31.7 (SD 6.5)
Cross-correlation	0.899 (SD 0.038)	0.914 (SD 0.017)
Test 2		
Score	18.5 (SD 2.56)	16.34 (SD 0.87)
Peak %	30.6 (SD 4.5)	39.3 (SD 7.0)
# Peaks	22.25 (SD 4.43)	23.00 (SD 4.53)

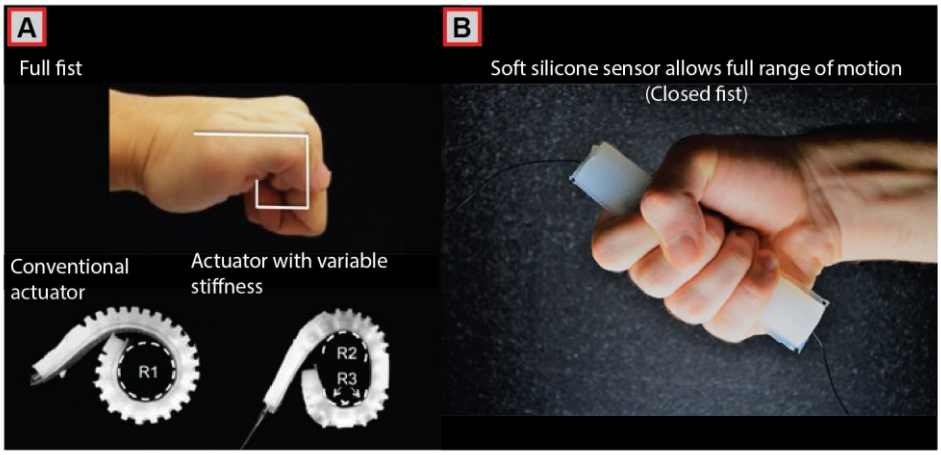


Figure 39 Closed fist using squeezable sensor (A) Comparison between the orientation of the fingers in a closed fist, in a conventional actuator and a more closely mimicking actuator with variable stiffness [148] (B) Soft silicone squeezable sensor in a closed fist allows user to full for their fist

In conclusion, we have presented an alternative to expensive and rigid devices, which are sometimes hard to use and exclude many demographics, least of all children whose development is crucial. We show how our device can be used in digital therapeutics and rehabilitation which is a field that can help patients get more personalised therapy, more often, and with less disruption to visit the clinic when they do not have to. We discuss the benefits of a device specifically designed with soft materials in order to allow users to fully form a closed grip. Rigid devices by design cannot let the user do this. Finally, we saw that contrary to what we expected test subjects applied more pressure to the softer device in order to be successful in their game activity. This opens up future

study in variable stiffness devices as well as multimodal and multidirectional sensing to better understand the effect of device hardness on gripping force, hand shape, and rehabilitation progress. We are working with occupational therapy and child cerebral palsy rehabilitation experts to deliver this technology.

7.3 - Commercial outlook

Despite major improvements in primary prevention and acute treatment over the last decades, neurological diseases are still devastating for patient quality of life. At the beginning of the 21st century, the standardized incidence of stroke in Europe were on average approximately 209 per 100,000 per year, with one-month case-fatality rates ranging from 13 to 35%. Approximately 1.1 million inhabitants of Europe suffer a stroke each year, and ischemic stroke accounts for approximately 80% of cases. In addition, because of the ageing population, the absolute number of stroke is expected to dramatically increase in coming years: by 2025, 1.5 million European people will suffer a stroke each year. [150]

The number of people in the UK alone living with an arm disability is 1.2 million, and 500 million worldwide. Their conditions include stroke, multiple sclerosis, Parkinson's, wrist fractures, arthritis, sporting injuries, car accidents, and more, with varying degrees of disabilities so they require sustained, long periods of rehabilitation sometimes lasting for years. This means that the demand is usually a lot higher than the supply of highly specialised therapy for these patients. Physical rehabilitation is a labour-intensive service, requiring professionally-trained therapists performing one-on-one assessment and therapy sessions with disabled patients. The most effective therapeutic intervention shown to improve movement is repetitive exercise, which means that the more therapy a patient receives, the faster they recover. Recommended therapy durations are often not realised due to resource limitations. The Covid-19 pandemic has compounded this challenge, placing significant additional strain on healthcare and social welfare resources. Hospitalised patients are discharged more rapidly to avoid contagion while therapy in a shared environment is more limited given social isolation and therapist reassignments.

As a service, current approaches to treat hand disability use subjective observation to assess and review progress. Therapeutic intervention is aimed at improving hand function, including the use of two hands together. However, there is no established method to monitor or assess current ability or to set therapy goals. A method to measure outcomes of training exercises using one or both hands, like a grip force sensor useable by all ages including children will help create specific therapy protocols including the planning stage, treatment stage, and measuring of outcomes.

One of the unique benefits of using soft sensors in hand rehabilitation is the inclusion of patients who were too weak to use conventional monitoring equipment and more importantly, children of young ages even around 2 years old. Additionally, the engagement with children in order to adhere to the training routine is critical since children who neglect to use their two hands together, have reduced function, neurological developmental changes and impaired independence. [151] A therapy course based on intense repetitions enables practice of skills in a familiar context, similar to common everyday activities, and promotes neuroplasticity which is especially important for children because early therapy is effective in improving psychological and future occupational abilities which tails off by age 2.5. [152–154]

The general impact of the solution presented in this Chapter aims to improve the current standard of hand grip therapeutic exercises in five ways: A) by bringing the rehabilitation at home, there is cost reduction as patients need to visit the clinic less, B) a larger audience is addressed by making a compliant monitoring device with tuneable softness commercially available, C) a larger audience can have access to digital tools which increase engagement and adherence of patients and in turn the effectiveness of the treatment, D) monitoring and training at the same time improves the course of treatment prescribed by the clinician thus decreasing the time of recovery, E) using a soft sensor other forms of data besides grip strength can be collected simultaneously such as individual finger strength, rolling motion on flat surface, and torsion using a single device. In future iterations of the device, a strain rosette sensor arrangement and multiple independently operating sensors should be investigated.

Conclusions and Outlook

In conclusion, we have presented a new technology for creating mechanically robust, covalently-bonded, Si-based electrical contacts for silicone-based stretchable CPC sensors and electrical devices. Unlike the existing solutions, the technology proposed is reliable, low-cost (cost of materials for two 5×5 mm^2 Cu-pSi contacts is $\$3\times10^{-3}$) and simple, consisting of only three steps for the fabrication and attachment of the contacts in a standard laboratory environment – *i.e.* formation of nanoporous Si, electroplating with Cu and plasma-bonding on silicone-based conductive composites. The Cu-pSi contact technology is compatible with large-volume manufacturing through the use of large Si wafers and has the potential to be the enabler of new classes of miniaturized silicone-based commercial stretchable devices with monolithically-integrated electrical contacts.[155–158] Low-cost devices enabled by this technology makes sensors more accessible and reduces the time and money needed to, for instance, go through an upper-limb rehabilitation process.

One of the most important features of the Cu-pSi technology is that the contacts do not fail gradually (regardless of whether the devices created are subjected to repeated, increasing or sustained mechanical stress) but instead fail catastrophically. This means that the devices produced using the Cu-pSi technology will either produce a correct signal or do not produce a signal at all; this is especially important for applications in healthcare – *e.g.,* disease diagnostics, rehabilitation monitoring – where wrong signals may lead to a different course of medical intervention.

The electrical behaviour of CB-CSC devices with Cu-pSi contacts under DC and AC showed a complex response for which a framework of assumptions was set forward to help in future studies. The sensors produced stable, repeatable resistance response to pressure at 300 kHz. In the future, a highly reliable, battery-powered, portable, wireless, low-cost and integrated sensing systems using silicone-based stretchable sensors can be created following the methodology in this work. Using a mobile device, such as a smartphone, the data generated by the sensors can be easily processed and stored on

the cloud with capabilities for remote-access, important for applications in connected/digital healthcare. [115,159]

The squeezable device developed, in particular, can find immediate applications in the rehabilitation of patients with neurological diseases. Healthy subjects were able to consistently complete two Tests using the device to control digital characters on a screen. The amount of pressure they exerted was controlled by the hardness of the encapsulation material. They were inclined to squeeze harder on the softer device because of the overall reduced sensitivity. The device was designed with clinical considerations in mind. A low-cost solution enables general access to the treatment too. A soft sensor that could be moulded to any shape, including everyday objects, increases accessibility and engagement with the sensor. Additionally, a soft sensor also allows for full range of motion. Finally, tuning the hardness of the sensor enables progressive training. This device can be manufactured in large scale using two-shot injection moulding of silicone rubber.

In summary, Cu-pSi creates robust contacts with silicone CPC sensors for wearable devices with applications in digital healthcare monitoring ranging from a breathing harness to hand rehabilitation tools. Next steps in the development of these devices should integrate portable LCR and sine wave (AC) generator electronics into a soft device that can communicate to phones and tablets via Bluetooth. Squeezable devices can then be used in the clinic to monitor and treat neurological, bimanual, and occupational therapy.

Bibliography

[1] J. Bardeen, W. H. Brattain, *Three Electrode Circuit Element Utilizing Semiconductive Materials*, 1948.

[2] W. Shockley, *Proceedings of the IEEE* 1998, *86*, 34.

[3] A. Chortos, G. I. Koleilat, R. Pfattner, D. Kong, P. Lin, R. Nur, T. Lei, H. Wang, N. Liu, Y.-C. Lai, M.-G. Kim, J. W. Chung, S. Lee, Z. Bao, *Advanced Materials* 2016, *28*, 4441.

[4] J. Xu, S. Wang, G. J. N. Wang, C. Zhu, S. Luo, L. Jin, X. Gu, S. Chen, V. R. Feig, J. W. F. To, S. Rondeau-Gagné, J. Park, B. C. Schroeder, C. Lu, J. Y. Oh, Y. Wang, Y. H. Kim, H. Yan, R. Sinclair, D. Zhou, G. Xue, B. Murmann, C. Linder, W. Cai, J. B. H. Tok, J. W. Chung, Z. Bao, *Science* 2017, *355*, 59.

[5] R. Herbert, J. H. Kim, Y. S. Kim, H. M. Lee, W. H. Yeo, *Materials* 2018, *11*, 187.

[6] C. O. Okoye, I. Jones, M. Zhu, Z. Zhang, D. Zhang, *Journal of Cleaner Production* 2021, *279*, 123336.

[7] J. W. Dally, G. A. Panizza, *Experimental Mechanics* 1972, *12*, 124.

[8] M. H. Lee, H. R. Nicholls, *Mechatronics* 1999, *9*, 1.

[9] J. A. Rogers, T. Someya, Y. Huang, *Science (New York, N.Y.)* 2010, *327*, 1603.

[10] F. Garnier, R. Hajlaoui, A. Yassar, P. Srivastava, *Science* 1994, *265*, 1684.

[11] D. H. Kim, N. Lu, R. Ma, Y. S. Kim, R. H. Kim, S. Wang, J. Wu, S. M. Won, H. Tao, A. Islam, K. J. Yu, T. il Kim, R. Chowdhury, M. Ying, L. Xu, M. Li, H. J. Chung, H. Keum, M. McCormick, P. Liu, Y. W. Zhang, F. G. Omenetto, Y. Huang, T. Coleman, J. A. Rogers, *Science* 2011, *333*, 838.

[12] K. Rajan, E. Garofalo, A. Chiolerio, *Sensors* 2018, *18*, 367.

[13] Z. Rao, F. Ershad, A. Almasri, L. Gonzalez, X. Wu, C. Yu, *Advanced Materials Technologies* 2020, *5*, DOI 10.1002/admt.202000233.

[14] C. Xu, Y. Yang, W. Gao, *Matter* 2020, *2*, 1414.

[15] S. Duan, K. Yang, Z. Wang, M. Chen, L. Zhang, H. Zhang, C. Li, *ACS Applied Materials & Interfaces* 2016, *8*, 2187.

[16] A. Bonyár, H. Sántha, B. Ring, M. Varga, J. Gábor Kovács, G. Harsányi, *Procedia Engineering* 2010, *5*, 291.

[17] D. Qi, K. Zhang, G. Tian, B. Jiang, Y. Huang, *Advanced Materials* 2021, *33*, 2003155.

[18] S. Nagels, W. Deferme, *Materials* 2018, *11*, 375.

[19] J. Chen, Q. Yu, X. Cui, M. Dong, J. Zhang, C. Wang, J. Fan, Y. Zhu, Z. Guo, *Journal of Materials Chemistry C* 2019, *7*, 11710.

[20] D. Qi, K. Zhang, G. Tian, B. Jiang, Y. Huang, *Advanced Materials* 2021, *33*, 2003155.

[21] D.-H. Kim, J.-H. Ahn, W. M. Choi, H.-S. Kim, T.-H. Kim, J. Song, Y. Y. Huang, Z. Liu, C. Lu, J. A. Rogers, *Science (New York, N.Y.)* 2008, *320*, 507.

[22] S. P. Lacour, J. Jones, S. Wagner, Teng Li, Zhigang Suo, *Proceedings of the IEEE* 2005, *93*, 1459.

[23] W. J. Arora, R. Ghaffari, *EXTREMELY STRETCHABLE ELECTRONICS* , 2019, US 10 , 383 , 219 B2.

[24] J. M. Engel, N. Chen, K. Ryu, *Technical Digest of the 12th Solid State Sensors, Actuator, and Microsystems Workshop (Hilton Head Island, SC, USA, 4-8 June 2006)* n.d., 316.

[25] M. Khatib, T. Huynh, Y. Deng, Y. D. Horev, W. Saliba, W. Wu, H. Haick, *Small* 2018, *15*, 1803939.

[26] S. Nagels, W. Deferme, *Materials* 2018, *11*, 375.

[27] M. Mosallaei, D. di Vito, B. Khorramdel, M. Mäntysalo, *Flexible and Printed Electronics* 2020, *5*, 015004.

[28] H. J. Shim, S. Sunwoo, Y. Kim, J. H. Koo, D. Kim, *Advanced Healthcare Materials* 2021, 2002105.

[29] T. Sekitani, T. Someya, *Advanced Materials* 2010, *22*, 2228.

[30] W. J. Song, M. Kong, S. Cho, S. Lee, J. Kwon, H. bin Son, J. H. Song, D. G. Lee, G. Song, S. Y. Lee, S. Jung, S. Park, U. Jeong, *Advanced Functional Materials* 2020, *30*, 2003608.

[31] "Stretchable Electronics Market Segment, Size, Share, Global Trends, 2026 | MRFR," can be found under https://www.marketresearchfuture.com/reports/stretchable-electronics-market-5826, n.d.

[32] E. Sen-Gupta, D. E. Wright, J. W. Caccese, J. A. Wright Jr., E. Jortberg, V. Bhatkar, M. Ceruolo, R. Ghaffari, D. L. Clason, J. P. Maynard, A. H. Combs, *Digital Biomarkers* 2019, *3*, 1.

[33] J.-H. Hong, J. M. Shin, G. M. Kim, H. Joo, G. S. Park, I. B. Hwang, M. W. Kim, W.-S. Park, H. Y. Chu, S. Kim, *Journal of the Society for Information Display* 2017, *25*, 194.

[34] S. S. Baishya, B. Bäuml, in *IEEE International Conference on Intelligent Robots and Systems*, Institute Of Electrical And Electronics Engineers Inc., 2016, pp. 8–15.

[35] S. B. Lao, *Wearable Tactile Pressure Sensing for Compression Garments and Control of Active Compression Devices*, University Of Waterloo, 2015.

[36] H. Q. Zhang, J. C. Teoh, J.-F. Wu, L. T. Yu, R.-H. Wang, D. M. Francis, C. T. Lim, *An Electronic Skin Readout System for Liquid Metal Based Flexible Resistive Sensor Array*, Preprints, 2020.

[37] D. H. Kang, J. H. Lee, J. W. Lee, H. S. Cho, S. H. Park, K. H. Lee, S. J. Kang, *Journal of Medical Systems* 2021, *45*, 1.

[38] S. Xu, Y. Zhang, L. Jia, K. E. Mathewson, K.-I. Jang, J. Kim, H. Fu, X. Huang, P. Chava, R. Wang, S. Bhole, L. Wang, Y. J. Na, Y. Guan, M. Flavin, Z. Han, Y. Huang, J. a Rogers, *Science* 2014, *344*, 70.

[39] Y.-S. Kim, J. Lu, B. Shih, A. Gharibans, Z. Zou, K. Matsuno, R. Aguilera, Y. Han, A. Meek, J. Xiao, M. T. Tolley, T. P. Coleman, *Advanced Materials* 2017, *29*, 1701312.

[40] G. S. Jeong, D.-H. Baek, H. C. Jung, J. H. Song, J. H. Moon, S. W. Hong, I. Y. Kim, S.-H. Lee, *Nature Communications* 2012, *3*, 977.

[41] Y. T. Kwon, Y. S. Kim, S. Kwon, M. Mahmood, H. R. Lim, S. W. Park, S. O. Kang, J. J. Choi, R. Herbert, Y. C. Jang, Y. H. Choa, W. H. Yeo, *Nature Communications* 2020, *11*, 1.

[42] J. Park, S. Wang, M. Li, C. Ahn, J. K. Hyun, D. S. Kim, D. K. Kim, J. A. Rogers, Y. Huang, S. Jeon, H. C. Ko, T. Someya, T. Someya, T. Sekitani, D.-Y. Khang, H. Jiang, Y. Huang, J. A. Rogers, T. Sekitani, K.-Y. Chun, T. Li, Z. Huang, Z. Suo, S. P. Lacour, S. Wagner, S. Jeon, J. Park, J. Park, S. Yoon, K. Kang, S. Jeon, S. Jeon, Y.-S. Nam, D. J.-L. Shir, J. A. Rogers, J. H. Moon, S. Yang, P. M. Dentinger, W. M. Clift, S. H. Goods, J. H. Jang, C. K. Ullal, T. Gorishnyy, V. v. Tsukruk, E. L. Thomas, J. H. Moon, J. Ford, S. Yang, J. N. Lee, C. Park, G. M. Whitesides, S. Jeon, S. Jeon, V. Malyarchuck, J. O. White, J. A. Rogers, L. Miao, J. C. Lötters, S. Singamaneni, M. D. Dickey, T. Sekitani, R. K. Kramer, C. Majidi, R. J. Wood, S. Cheng, Z. Wu, D. J. Lipomi, M. Kubo, H.-J. Kim, C. Son, B. Ziaie, J.-H. So, *Nature Communications* 2012, *3*, 916.

[43] A. Larmagnac, S. Eggenberger, H. Janossy, J. Vörös, *Scientific Reports* 2014, *4*, DOI 10.1038/srep07254.

[44] S. P. Stier, H. Böse, *Micromachines* 2021, *12*, 255.

[45] Y. Liu, H. Wang, W. Zhao, M. Zhang, H. Qin, Y. Xie, *Sensors* 2018, *18*, 645.

[46] B. Caulfield, B. Reginatto, P. Slevin, *npj Digital Medicine* 2019, *2*, 1.

[47] H. R. Shanks, P. D. Maycock, P. H. Sidles, G. C. Danielson, *Physical Review* 1963, *130*, 1743.

[48] by E. James Mark, by Nino Russo, V. Ya Antochencko, *Journal of the American Chemical Society* 2009, *131*, 16330.

[49] H. Watanabe, N. Yamada, M. Okaji, *International Journal of Thermophysics* 2004, *25*, 221.

[50] Z. Xie, R. Avila, Y. Huang, J. A. Rogers, *Advanced Materials* 2020, *32*, 1902767.

[51] Y. Zhang, Z. Huo, X. Wang, X. Han, W. Wu, B. Wan, H. Wang, J. Zhai, J. Tao, C. Pan, Z. L. Wang, *Nature Communications* 2020, *11*, 1.

[52] T. Nguyen, M. Khine, *Polymers* 2020, *12*, 1.

[53] A. Hirsch, L. Dejace, H. O. Michaud, S. P. Lacour, *Accounts of Chemical Research* 2019, *52*, 534.

[54] A. L. Kadilak, Y. Liu, S. Shrestha, J. R. Bernard, W. E. Mustain, L. M. Shor, *Journal of Electroanalytical Chemistry* 2014, *727*, 141.

[55] J.-H. Kong, N.-S. Jang, S.-H. Kim, J.-M. Kim, *Carbon* 2014, *77*, 199.

[56] Y. Zheng, Y. Li, Z. Li, Y. Wang, K. Dai, G. Zheng, C. Liu, C. Shen, *Composites Science and Technology* 2017, *139*, 64.

[57] N. Lu, C. Lu, S. Yang, J. Rogers, *Advanced Functional Materials* 2012, *22*, 4044.

[58] Y. Zare, K. Y. Rhee, *Composites Science and Technology* 2018, *155*, 252.

[59] I. Kang, M. J. Schulz, J. H. Kim, V. Shanov, D. Shi, *Smart Materials and Structures* 2006, *15*, 737.

[60] H. Münstedt, Z. Starý, *Polymer* 2016, *98*, 51.

[61] T. Lu, L. Finkenauer, J. Wissman, C. Majidi, *Advanced Functional Materials* 2014, *24*, 3351.

[62] M. D. Bartlett, E. J. Markvicka, C. Majidi, *Advanced Functional Materials* 2016, 8496.

[63] M. Tavakoli, R. Rocha, L. Osorio, M. Almeida, A. de Almeida, V. Ramachandran, A. Tabatabai, T. Lu, C. Majidi, *Journal of Micromechanics and Microengineering* 2017, *27*, 035010.

[64] M. Amjadi, K. U. Kyung, I. Park, M. Sitti, *Advanced Functional Materials* 2016, *26*, 1678.

[65] M. Amjadi, A. Pichitpajongkit, S. Lee, S. Ryu, I. Park, *ACS Nano* 2014, *8*, 5154.

[66] E. Roh, B.-U. Hwang, D. Kim, B.-Y. Kim, N.-E. Lee, *ACS Nano* 2015, *9*, 6252.

[67] M. Amjadi, Y. J. Yoon, I. Park, *Nanotechnology* 2015, *26*, 375501.

[68] Y. Sun, W. M. Choi, H. Jiang, Y. Y. Huang, J. A. Rogers, *Nature Nanotechnology* 2006, *1*, 201.

[69] S. Jeong, K. Hjort, Z. Wu, S. H. Jeong, K. Hjort, Z. Wu, *Sensors* 2014, *14*, 16311.

[70] J. van den Brand, R. Kusters, M. Barink, A. Dietzel, *Microelectronic Engineering* 2010, *87*, 1861.

[71] D. Ruh, P. Reith, S. Sherman, M. Theodor, J. Ruhhammer, A. Seifert, H. Zappe, *Advanced Materials* 2014, *26*, 1706.

[72] N. Salowitz, Z. Guo, Y.-H. Li, K. Kim, G. Lanzara, F.-K. Chang, *Journal of Composite Materials* 2013, *47*, 97.

[73] P. Mach, A. Geczy, R. Polanský, D. Bušek, *Journal of Materials Science: Materials in Electronics* 2019, *30*, 4895.

[74] M. J. Owen, *Journal of Applied Polymer Science* 1988, *35*, 895.

[75] J. Kim, A. Banks, H. Cheng, Z. Xie, S. Xu, K. I. Jang, J. W. Lee, Z. Liu, P. Gutruf, X. Huang, P. Wei, F. Liu, K. Li, M. Dalal, R. Ghaffari, X. Feng, Y. Huang, S. Gupta, U. Paik, J. A. Rogers, *Small* 2015, *11*, 906.

[76] S. Xu, Y. Zhang, L. Jia, K. E. Mathewson, K.-I. Jang, J. Kim, H. Fu, X. Huang, P. Chava, R. Wang, S. Bhole, L. Wang, Y. J. Na, Y. Guan, M. Flavin, Z. Han, Y. Huang, J. A. Rogers, *Science (New York, N.Y.)* 2014, *344*, 70.

[77] K.-I. Jang, A. Banks, P. Won, Y. Li, J. A. Rogers, B. H. Kim, R. Xu, S. Ma, J. W. Lee, U. Paik, J. Kim, Y. H. Kwon, Y. Huang, K. J. Yu, J. Y. Choe, S. W. Jang, S. Huh, S. Lee, S. Xu, Y. Yang, *Proceedings of the National Academy of Sciences* 2016, *113*, 6131.

[78] S. Biswas, J. Reiprich, T. Cohrs, D. T. Arboleda, A. Schoeberl, M. Mozafari, L. Schlag, T. Stauden, J. Pezoldt, H. O. Jacobs, *Advanced Materials Technologies* 2017, *2*, 1700131.

[79] H. Kaneko, J. Horie, *Respiratory Care* 2012, *57*, 1442.

[80] W. Wu, J. Wu, J. H. Kim, N. Y. Lee, *Lab on a Chip* 2015, *15*, 2819.

[81] M. K. Chaudhury, G. M. Whitesides, *Langmuir* 1991, *7*, 1013.

[82] R. Peng, D. Li, *Lab on a Chip* 2016, *16*, 3767.

[83] T. Trantidou, Y. Elani, E. Parsons, O. Ces, *Microsystems and Nanoengineering* 2017, *3*, 1.

[84] M. I. Butrón-García, J. A. Jofre-Reche, J. M. Martín-Martínez, *Applied Surface Science* 2015, *332*, 1.

[85] A. Tiwari, L. Dorogin, A. I. Bennett, K. D. Schulze, W. G. Sawyer, M. Tahir, G. Heinrich, B. N. J. Persson, *Soft Matter* 2017, *13*, 3602.

[86] E. M. Liston, L. Martinu, M. R. Wertheimer, *Journal of Adhesion Science and Technology* 1993, *7*, 1091.

[87] L. Li, C. P. Wong, in *Proceedings - Electronic Components and Technology Conference*, 2013, pp. 2326–2331.

[88] Z. Huang, N. Geyer, P. Werner, J. de Boor, U. Gösele, *Advanced Materials* 2011, *23*, 285.

[89] X. Leng, C. Wang, Z. Yuan, in *Procedia CIRP*, Elsevier B.V., 2020, pp. 26–32.

[90] A. Backes, U. Schmid, *Sensors and Actuators, B: Chemical* 2014, *193*, 883.

[91] S. Jana, S. Mondal, S. R. Bhattacharyya, *Journal of Nanoscience and Nanotechnology* 2013, *13*, 3983.

[92] Y. Qu, L. Liao, Y. Li, H. Zhang, Y. Huang, X. Duan, *Nano Lett.* 2009, *9*, 4539.

[93] Z. Huang, N. Geyer, P. Werner, J. de Boor, U. Gösele, *Advanced Materials* 2011, *23*, 285.

[94] H. Han, Z. Huang, W. Lee, *Nano Today* 2014, *9*, 271.

[95] S. A. Znati, N. Chedid, H. Miao, L. Chen, E. E. Bennett, H. Wen, *Journal of surface engineered materials and advanced technology* 2015, *5*, 207.

[96] C. Fang, E. Foca, S. Xu, J. Carstensen, H. Föll, *Journal of The Electrochemical Society* 2007, *154*, D45.

[97] H. Oppermann, L. Dietrich, *Microelectronics Reliability* 2012, *52*, 356.

[98] F. Güder, Y. Yang, U. M. Kücìükbayrak, M. Zacharias, *ACS Nano* 2013, *7*, 1583.

[99] M. Grell, C. Dincer, T. Le, A. Lauri, E. Nunez Bajo, M. Kasimatis, G. Barandun, S. A. Maier, A. E. G. Cass, F. Güder, *Advanced Functional Materials* 2019, *29*, 1804798.

[100] R. A. Lai, T. M. Hymel, V. K. Narasimhan, Y. Cui, *ACS Applied Materials and Interfaces* 2016, *8*, 8875.

[101] C. Boehler, F. Güder, U. M. Kücükbayrak, M. Zacharias, M. Asplund, *Scientific Reports* 2016, *6*, 19574.

[102] K. Fukami, K. Kobayashi, T. Matsumoto, Y. L. Kawamura, T. Sakka, Y. H. Ogata, *Journal of The Electrochemical Society* 2008, *155*, D443.

[103] US Department of Health and Human Services, "No Title," n.d.

[104] J. Kim, M. Lee, H. J. Shim, R. Ghaffari, H. R. Cho, D. Son, Y. H. Jung, M. Soh, C. Choi, S. Jung, K. Chu, D. Jeon, S. T. Lee, J. H. Kim, S. H. Choi, T. Hyeon, D. H. Kim, *Nature Communications* 2014, *5*, DOI 10.1038/ncomms6747.

[105] D.-Y. Khang, H. Jiang, Y. Huang, J. A. Rogers, *Science (New York, N.Y.)* 2006, *311*, 208.

[106] J.-H. So, A. S. Tayi, F. Güder, G. M. Whitesides, *Advanced Functional Materials* 2014, *24*, n/a.

[107] S. Roy, A. Kumar, *Composite Structures* 2017, *181*, 1.

[108] M. A. Kashfipour, N. Mehra, J. Zhu, n.d., DOI 10.1007/s42114-018-0022-9.

[109] S. Seyedin, J. M. Razal, P. C. Innis, R. Jalili, G. G. Wallace, *Advanced Materials Interfaces* 2016, *3*, 1500672.

[110] J. Diani, B. Fayolle, P. Gilormini, *European Polymer Journal* 2009, *45*, 601.

[111] P. Mazurek, S. Vudayagiri, A. L. Skov, *Chemical Society Reviews* 2019, *48*, 1448.

[112] W. Ma, W. Zhang, P. Li, J. Hu, G. Li, S. Sang, in *2012 International Conference on Computing, Measurement, Control and Sensor Network*, IEEE, 2012, pp. 195–198.

[113] H. Elhadidy, J. Sikula, J. Franc, *Semiconductor Science and Technology* 2012, *27*, 015006.

[114] S. Halas, T. Durakiewicz, *Journal of Physics: Condensed Matter* 1998, *10*, 10815.

[115] F. Güder, A. Ainla, J. Redston, B. Mosadegh, A. Glavan, T. J. Martin, G. M. Whitesides, *Angewandte Chemie International Edition* 2016, *55*, 5727.

[116] N. Li, T. Han, F. Tian, J. Huang, M. Sun, P. Irani, J. Alexander, in *Conference on Human Factors in Computing Systems - Proceedings*, Association For Computing Machinery, New York, NY, USA, 2020, pp. 1–13.

[117] X. Xu, C. Yu, A. K. Dey, J. Mankoff, in *Conference on Human Factors in Computing Systems - Proceedings*, Association For Computing Machinery, New York, NY, USA, 2019, pp. 1–12.

[118] D. Cami, F. Matulic, R. G. Calland, B. Vogel, D. Vogel, in *UIST 2018 - Proceedings of the 31st Annual ACM Symposium on User Interface Software and Technology*, Association For Computing Machinery, Inc, New York, New York, USA, 2018, pp. 825–837.

[119] P. Quinn, S. C. Lee, M. Barnhart, S. Zhai, in *Conference on Human Factors in Computing Systems - Proceedings*, Association For Computing Machinery, 2019.

[120] A. Ng, S. A. Brewster, F. Beruscha, W. Krautter, in *Conference on Human Factors in Computing Systems - Proceedings*, Association For Computing Machinery, New York, NY, USA, 2017, pp. 2845–2851.

[121] N. A. Borghese, J. Essenziale, R. Mainetti, E. Mancon, R. Pagliaro, G. Pajardi, *Sensors (Switzerland)* 2019, DOI 10.3390/s19245517.

[122] J. Parker, L. Powell, S. Mawson, *Journal of Medical Internet Research* 2020, *22*, DOI 10.2196/15981.

[123] M. Amit, L. Chukoskie, A. J. Skalsky, H. Garudadri, T. N. Ng, *Advanced Functional Materials* 2020, *30*, 1905241.

[124] J. L. Whittaker, N. Booysen, S. de La Motte, L. Dennett, C. L. Lewis, D. Wilson, C. McKay, M. Warner, D. Padua, C. A. Emery, M. Stokes, *British Journal of Sports Medicine* 2017, *51*, 580.

[125] A. I. Faisal, S. Majumder, R. Scott, T. Mondal, D. Cowan, M. Jamal Deen, *IEEE Sensors Journal* 2021, *21*, 8253.

[126] K. Hutchinson, R. Sloutsky, A. Collimore, B. Adams, B. Harris, T. D. Ellis, L. N. Awad, *Neurorehabilitation and Neural Repair* 2020, 154596832096111.

[127] F. Tian, F. Lyu, X. (Luke) Zhang, X. Ren, H. Wang, *International Journal of Human–Computer Interaction* 2017, *33*, 565.

[128] C.-C. Huo, Y. Zheng, W.-W. Lu, T.-Y. Zhang, D.-F. Wang, D.-S. Xu, Z.-Y. Li, *Neural Regeneration Research* 2021, *16*, 264.

[129] K. Larson, *Dow* 2019.

[130] C. Guo, H. Ashrafian, S. Ghafur, G. Fontana, C. Gardner, M. Prime, *npj Digital Medicine* 2020, *3*, 1.

[131] H. Tchero, M. T. Teguo, A. Lannuzel, E. Rusch, *Journal of Medical Internet Research* 2018, *20*, e10867.

[132] K. E. Laver, Z. Adey-Wakeling, M. Crotty, N. A. Lannin, S. George, C. Sherrington, *Cochrane Database of Systematic Reviews* 2020, *2020*, DOI 10.1002/14651858.CD010255.pub3.

[133] Z. Adey-Wakeling, M. Crotty, *Aging Health* 2013, *9*, 629.

[134] A. Vratsistas-Curto, C. Sherrington, A. McCluskey, *Disability and Rehabilitation* 2019, *43*, 1.

[135] C. Musalek, S. Kirchengast, *International Journal of Environmental Research and Public Health* 2017, *14*, 1447.

[136] T. H. Wagner, A. C. Lo, P. Peduzzi, D. M. Bravata, G. D. Huang, H. I. Krebs, R. J. Ringer, D. G. Federman, L. G. Richards, J. K. Haselkorn, G. F. Wittenberg, B. T. Volpe, C. T. Bever, P. W. Duncan, A. Siroka, P. D. Guarino, *Stroke* 2011, *42*, 2630.

[137] K. Thomson, A. Pollock, C. Bugge, M. C. Brady, *Disability and Rehabilitation: Assistive Technology* 2015, *11*, 1.

[138] I. Jakob, A. Kollreider, M. Germanotta, F. Benetti, A. Cruciani, L. Padua, I. Aprile, *PM and R* 2018, *10*, S189.

[139] R. Stock, G. Thrane, T. Askim, A. Anke, P. J. Mork, *Journal of Rehabilitation Medicine* 2019, *51*, 248.

[140] S. M. Hatem, G. Saussez, M. della Faille, V. Prist, X. Zhang, D. Dispa, Y. Bleyenheuft, *Frontiers in Human Neuroscience* 2016, *10*, 442.

[141] B. G. Subramani, P. R. Selvaganapathy, 2008, DOI 10.1088/0960-1317/18/6/067001.

[142] Y. Yabuki, K. Tanahashi, Y. Mouri, Y. Murai, S. Togo, R. Kato, Y. Jiang, H. Yokoi, *Robotics and Autonomous Systems* 2019, DOI 10.1016/j.robot.2018.09.004.

[143] T. Feix, J. Romero, H.-B. Schmiedmayer, A. M. Dollar, D. Kragic, *IEEE TRANSACTIONS ON HUMAN-MACHINE SYSTEMS* 2016, *46*, DOI 10.1109/THMS.2015.2470657.

[144] B. Huang, M. Li, T. Mei, D. McCoul, S. Qin, Z. Zhao, J. Zhao, *Sensors (Switzerland)* 2017, *17*, DOI 10.3390/s17122708.

[145] J. H. Kong, N. S. Jang, S. H. Kim, J. M. Kim, *Carbon* 2014, *77*, 199.

[146] R. Bertani, C. Melegari, M. C. de Cola, A. Bramanti, P. Bramanti, R. S. Calabrò, *Neurological Sciences* 2017, *38*, 1561.

[147] L. R. Borges, A. B. Fernandes, L. P. Melo, R. O. Guerra, T. F. Campos, *Cochrane Database of Systematic Reviews* 2018, *2018*, DOI 10.1002/14651858.CD011887.pub2.

[148] H. K. Yap, J. H. Lim, F. Nasrallah, J. C. H. Goh, R. C. H. Yeow, in *Proceedings - IEEE International Conference on Robotics and Automation*, Institute Of Electrical And Electronics Engineers Inc., 2015, pp. 4967–4972.

[149] H. K. Yap, J. H. Lim, F. Nasrallah, C. H. Yeow, *Frontiers in Neuroscience* 2017, DOI 10.3389/fnins.2017.00547.

[150] A. G. Thrift, T. Thayabaranathan, G. Howard, V. J. Howard, P. M. Rothwell, V. L. Feigin, B. Norrving, G. A. Donnan, D. A. Cadilhac, *International Journal of Stroke* 2017, *12*, 13.

[151] B. Hoare, S. Greaves, *Journal of pediatric rehabilitation medicine* 2017, *10*, 47.

[152] L. Nordstrand, A.-C. Eliasson, M. Holmefur, *Developmental Medicine & Child Neurology* 2016, *58*, 1042.

[153] A. C. Eliasson, L. Nordstrand, L. Ek, F. Lennartsson, L. Sjöstrand, K. Tedroff, L. Krumlinde-Sundholm, *Research in Developmental Disabilities* 2018, *72*, 191.

[154] I. Novak, I. Honan, *Australian Occupational Therapy Journal* 2019, *66*, 258.

[155] C. H. Hsu, J. R. Wu, Y. T. Lu, D. J. Flood, A. R. Barron, L. C. Chen, *Materials Science in Semiconductor Processing* 2014, *25*, 2.

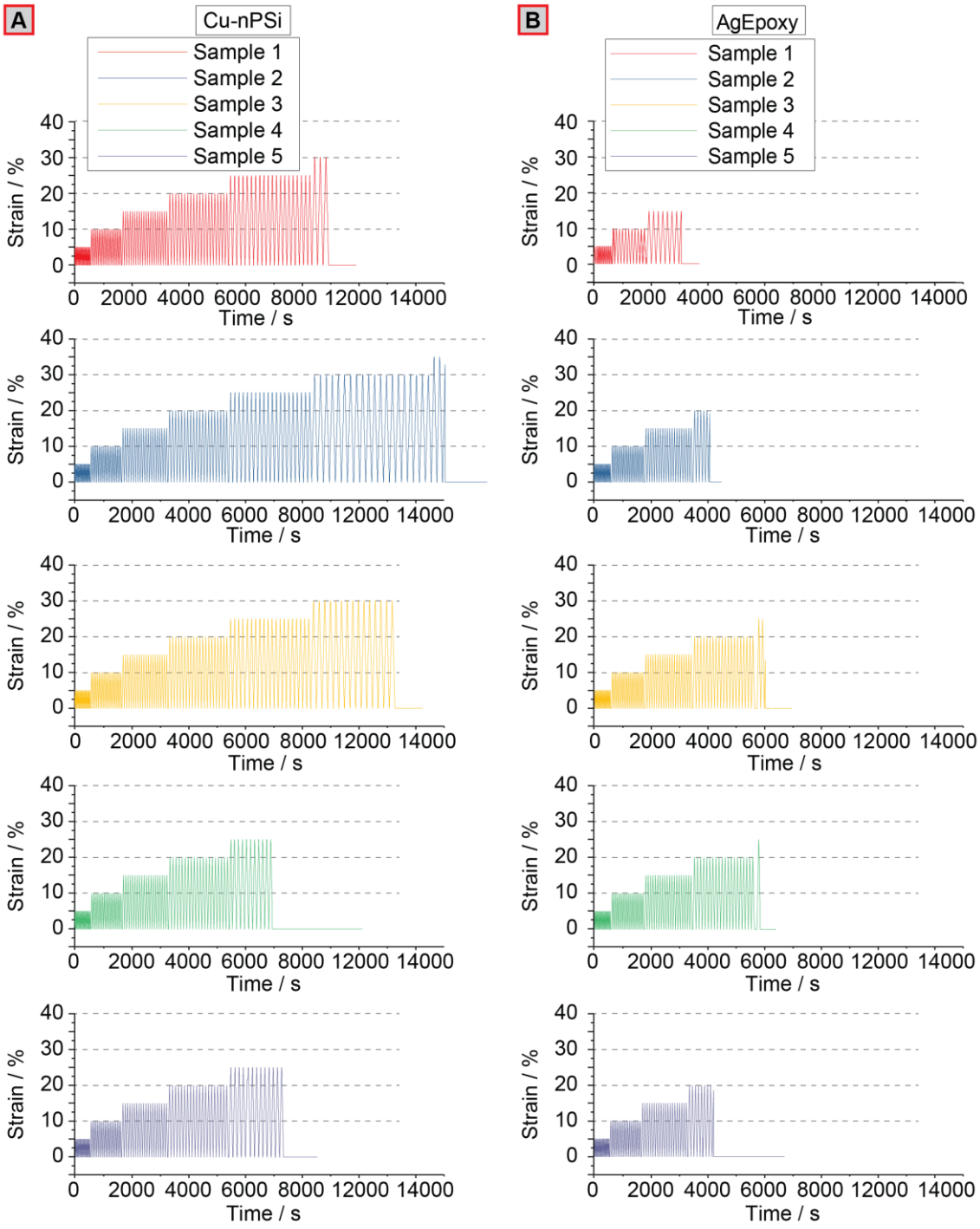
[156] F. Güder, E. Frei, U. M. Kücükbayrak, A. Menzel, R. Thomann, R. Luptak, B. Hollaender, I. Krossing, M. Zacharias, *ACS Applied Materials & Interfaces* 2014, *6*, 1576.

[157] P. Rai-Choudhury, *Handbook of Microlithography, Micromachining, and Microfabrication, Volume 2: Micromachining and Microfabrication*, SPIE PRESS, 1997.

[158] L. Gervais, N. de Rooij, E. Delamarche, *Advanced Materials* 2011, *23*, DOI 10.1002/adma.201100464.

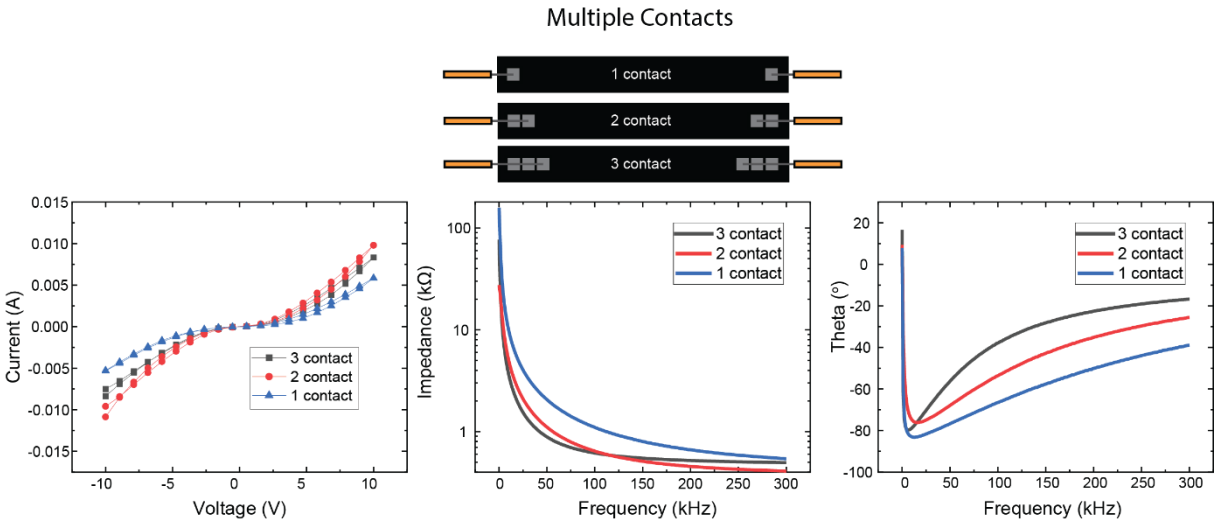
[159] A. Pal, H. E. Cuellar, R. Kuang, H. F. N. Caurin, D. Goswami, R. v. Martinez, *Advanced Materials Technologies* 2017, *2*, DOI 10.1002/admt.201700130.

Appendix

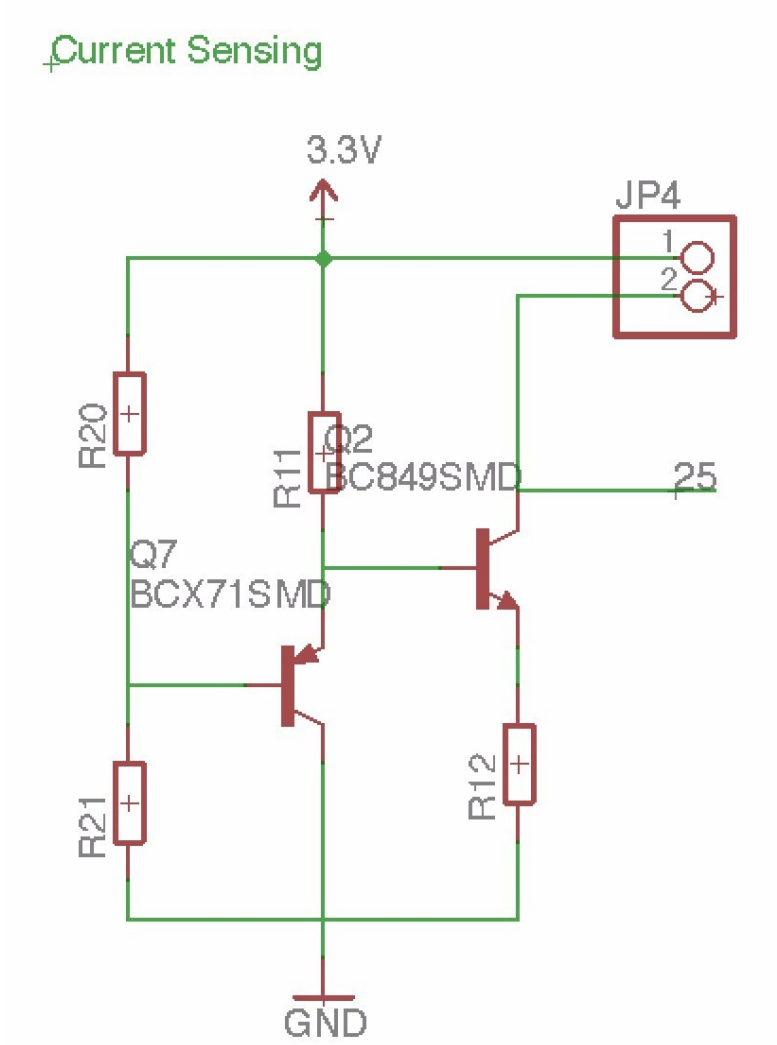


Appendix: Figure 40 Cyclic CB-PDMS test repeats (A) Strain values for Cu-pSi contact samples during cyclic stretching with increasing strain levels until failure, showing samples failing on average at 30%; during our tests, some samples were able to withstand strains of up to 35% before failure of CB-

PDMS; (B) Strain values for AgEpoxy contacts during cyclic stretching at incremental strain levels starting from 5% and increasing by 5% every 20 cycles until failure.



Appendix: Figure 41 Multiple contacts AC/DC measurements Multiple contacts tests showed negligible difference between devices when we increased the number of contacts on each one.



Appendix: Figure 42 Schematic of the custom-built constant current circuit for measuring the resistance of the silicone-based piezoresistive CPC sensors.

Curriculum Vitae

Michael Kasimatis

Education

M.Sc., Nanotechnology and Regenerative Medicine 2013 – 2014

Division of Surgery and Interventional Science

University College London, London, UK

B.Sc., Chemistry 2010 – 2013

Department of Chemistry

Durham University, Durham, UK

Research Experience

Ph.D. Candidate 2016 – 2021

Güder Research Group

Department of Bioengineering

Imperial College London, London, UK

Research Position 2015-2016

'Manufacturing bespoke human organs; 3D printed nanocomposite trachea' - EP/L020904/1

Division of Surgery and Interventional Science, UCL

Stevenage Bioscience Catalyst, Stevenage, UK

Master's Thesis 2013-2014

'Nanocomposite Polyurethane Synthesis for Vascular Implant Self-Endothelialisation' – Poster Presentation, Medical Engineering Centres Annual Meeting and Bioengineering '14 conference, Imperial College London

Centre for Nanotechnology and Regenerative Medicine

University College London, London, UK

Research Project 2012-2013

'Nanodiscs as tools for evaluating Membrane Protein Structure'

Durham University, Durham, UK

List of Publications

Published

1. Gui Zhen Teoh, Poramate Klanrit, Michael Kasimatis, Alexander M. Seifalian, *Role of nanotechnology in development of artificial organs.* Minerva Med. 2015, 106, 17

2. Max Grell, Can Dincer, Thao Le, Alberto Lauri, Estefania Nunez-Bajo, Michael Kasimatis, Giandrin Barandun, Stefan A. Maier, Anthony E. G. Cass, Firat Güder, *Autocatalytic Metallization of Fabrics Using Si Ink, for Biosensors, Batteries and Energy Harvesting,* Advanced Functional Materials 2018, 29, 1804798

3. Giandrin Barandun, Matteo Soprani, Sina Naficy, Max Grell, Michael Kasimatis, Kwan Lun Chiu, Andrea Ponzoni, Firat Güder, *Cellulose Fibers Enable Near-Zero-Cost Electrical Sensing of Water-Soluble Gases*, ACS Sensors 2019, 4, 6, 1662-1669

4. Michael Kasimatis, Estefania Nunez-Bajo, Max Grell, Yasin Cotur, Giandrin Barandun, Ji-Seon Kim, Firat Güder, *Monolithic Solder-On Nanoporous Si-Cu Contacts for Stretchable Silicone Composite Sensors*, ACS Appl. Mater. Interfaces 2019, 11, 50, 47577-47586

5. Yasin Cotur, Michael Kasimatis, Matti Kaisti, Selin Olenik, Charis Georgiou, Firat Güder*, Stretchable Composite Acoustic Transducer for Wearable Monitoring of Vital Signs,* Advanced Functional Materials 2020, 30, 1910288

6. Estefania Nunez-Bajo, Alexander Silva Pinto Collins, Michael Kasimatis, Yasin Cotur, Tarek Asfour, Ugur Tanriverdi, Max Grell, Matti Kaisti, Guglielmo Senesi, Karen Stevenson, Firat Güder, *Disposable Silicon-based All-in-One Micro-qPCR for Rapid On-Site Detection of Pathogens*, Nature Communications 2020, 11, 6176

7. Max Grell, Giandrin Barandun, Michael Kasimatis, Alex Collins, Jieni Wang, Tarek Asfour, Firat Güder, *Determining and Predicting Soil Chemistry with a Point-*

of-Use Sensor Toolkit and Machine Learning Model, bioRxiv 2020, Submission for peer review

In Preparation

8. Giandrin Barandun, Max Grell, Michael Kasimatis, Yubang Shen, Chun Lin Yap, Jeremy Levy, Firat Güder, *Cellulose Fibers in a Sensor Array Enable Low-Cost Point-of-Care Diagnostics of Breath Ammonia Levels*

9. Fahad Alshabouna, Hong Seok Lee, Giandrin Barandun, Estefania Nunez-Bajo, Yasin Cotur, Michael Kasimatis, Firat Güder, *All-Organic Textile-Based Wearable Sensors by Computerized Embroidery (from Fibres to Wearable Sensors)*

10. Michael Kasimatis, Giandrin Barandun, Michael Mace, Max Grell, Paul Rinne, Nicola Goldsmith, Firat Güder, *Soft Stretchable Sensor for Enhanced Handgrip Performance in Point-of-Care Rehabilitation and Digital Therapeutics*

11. Michael Kasimatis, Firat Güder, *A Review of Monolithic Stretchable Strain Sensors in Digital Therapeutics*

12. Yasin Cotur, Selin Olenik, Ugur Tanriverdi, Tarek Asfour, Guglielmo Senesi, Michael Kasimatis, Laura Gonzalez-Macia, and Firat Güder, *Flexible Composite Pressure Transducer for Wearable Monitoring of Breathing Patterns*

Patents

1. Giandrin Barandun, Max Grell, Michael Kasimatis, Electrical Sensing of Gases in Packaged Products and Monitoring Freshness of Perishable Food Products, Application No. GB 2006737.7 (Filed May 2020)

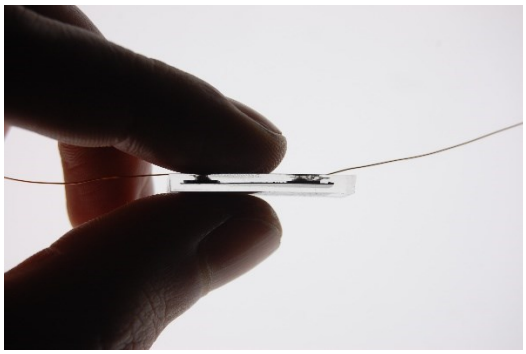
2. Michael Kasimatis, Max Grell, Yasin Cotur, Giandrin Barandun, Firat Güder, *Component for a Stretchable Electronic Device*, Application No. GB 1907270.1 (Filed May 2019)

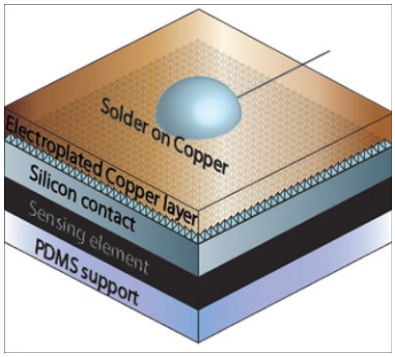
3. Yasin Cotur, Michael Kasimatis, Firat Güder, *Flexible Stretchable Wearable Transducer*, Application No. GB 1813568.1 (Filed August 2019)

4. Max Grell, Can Dincer, Thao Le, Alberto Lauri, Estefania Nunez-Bajo, Michael Kasimatis, Giandrin Barandun, Stefan A. Maier, Anthony E. G. Cass, Firat Güder, *Metal Fabrics and Membranes,* Application No. GB 1805131.8 (Filed March 2018)

Media

"Stretchy and squeezy soft sensors one step closer thanks to new bonding method"





Available by:

THE ENGINEER
Imperial College London
TI
FIERCE Technology
ELSEVIER materialstoday
ZENOPA
Medical EXPO
Over Smart Watch
A
body electron
medgadget
AZO SENSORS
TECTALES tagging medical technologies
INVERSE
AT TODAY

Awards & Grants

Innovate UK Smart Grants, Non-destructive wireless monitoring of food quality using near zero-cost printed electrical gas sensors, 2019, Innovate UK

Cisco Global Problem Solver Challenge Winner, *BlakBear – Optimize food production*, 2019, Cisco Systems

Vodafone Techstarter Award, BlakBear – Low cost paper-based sensors combined with software to increase yields in agriculture, 2018, Vodafone UK

Venture Catalyst Challenge Runner-up, *Opensense – Low cost paper-based pollution sensor*, 2017, Imperial College London Enterprise Lab